Table 5.4.c: Averaged effects (hPa/hour) of each factor during the different phases of the cases at the central pressure value of the medicane. See table 5.4.b for the period of each phase

	950116		**960912**		**030527**	
	Ist phase	IInd phase	Ist phase	IInd phase	Ist phase	IInd phase
1st	e_{24} (-3.07)	e_{124} (-4.28)	e_{123} (2.84)	e_{124} (-5.47)	e_{3} (-2.87)	e_{123} (4.23)
2nd	e_{3} (-2.36)	e_{1234} (2.97)	e_{12} (-1.80)	e_{123} (4.41)	e_{24} (-2.35)	e_{14} (-2.65)
3rd	e_{14} (-1.51)	e_{134} (-2.35)	e_{14} (-1.66)	e_{14} (-2.16)	e_{14} (-1.39)	e_{4} (-1.37)
4th	e_{1} (-1.04)	e_{24} (-2.10)	e_{24} (-1.64)	e_{13} (-1.44)	e_{4} (-1.11)	e_{1} (-0.70)
5th	e_{124} (-0.98)	e_{234} (-1.43)	e_{3} (-1.62)	e_{134} (1.41)	e_{1234} (-0.94)	e_{134} (-0.53)
6th	e_{134} (-0.97)	e_{1} (-1.27)	e_{4} (-1.24)	e_{4} (-1.32)	e_{23} (0.76)	e_{124} (-0.47)
7th	e_{234} (-0.91)	e_{3} (-1.15)	e_{1234} (-1.18)	e_{24} (-1.08)	e_{234} (-0.64)	e_{24} (0.29)
8th	e_{23} (0.70)	e_{13} (-1.08)	e_{2} (0.83)	e_{1} (-0.71)	e_{134} (0.52)	e_{12} (0.29)
9th	e_{123} (-0.46)	e_{4} (-0.85)	e_{234} (-0.78)	e_{23} (-0.57)	e_{123} (0.43)	e_{13} (-0.24)
10th	e_{2} (-0.35)	e_{14} (-0.79)	e_{134} (0.62)	e_{34} (-0.54)	e_{2} (0.35)	e_{3} (-0.17)
11th	e_{13} (-0.35)	e_{34} (-0.63)	e_{124} (-0.42)	e_{12} (-0.42)	e_{1} (-0.22)	e_{234} (-0.17)
12th	e_{4} (-0.33)	e_{2} (-0.55)	e_{23} (0.30)	e_{3} (-0.38)	e_{124} (0.16)	e_{1234} (0.14)
13th	e_{1234} (-0.30)	e_{123} (0.54)	e_{1} (-0.25)	e_{1234} (0.18)	e_{12} (0.06)	e_{23} (0.07)
14th	e_{12} (0.20)	e_{23} (0.33)	e_{34} (0.20)	e_{234} (0.14)	e_{13} (-0.02)	e_{2} (-0.03)
15th	e_{34} (-0.06)	e_{12} (-0.31)	e_{13} (-0.18)	e_{2} (-0.13)	e_{34} (-0.02)	e_{34} (-0.01)

among January 1995, September 1996 and assumed more baroclinic May 2003 case). In other baroclinic studies a cyclolitc role was attributed to the surface fluxes (Kuo et al., 1991a; Horvath et al., 2006) due to a weakening of the surface baroclinic conditions that is proposed to be reinforced in the e_{123} synergy that includes the upper-level disturbance. At the same time, synergy is also proposed to be related to the strength of the capping inversion at the top of the PBL. Surface fluxes define PBL characteristics, meanwhile upper-level disturbances promotes mid-level instability. Their mutual interaction might be related to weaker differences between PBL and free atmosphere layers. Changes on the characteristics of the capping inversion introduced changes in the important energy budget (trough the $\overline{(w'\theta_e)}_h$, see figure 5.2.1) at the top (h) of the boundary layer at outer regions of the medicane (Emanuel, 1986).

Effects on maximum averaged horizontal wind speed

Effects on the maximum azimuthally averaged horizontal wind speed present a large variety of roles (figure 5.4.16). Looking to the fifth more important ones, a quite different sensitivities is obtained for both phases of each medicane (see table 5.4.d). Same factors like, e_{123}, e_{134} have different effectivity sign in 950116 and 960912 cases. This merge of roles and effects of the factors, could be a reflection of the mixture of mechanisms from which the system is developed, since no clear baroclinic or tropical-like structure is formed. In lower degree the initial dominance of the upper level disturbance (e_3) and SST and surface fluxes synergies (e_{24}, e_{14}) as in previous effect is also shown.

During the second phase of the storm evolution, the main effects on the maximal horizontal wind speed at 950 hPa become better identified, since their roles become stronger and much more well defined as a reflection of the well-formed structure. This is summarised in less number of principal effects for the three cases than in the formation phase (see table 5.4.d). Storms are still reinforced by surface factors, meanwhile upper level disturbance lost importance. In January 1995 case three of the five most important effects are the same than in the effects on the central sea level pressure (e_{124}, e_{134}, e_{24}). Moreover the effects present the same behaviour. Cyclogenetic effects e_{124}, e_{24}, e_{134} increase the wind speed of the system. This well correspondence between effects, could reflect a well formation of the case as a tropical-like storm driven by the air-sea mechanism.

Effects on relative vorticity

Effects on the Relative Vorticity at 950 hPa at the centre of the storm (see figure 5.4.17) clearly show the previous defined two phases of the evolution of these kind of systems. There is a clear signal of the formation of the 960912 and 030527 medicanes in the vorticity effects (see middle and bottom plots in figure 5.4.17), which are null until the storms

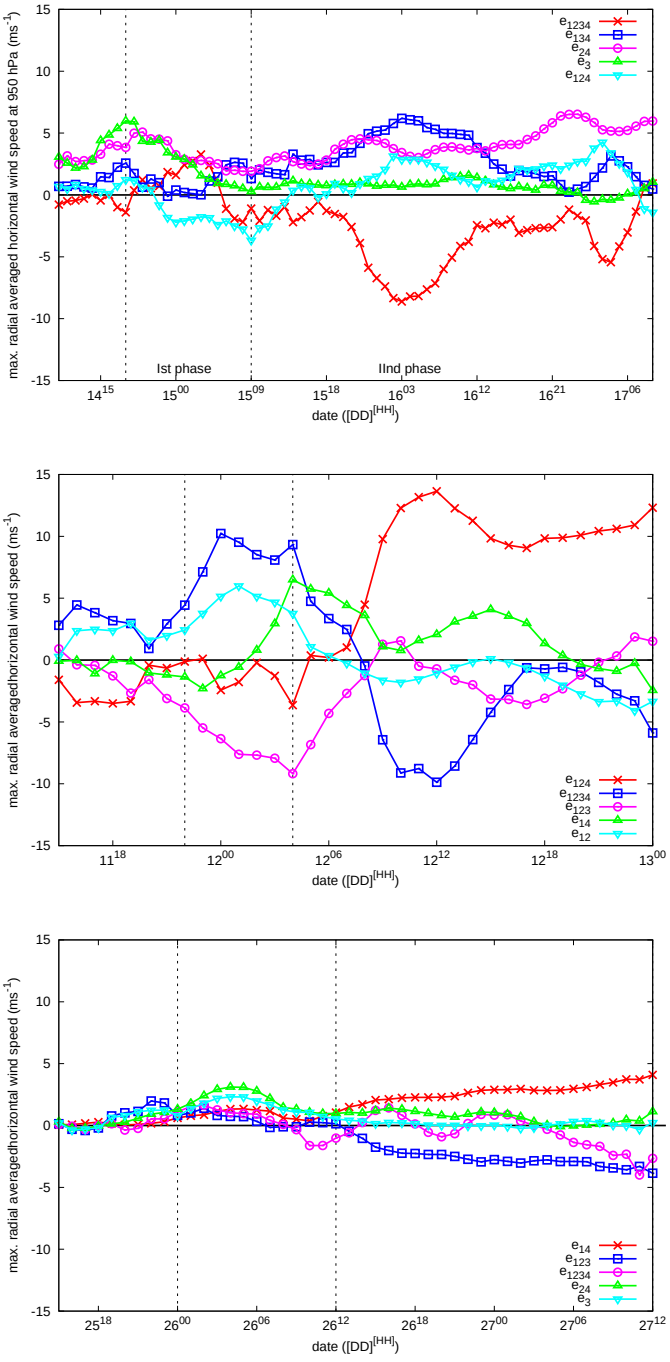

Figure 5.4.16: As in 5.4.15, but for the maximum azimuthally averaged horizontal wind speed at 950 hPa.

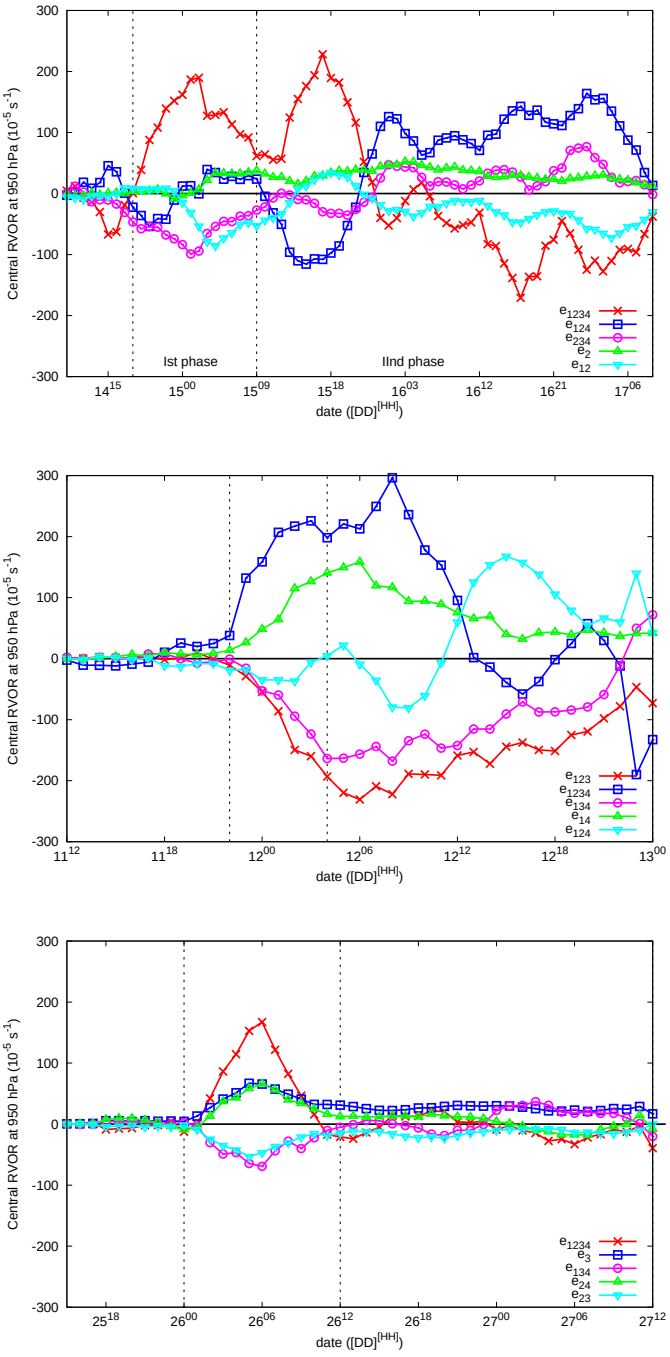

Figure 5.4.17: Like in 5.4.15 but for the Relative Vorticity ($10^{-5}s^{-1}$) at 950 hPa at the centre of the storm.

Table 5.4.d: Averaged effects (ms^{-1}/hour) of each factor during the different phases of the cases at the maximal azimuthal averaged horizontal wind speed at 950 hPa of the medicane. See table 5.4.b for the period of each phase

	950116		**960912**		**030527**	
	Ist phase	IInd phase	Ist phase	IInd phase	Ist phase	IInd phase
1st	e_{24} (3.57)	e_{24} (4.23)	e_{1234} (9.58)	e_{124} (8.67)	e_{24} (2.22)	e_{14} (2.74)
2nd	e_{3} (3.04)	e_{1234} (-3.54)	e_{123} (-7.79)	e_{34} (2.73)	e_{3} (1.69)	e_{123} (-2.57)
3rd	e_{14} (1.73)	e_{134} (3.06)	e_{12} (5.43)	e_{14} (2.52)	e_{14} (0.98)	e_{134} (0.99)
4th	e_{124} (-1.35)	e_{14} (1.83)	e_{4} (2.22)	e_{1234} (-2.48)	e_{2} (-0.59)	e_{24} (0.72)
5th	e_{134} (1.29)	e_{124} (1.33)	e_{134} (-2.03)	e_{123} (-2.15)	e_{123} (0.54)	e_{1} (0.54)
6th	e_{234} (1.04)	e_{13} (1.19)	e_{13} (1.29)	e_{134} (-1.86)	e_{1234} (0.49)	e_{1234} (-0.48)
7th	e_{23} (-1.01)	e_{34} (1.06)	e_{2} (-1.22)	e_{234} (-1.73)	e_{124} (-0.48)	e_{124} (-0.42)
8th	e_{1} (0.93)	e_{2} (-0.97)	e_{124} (-1.14)	e_{12} (-1.08)	e_{23} (0.31)	e_{13} (0.29)
9th	e_{1234} (0.82)	e_{234} (0.79)	e_{1} (-0.62)	e_{1} (0.45)	e_{12} (0.28)	e_{12} (-0.23)
10th	e_{13} (-0.47)	e_{1} (0.74)	e_{3} (0.49)	e_{13} (0.40)	e_{234} (-0.23)	e_{23} (0.16)
11th	e_{123} (0.34)	e_{3} (0.67)	e_{34} (-0.38)	e_{2} (0.35)	e_{13} (0.17)	e_{4} (0.11)
12th	e_{2} (-0.32)	e_{4} (-0.66)	e_{14} (-0.35)	e_{3} (-0.31)	e_{1} (-0.14)	e_{3} (0.10)
13th	e_{4} (0.25)	e_{123} (-0.30)	e_{23} (-0.34)	e_{23} (0.28)	e_{4} (0.09)	e_{2} (0.11)
14th	e_{34} (-0.07)	e_{12} (0.24)	e_{234} (-0.21)	e_{24} (0.20)	e_{34} (0.06)	e_{234} (0.09)
15th	e_{12} (-0.06)	e_{23} (-0.10)	e_{24} (0.17)	e_{4} (-0.01)	e_{134} (0.04)	e_{34} (-0.01)

Table 5.4.e: Averaged effects (10^{-5} s^{-1}/hour) of each factor during the different phases of the cases on the Relative Vorticity at the centre of the medicane at 950 hPa. See table 5.4.b for the period of each phase

	950116		**960912**		**030527**	
	Ist phase	IInd phase	Ist phase	IInd phase	Ist phase	IInd phase
1st	e_{1234} (125.47)	e_{124} (59.74)	e_{1234} (195.71)	e_{123} (-167.27)	e_{1234} (72.67)	e_3 (27.25)
2nd	e_{234} (-65.51)	e_2 (32.49)	e_{234} (-102.27)	e_{134} (-110.14)	e_3 (43.79)	e_4 (22.71)
3rd	e_{12} (-32.62)	e_{23} (-29.15)	e_{123} (-97.85)	e_{1234} (84.33)	e_{234} (38.18)	e_{124} (22.45)
4th	e_{134} (-19.29)	e_{24} (-27.90)	e_{23} (84.71)	e_{13} (83.29)	e_{134} (-36.87)	e_{123} (-16.36)
5th	e_1 (18.61)	e_{12} (-25.26)	e_{14} (78.75)	e_{14} (80.82)	e_{24} (34.02)	e_{23} (-14.48)
6th	e_2 (14.29)	e_{14} (-24.98)	e_{34} (76.78)	e_{12} (65.53)	e_{23} (-30.63)	e_{34} (-12.49)
7th	e_{34} (13.30)	e_1 (17.36)	e_{13} (73.88)	e_{24} (61.31)	e_{14} (20.17)	e_{134} (8.52)
8th	e_{123} (11.58)	e_{234} (16.69)	e_{24} (73.36)	e_{124} (55.91)	e_4 (18.28)	e_{1234} (-6.80)
9th	e_3 (-9.54)	e_{1234} (-13.21)	e_2 (-69.83)	e_1 (-25.64)	e_{123} (-17.42)	e_{234} (5.51)
10th	e_4 (-9.05)	e_4 (11.53)	e_1 (-69.58)	e_{234} (-25.34)	e_{124} (12.01)	e_{24} (3.37)
11th	e_{24} (8.71)	e_{34} (-5.90)	e_{134} (-69.31)	e_{34} (19.39)	e_2 (-9.43)	e_{13} (-2.95)
12th	e_{13} (4.88)	e_3 (-2.26)	e_3 (-60.90)	e_{23} (15.24)	e_{13} (-6.88)	e_1 (1.75)
13th	e_{23} (-4.85)	e_{134} (-2.01)	e_4 (-60.14)	e_3 (-12.78)	e_1 (5.96)	e_{14} (0.32)
14th	e_{14} (1.01)	e_{13} (1.02)	e_{12} (56.66)	e_2 (-10.82)	e_{12} (-4.02)	e_{12} (-0.10)
15th	e_{124} (-0.24)	e_{123} (-0.23)	e_{124} (-29.91)	e_4 (-5.61)	e_{34} (-0.95)	e_2 (-0.04)

are starting to form (11^{21} and 25^{23} UTC, respectively). mature and dissipative phase is depicted as a change in the roles of the factors in the 950116 and 030527 cases at 15^{23} and 26^{10} UTC respectively. Similar change of the roles is observed in the 960912 case at 12^{12} UTC. The principal roles in the January 950116 shown a mixture of factors and cyclolitic/cyclogenetic effects (see top panel in figure 5.4.17). On the other hand, 960912 and 030527 main effects follow two different characteristics. One group of the factors maintain their effect after the genesis of the meso-cyclone (as it is shown by the fifth most important effects of 960912 in the table 5.4.e). Other group of factors only are effective during the initial period of formation of the system (shown by fifth most important effects of 030527 case). The difference between effects of the cases, can be another evidence of the strong dynamical differences between two tropical-like episodes of 950116 and 960912 and a not well defined tropical-like 030527 case.

5.5 Sensitivity study on January 1995 medicane

January 1995 case has been described as the clearest case of tropical-like structure among the three studied cases in the previous section. In addition, from a collection of about 40 cases, the January 1995 event shows the most clear hurricane-like structure on satellite imagery[2].

MM5 model has been shown as a quite adequate tool to simulate tropical storms, like hurricane Andrew (Liu et al., 1997) and Mediterranean tropical-like systems (Reed et al., 2001; Homar et al., 2003b). Since MM5 numerical simulations provide a quite good simulation of the episode (see previous section), a detailed study of the air-sea mechanism in this case can be done.

Analysis of January 1995 case is done following azimuthal averages of 16 radius (100 km long) taken equidistributed at all directions from the centre of the storm. Azimuthal averaged values assume axisymmetry of the storm. Moreover, provides an unique way to represent the results with spatial and temporal independence. However, due to average computations, obtained fields are smoothed and some details are missed. Moreover, azimuthal averaged values are used as a way to ensure that the values of the fields are describing the global characteristic of the system. Analysis is carried out in two ways: a study of the correspondence of the characteristics of MM5 simulated case with the air-sea idealised characteristics, and factor separation results for four selected factors: sea surface temperature (SST), latent heat flux from sea (LHF), sensible surface heat flux (SSHF) and Upper level cold low on a different set of variables.

5.5.1 Methodology of 2-d effects

In order to study the role of the air-sea mechanism, the effect of four factors as well as their synergies are analysed. Simulation without any factor is carried out with sea surface temperature (SST, factor 4) cooled 5°C, sensible surface heat flux (SSHF, factor 2) and latent heat flux from the sea (LHF, factor 1) are switched off in the PBL scheme. Finally, upper level disturbances (ULd, factor 3), selected as all the potential vorticity (PV) field between 500 and 100 hPa, is decreased a 10% of its value at each time when the boundary conditions on the coarse domain (global analyses from ECMWF) are actualised (every 6 hours). Instead FS provide a way to analyse the effect of the tetra- synergy it is not analysed due to the high complexity and large variety of non-linear roles that are included in this synergy (see table 5.4.a for a description of each simulation). It is assumed that selected four factors provide a complete scope of the energetic cycle of the air-sea mechanism. However, one should bear in mind that the latent heat release of the

[2] http://www.uib.es/depart/dfs/meteorologia/METEOROLOGIA/MEDICANES/

strong, deep and vigorous cloud formation essential for the development of these storms, as it was shown in another similar case by Homar et al. (2003b).

Study of the non-linearity of the effects on some point characteristics of the storm (central sea level pressure, vorticity and maximum azimuthal averaged wind speed) has been done in the previous section. Here the 2-dimensional effects of the factors following 16-radius azimuthal averaged fields (with a radius of 100 km from the centre of the storm) will be presented. Previous studies (Homar et al., 2003b; Horvath et al., 2006) used FS in the study of a single characteristic of the system (central pressure), others one (Stein and Albert, 1993; Romero et al., 1997; Homar et al., 1999; García-Ortega et al., 2007) showed the effects on 2-dimensional patterns. In this case, FS technique is applied in a Lagrangian way (following the centre of the simulated system) that provided results will be focused on the structure of the system by itself. Thus, FS is not focused on the results on a single control simulation, otherwise on the simulated feature that wants to be studied. Showing the results on azimuthal averaged vertical sections of the storm is the proposed way from which a generic scope of the role of the effect should be obtained in both sense: the structure and induced dynamics. The azimuthal averaged effects should provide a detailed view of the roles according to their relative position within the studied feature. This increases the complexity of the study, since an interpretation of the effect should be provide taking into account its positional dependence. At the same time that a tropical-like storm has strong dynamically differentiated eye, wall and outer regions.

5.5.2 Validation of control simulation

Validation

Simulated trajectory and vertical structure of the cyclone present quite semblances with the satellite-based tropical-like observed structure and storm trajectory (see figure 5.5.1). At the same time, radial perspective of the simulated storm present clear tropical characteristics (see figure 5.5.2). Unfortunately sparse observations are in this maritime area and a verification following few ship measurements can only be done.

In order to analyse the goodness of the MM5 simulation of the case, BUFR files from ECMWF were used. According to specifications of the observational stations they can provide observations every 3, 6 or 12 hours. In this case 7 ship measurements available during mature phase of the storm (when a clear eye was observed) are considered.

Simulated trajectory of the storm is quite similar to the satellite-based derived one. However, simulated trajectory presents a temporal shift. Numerical storm evolves much faster and last less time that the observed (see figures 5.5.1 and 5.5.3). Instead poor temporal coincidence between observed and simulated trajectories of the storm, a com-

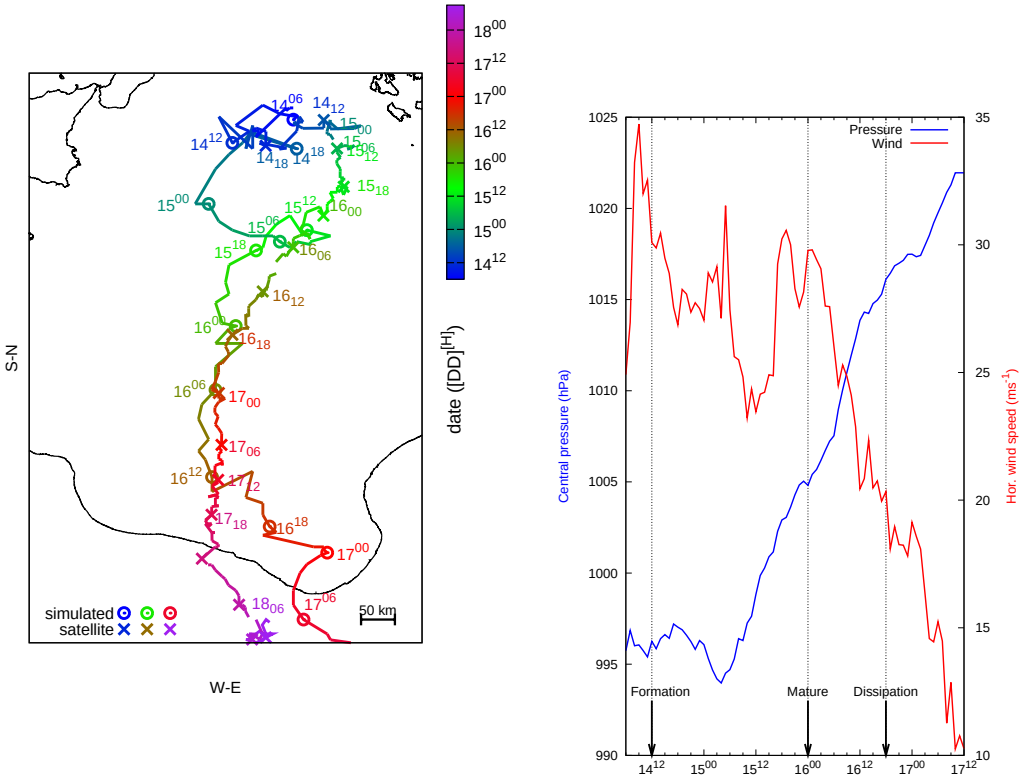

Figure 5.5.1: Control simulation results (f_{1234}). Left panel: MM5 simulated (line with circles and dates in $[DD]^{[HH]}$ format) and satellite derived (line with crosses and dates in $[DD]_{[HH]}$ format) medicane trajectories for the 950116 case with the corresponding date ($[DD]^{[HH]}$, format). Line colour according to box. Right panel: Temporal evolution of the simulated sea level pressure at the centre of the storm (blue line, hPa) and maximum horizontal wind speed at 950 hPa within a radius of 200 km from the centre (red line, ms^{-1}) date in $[DD]^{[HH]}$ format

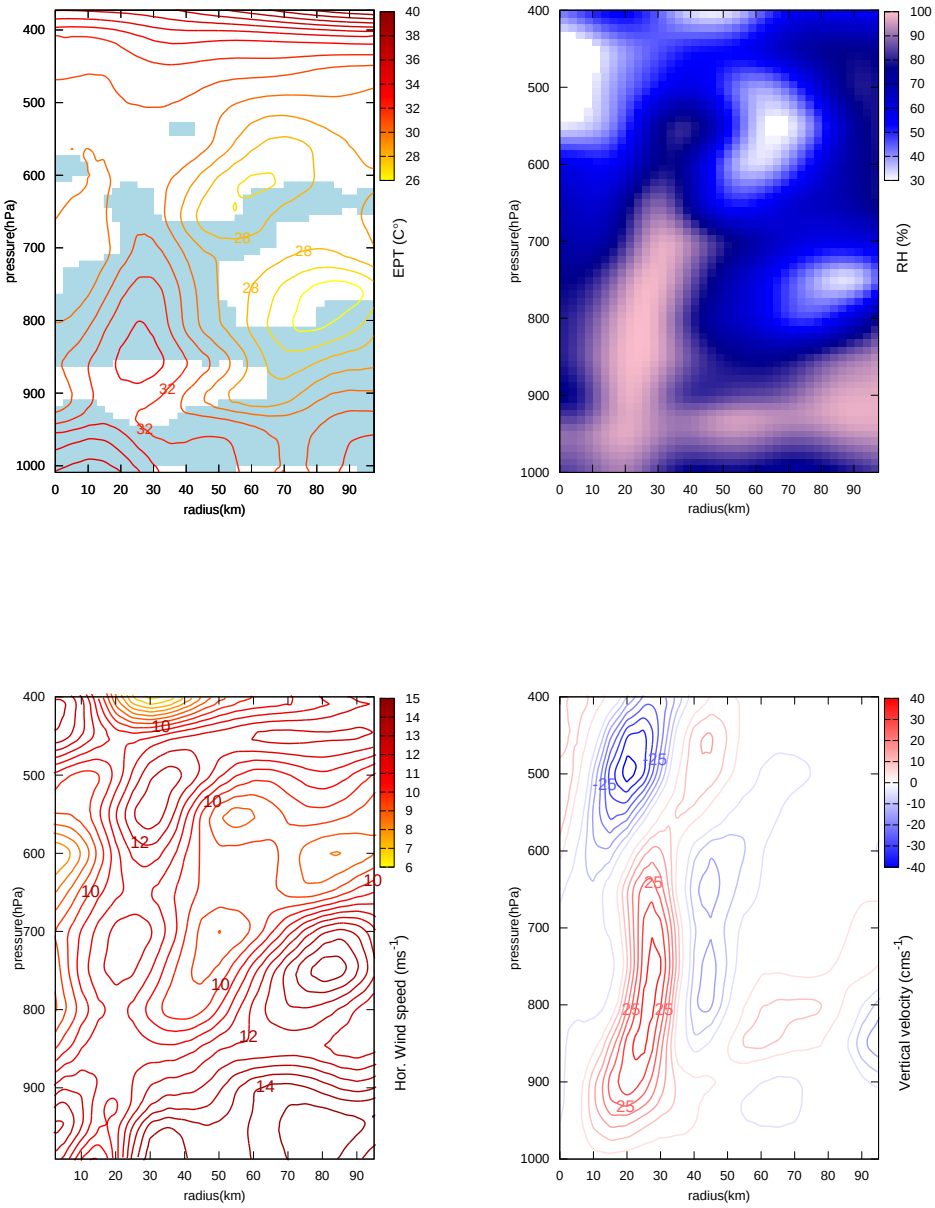

Figure 5.5.2: Averaged time-azimuthal fields (from the centre of the storm) of MM5 control simulated 950116 medicane during the period of maximum intensity (from 15th Jan. 95 at 16 UTC to 16th Jan. 95 at 05 UTC, defined as maximum horizontal wind speed and radial surface pressure gradient). x-axis (radial distance from the centre of the storm, km), y-axis (pressure, hPa). Negative vertical gradients of EPT are blue shaded ($\partial_z EPT < 0$, convective instability). Top left panel: Equivalent Potential Temperature (coloured line, every 1. $°C$). Top right panel: Relative Humidity from 30 %. Bottom left panel: Horizontal velocity (lines every 0.5 ms^{-1}). Bottom right panel: Vertical velocity (lines every 5 cms^{-1}), upward (red line), downward (blue line)

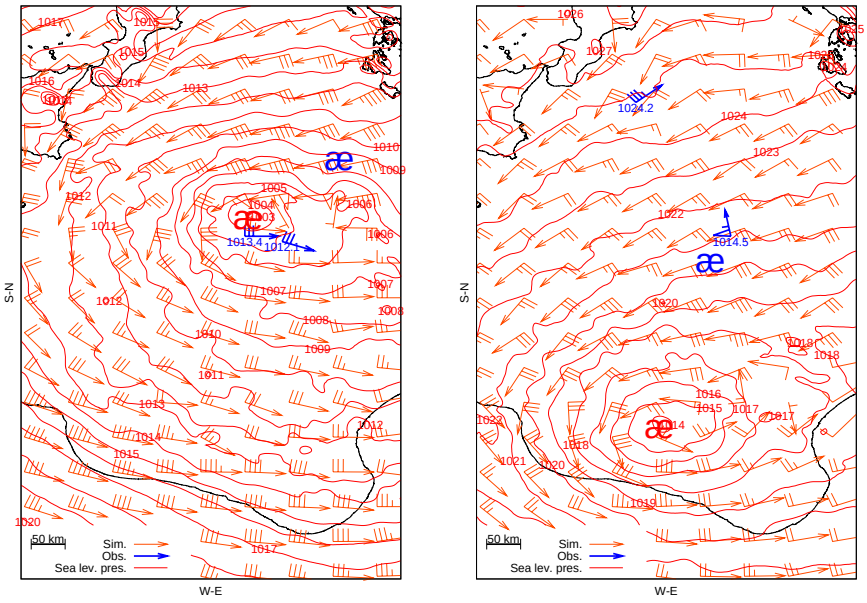

Figure 5.5.3: MM5 Control simulation results results for the January 1995 case (in reds; wind speed at 950 hPa, Sea surface pressure field every 1 hPa and centre of the medicane cross) and the observations (in blue: wind, surface pressure and satellite-based position of the medicane). On January 15th at 18 UTC (left), and January 16th at 12 UTC (right). Symbol æ denotes medicane keeping § for hurricane

parison among the structures of simulated and observed storms is attempted to be done. Trajectory and warm-core simulated structures are taken as realistic enough to assume well correspondence with observed one and for the porpoises of the study. Since at least, a tropical-like cyclone is obtained in the MM5 simulations and the role of different features related to the air-sea mechanism want to be studied.

Obtained fields during the maximum intensity of the simulated storm (between January 15th at 16 UTC and 16th 05 UTC, defined as a horizontal wind maximum at 950 hPa close to the centre of the storm in figure 5.5.1, and stronger radial pressure gradients) are compared to the observations meanwhile an eye-like structure in the centre of the storm can be observed on satellite imagery (from January 15th at 07 UTC to 18th at 06 UTC). Observed characteristics of the storm are taking as a composite of all the measurements located at the corresponding distance of the centre of the storm at the moment of the measurement. Resultant storm is considered to have preservative structure avoiding temporal changes or evolutions of its characteristics. Should beard in mind that this validation have strong approximations: an artificial construction of the characteristics of the observed storm and comparison will be made between smoothed simulated fields (they are spatial and time averaged) and punctual observations. However, according to the available observations, and knowing the temporal shift of the simulations, this methodology is the proposed most accurate way from which the validation of the simulated mature state of the medicane can be done with sparse and temporally shifted ship measurements.

MM5 simulation presents a deeper low pressure disturbance with winds increasing radius ward (see figure 5.5.4). A warm core can be derived (the centre of the storm is warmer that the outer values, bottom left). Moreover a possible wall can be derived from the maximum humidity value and lowest boundary layer height at a distance of 10 km from the centre of the storm (bottom right). Observational composite presented somewhat similar to a tropical-like storm (cross values). Inner low core is warmer with a maximum wind speed and humidity and low cloud base. However, observational and simulated values are quite different. The most notorious difference is that meanwhile MM5 gives a deeper low than the observational compose one (top left), observations give a stronger wind profile (top right).

Vortex characteristics

In order to analyse main characteristics of the mature state of the medicane, some vortex mean fields are computed. Following to the trajectory of the storm, grid boxes of 400x400 km are taken of different fields centred at the storm maximum intensity (between January 15 at 16 UTC and 16th at 05 UTC). Equivalent potential temperature at 850 hPa (EPT), relative vorticity at 950 hPa (RVOR), geopotential height at 500 hPa (H), sea level pressure and mixing ratio at 2 m (Q) give an idea of a rounded clear structure (see

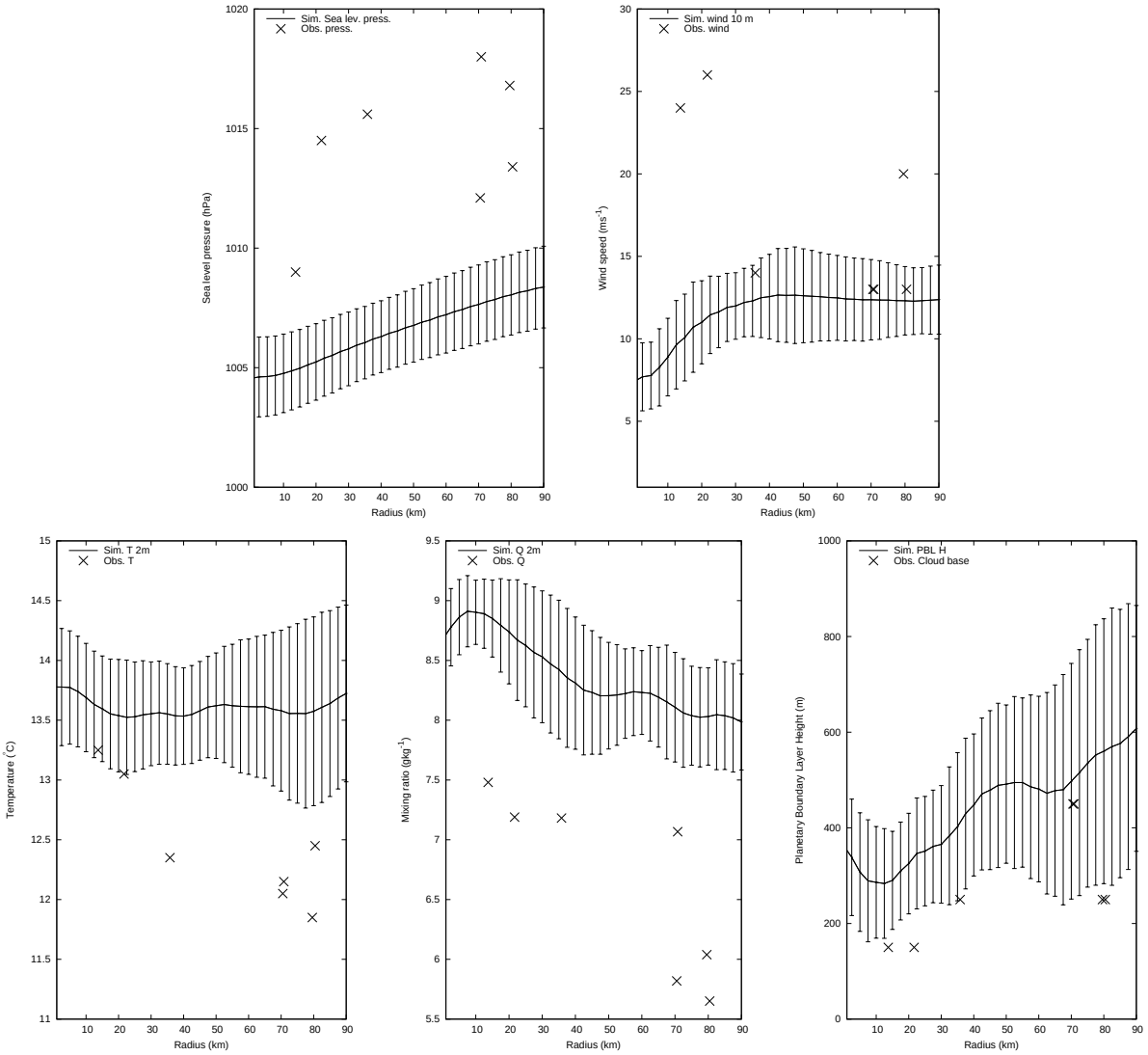

Figure 5.5.4: Radial distribution from the centre of the storm of the MM5 control results for the January 1995 case azimuthal and time averaged values during the maximum intensity of the storm (between January 15th at 16 UTC and 16th 05 UTC) and observations during the existence of an eye (from January 15th at 07 UTC to 18th 06 UTC). Each value has been referred to its individual position of the storm. Sea level pressure (hPa, top left), Wind speed at 10 m (ms^{-1}, top right), Temperature at 2 m (°C, bottom left), Mixing ratio at 2 m (gkg^{-1}, bottom middle) and simulated planetary boundary layer height (m) and observed base of the clouds (m, bottom right). Bars show standard deviation of azimuthal averaging

figure 5.5.5). However, Radiative tendency at 850 hPa RADTEND), temperature at 2 m (T2), planetary boundary layer height (PBLHGT), horizontal and vertical wind at 500 hPa and isoentropic Ertel potential vorticity (ErPV Is) (see figures 5.5.6 and 5.5.7) do not give any kind of clear organised structure.

It is shown how the storm is structured as a warm core low with high vorticity and quasi-saturated centre (see figure 5.5.5). Significant down drafts are obtained during the mature phase of the storm at its centre (see top right panel in figure 5.5.6). At the same time, horizontal wind field do not show an enclosed homogeneous vortex circulation (see figure 5.5.7). It is also obtained that the storm presented a maximum wind profile in the back part of the storm (northern region).

The non-vortex characteristics of the storm are more evident at low levels than at upper levels (see figure 5.5.7). A clear lower winds zone is extended eastward and it is reflected at all levels. This could be a signature of the environmental influences of the upper level anomalies that presented a clear meridional distribution (see ErPV Is field in bottom right panel in figure 5.5.6). It should be also mentioned the shifted relative distribution of the upper and low level disturbances. Geopotential height minimum (top right panel in figure 5.5.5), is shifted eastward from the centre of the storm. The persistence of the shift between upper and low level disturbances is also shown by the horizontal wind profile in which there is a coincidence of a minimal wind intensity (see middle and bottom figures in figure 5.5.7). The no clear existence of an axisymmetric vortex structure of the storm can be considered as a reflect of the weakness of the tropical characteristics of the storm as air masses with different thermal characteristics that confluence at the central part of the medicane (see top left panel in figure 5.5.6). This point is also mentioned by Montgomery and Farrell (1992) in the polar lows as a possible reflect of the warm air swirl by cold air. Finally frictional effects are shown in the wind profile, since wind strength at 950 hPa is stronger than at 2 m (see figure 5.5.7).

5.5.3 PBL Air-sea structure correspondence

As has been said, MM5 numerical simulations present a cyclone with tropical-like characteristics. Assuming well enough coincidence of the behaviour of the simulated storm, MM5 simulations will be used to study the importance of the air-sea mechanism in these type of Mediterranean tropical-like storms.

General characteristics of the planetary boundary layer (hereafter, PBL) of the storm do not present a clear structure as it is described by theory. Temporal evolution of simulated regime (defined throughout the Bulk Richardson number and Monin-Obukhov length) shows a pattern in which a signature of a wall and three related PBL zones can

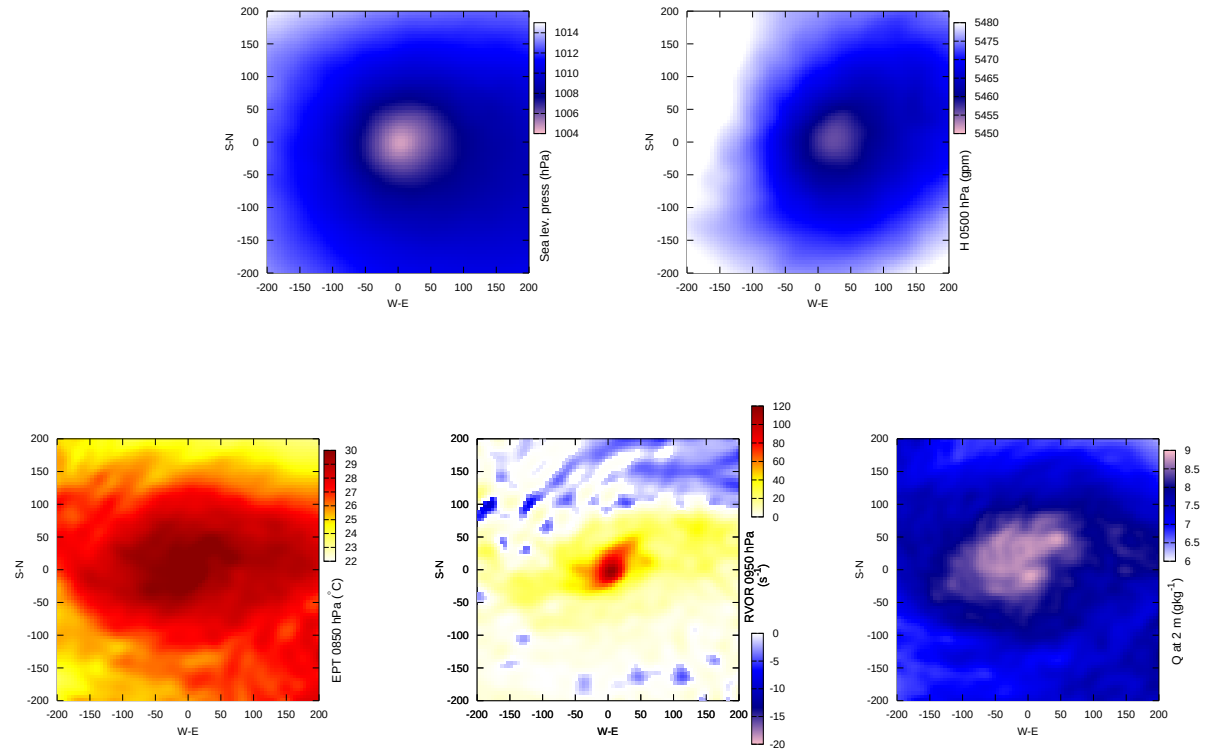

Figure 5.5.5: Time averaged fields in a grid box of 400x400 km centred at the centre of the storm following its trajectory during its maximum intensity (From January 15th at 16 UTC to 16th at 05 UTC). For the Sea level pressure (hPa, top left) and Geopotential Height at 500 hPa (gpm, top right). Equivalent Potential Temperature at 850 hPa (°C, bottom left), Relative vorticity at 950 hPa (s^{-1}, bottom middle) and Mixing ratio at 2 m (bottom right, gkg^{-1})

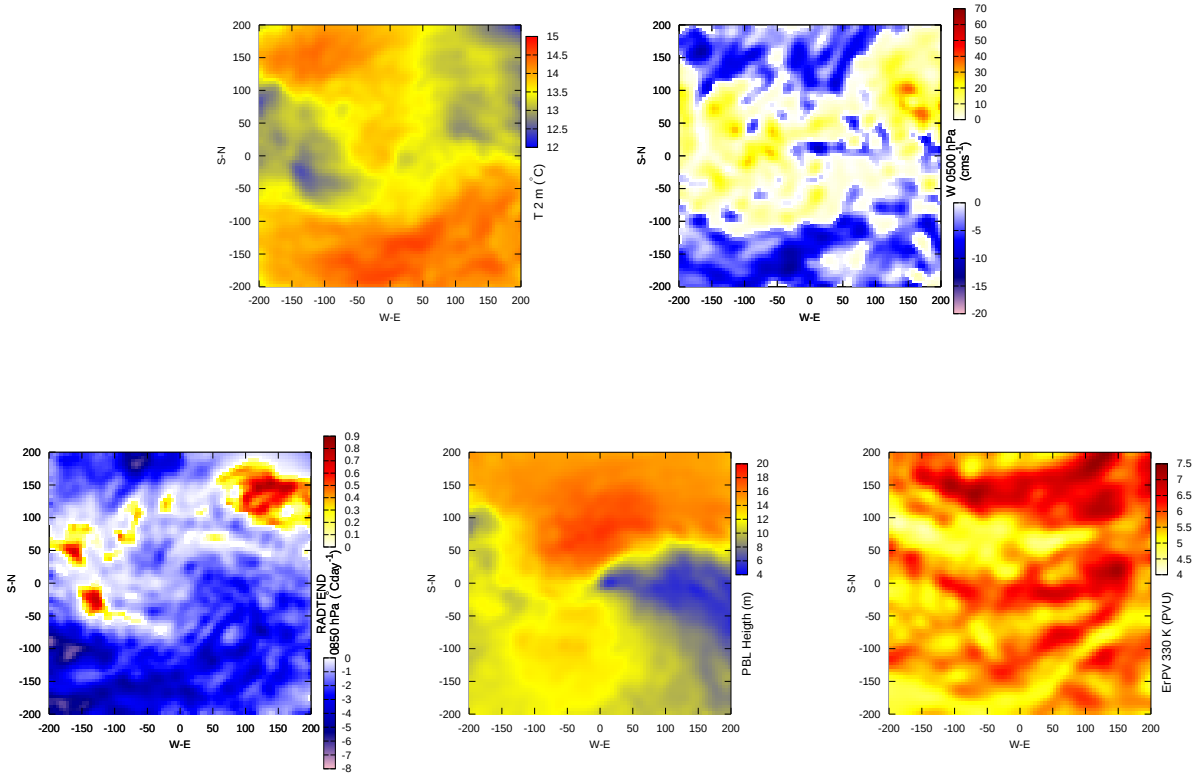

Figure 5.5.6: As in 5.5.5, but for the Temperature at 2 m ($^{\circ}C$, top left), vertical velocity at 500 hPa (cms^{-1}, top right), radiative tendency at 850 hPa ($^{\circ}Cday^{-1}$, bottom left), planetary boundary layer height (m, bottom middle) and Ertel potential vorticity on an isentropic surface at 330 K ($PVU = 10^{-6}m^2Ks^{-1}kg^{-1}$, bottom right)

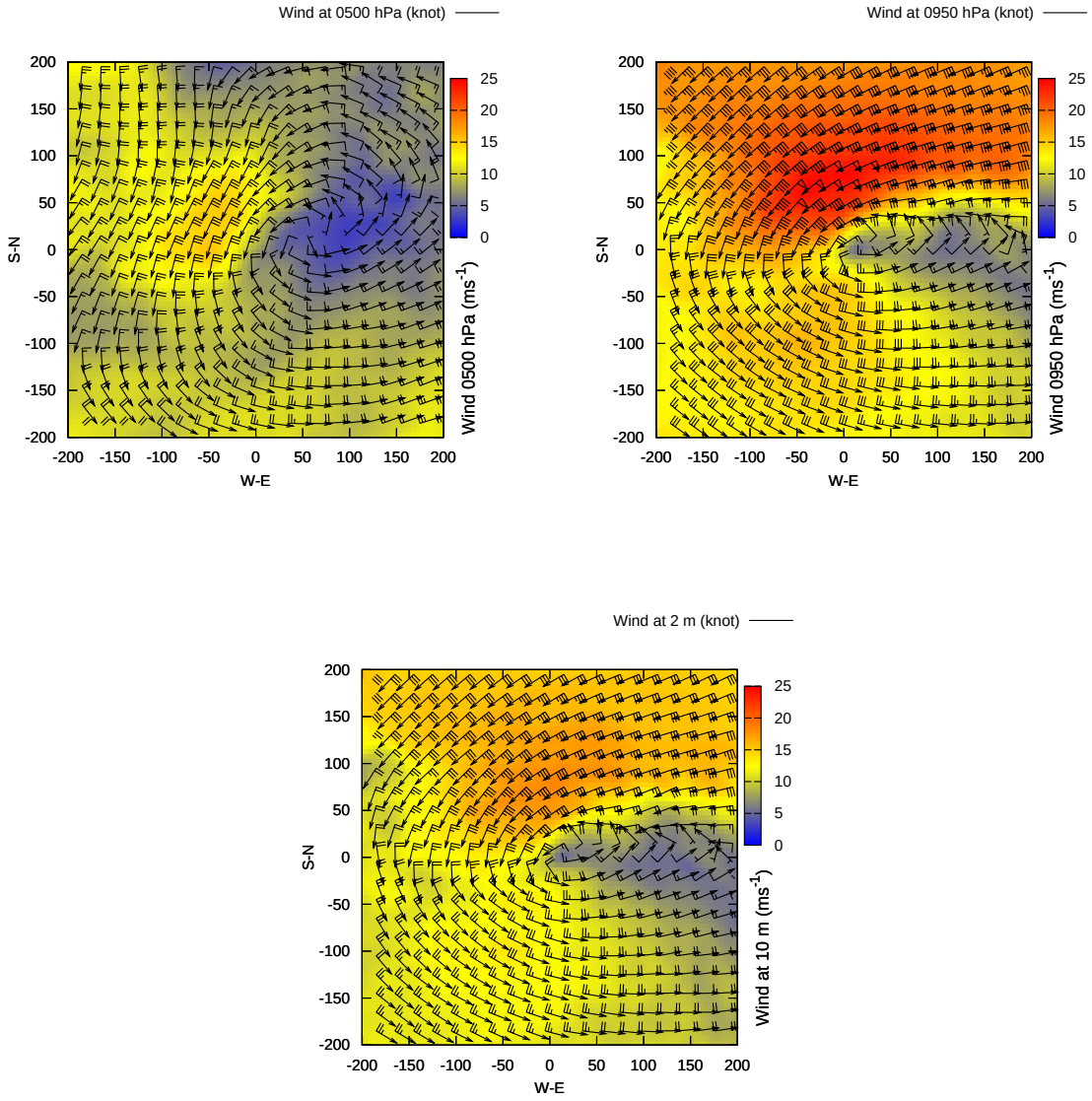

Figure 5.5.7: As in 5.5.5, but for horizontal wind speed at 500 hPa (ms^{-1}, top left), at 950 hPa (ms^{-1}, top right) and at 10 m (ms^{-1}, bottom), superimposed in barb notation (triangle 50 knot, full pennant 10 knot and half pennant 5 knot)

be observed. At specific times three boundary regimes are simulated and presented a well agreement with an eye-wall-convection regions (see figure 5.5.8). Changes in PBL regime have correspondence with the lowest and most saturated region of the radius section that can be identified with the wall zone. Due to subsidence in the eye, this zone should present a stable boundary layer, meanwhile MM5 boundary layer scheme gives a free convective regime. Blackadar PBL is a simple scheme that considers only two regimes (Grell et al., 1995): free-convection and nocturnal regime given by a comparison between the critical and the bulk Richardson Richardson numbers (Stull, 1988). The simplicity of the scheme might not be accurate enough to provide an adequate view of the PBL.

However, temporal evolution of boundary layer characteristics reflect the complete establishment of tropical-like characteristics of the storm (See figure 5.5.8); it is shown how the centre of the storm is warming due to warm core characteristics (see increasing centre temperature in thermal evolution in the top right panel). At the same time, inner regions presented the lowest turbulent characteristics (lowest values of the friction velocity, u_*, bottom right panel) and the enhancing of the eye as a wider section with the lowest boundary layer heights (top left panel). However, as has been seen in temporal evolution of the central pressure (see right panel in figure 5.5.1), surface pressure increases with time (bottom panel in figure 5.5.8).

5.5.4 Effects on the vertical radial structure

Effects obtained for the January 1995 case have a relatively good relation to the dynamics of the air-sea interaction (see previous section). For a more detailed study effects on 16 azimuthal averaged vertical cross sections of the system from the centre of the storm are shown. These radial vertical cross sections are taken at three time steps. One on January 14th at 12 UTC (six hour after the starting time of the simulations avoiding model spin up effects), on January 16th at 00 UTC (at mature state of the system) and during dissipation phase on January 16th at 18 UTC.

The effects of the factors could be focused in two principal aspects of the storm; thermodynamic aspects such as temperature, humidity and cloudiness and dynamical aspects such us geopotential height and wind field. Even so, air-sea mechanism establishes a thermodynamic base for the formation and evolution of a tropical storm that makes possible the treatment of a hurricane as a Carnot engine (Emanuel, 1986, 1995). Thus a well understanding of the evolution and structure of the EPT can give a wide idea of the thermodynamic aspects of the system, even though other characteristics are not well described by the variable. Some important aspects obtained from other variables will be also mentioned when it is necessary, since some factors could have a strong impact on specific other aspects of the system.

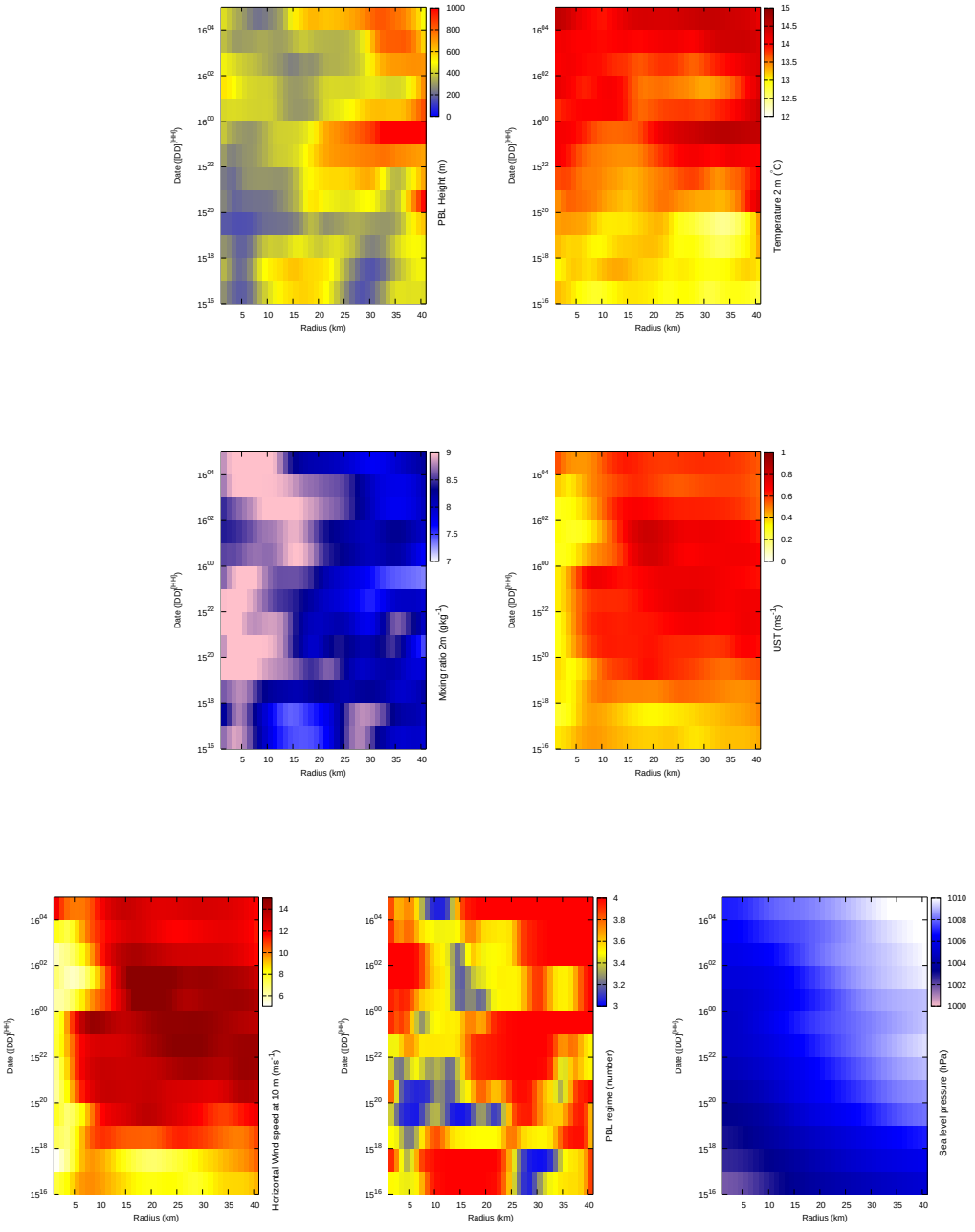

Figure 5.5.8: Temporal evolution (from January 15th at 16^{00} to January 16th 05^{00} UTC) of azimuthal averaged values PBL Height (top left), Temperature at 2 m (top right), mixing ratio (gkg^{-1}, middle left), u_* (ms^{-1}, middle right), wind speed at 10 m (ms^{-1}, bottom left), PBL regime (3: Forced convection, 4: Free convection; bottom middle) and Sea level pressure (hPa, bottom right)

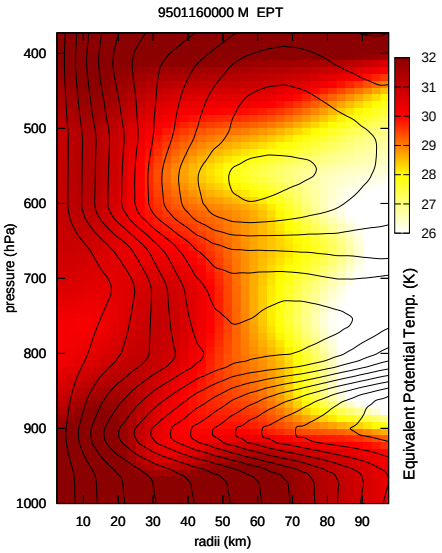

Figure 5.5.9: Storm centred azimuthal averaged vertical cross section of constant angular momentum surfaces M ($m^2 s^{-1}$, solid lines) and equivalent potential temperature (K, shaded) on 16th January 1995 at 00 UTC. x axes radius distance from centre, y axes pressure)

If the air-sea mechanism is active during the medicane evolution, in somehow vertical cross sections of the fields exhibit some peculiarities of the tropical-like structure of the storm. Radial azimuthal averaged vertical cross section of the simulated mature state of the storm (see figure 5.5.9), have some similarities with the radial structure of a hurricane (Rotunno and Emanuel, 1987) (see figure 5.2.1). Constant angular momentum surfaces draw two distinct zones: at low level, surfaces are radially equi-distributed; at mid-levels, surfaces show up-outward distribution. A warm core structure is also shown with a signature of an eye-wall.

Effects are given at a specific moment of the simulation, which provide a time-dependant description of the result. However, they provide a not smoothed view of the storm that is given by averaged fields in storm's mature phase discussed in the validation subsection. Moreover, azimuthal averaged fields assume axis-symmetric structure of the storm, and an unique and equal radius for all the periods of the storm, that might help to

obtain an objective scope of the phases of the cyclone. Due to hurricane-like characteristics of the storm, effects might have two distinguished values: at the centre and outer regions.

Effects during formation

At the beginning of the storm (January 14th at 12 UTC) a weak vortex about 800 hPa height, and a radii about 40 km is observed (see top left in figure 5.5.10). It is shown the positive role of the surface fluxes in the storm as it was found by Kuo et al. (1991b). LHF warms and moistens the surface layers (e_1, top right), meanwhile SSHF (e_2 bottom left) warms and dries surface layers and deepens the storm cooling, moistening and increasing wind speed at its centre (not shown). Enhancing effect in the core of the vortex, might be a reflect of the positive role of the SSHF in maritime low disturbances described by Mak (1997). Upper level disturbances (ULd hereafter, effect e_3, bottom middle), provokes a decrease of the EPT all over the storm, except at the top of the centre of the vortex, where the column of air at this zone is moistened and vorticity is raised until 700 hPa as a result of the factor (not shown). Meanwhile induced down drafts of upper air dried. At this moment, control simulation (in the f_{1234}) disturbance is beneath an upper level cold pool zone (not shown).

The synergy between the SSHF and the Upper level disturbances e_{23} (bottom right in figure 5.5.10) has a differenced role in the centre of the vortex and the outer regions, with a vertical dependence according to the height of the vortex. It plays a role heating and drying the centre of the storm, meanwhile the environment is cooled and moistened. At the same time it reduces the wind speed at the centre of the storm (not shown). In terms of the baroclinic development of the vortex, it plays a cyclolitic role, but it has a positive effect towards the characteristics of an hurricane-like eye and it destabilises the environment of the vortex. SST enhances the turbulent mixing and transports in the surface (see bulk parametrisation of LHF and SSHF fluxes, Emanuel (1986)) and the synergy (e_{24}, left panel in figure 5.5.11) has a stronger equivalent effect than in the e_2 pure effect.

Similar role is obtained by the triple synergy e_{124} (middle) between surface fluxes (LHF and SSHF) and SST from which a tropical driven effect on the evolution of the storm can be derived. Mid level humidity is enhanced and cloud formation is promoted at outer regions of the vortex (Cloud liquid water at middle levels is enhanced (not shown)). At the same time it reduces wind speed and vorticity at the centre of the storm increasing wind speed at outer regions (not shown). Finally, e_{234} reproduces the same pattern of the SSHF by it self (right). It is remarkable that the mutual interaction of two factors e_{23} without taking into account influences of SST has the opposite sign. This result shows the

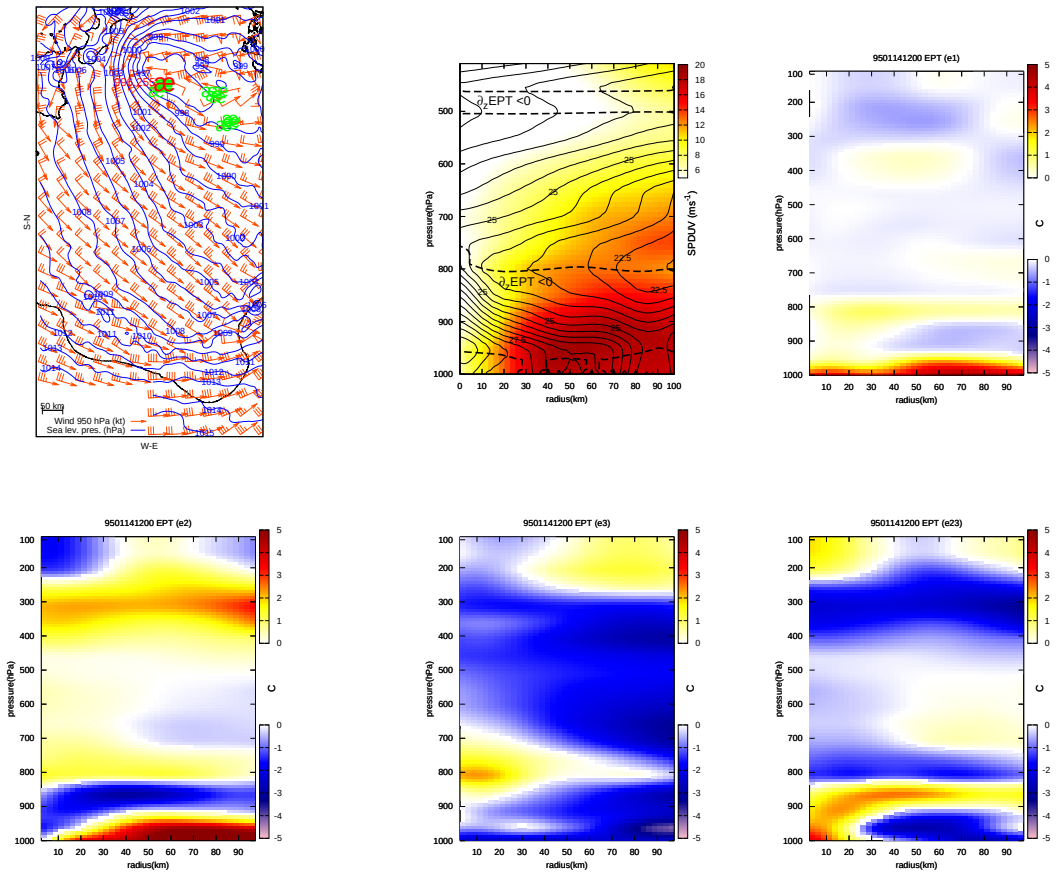

Figure 5.5.10: Values on January 14th at 12 UTC. Top left panel: Control simulation sea level pressure (f_{1234}, simulation; every 1 hPa, blue lines), horizontal wind at 950 hPa (orange vectors in barb notation; triangle: 50 kt, pennant 10 kt, half pennant 5 kt) and central position and pressure of the storm (red æ, red label in hPa), rest of simulated medicanes positions (green æ). Top middle panel: Control simulation vertical cross sections of azimuthal averaged horizontal wind speed (shaded in ms^{-1}) and equivalent potential temperature (EPT, solid lines in $°C$, convective instability zone $\partial_z EPT < 0$ is shown as thick dashed line). Rest of panels: Azimuthal averaged effects on EPT (dashed in $°C$; blues: negative effect, reds: positive effect). e_1 (LHF, top right), e_2 (SSHF, bottom left), e_3 (ULd, bottom middle), e_{23} (SSHF and ULd synergy, bottom right)

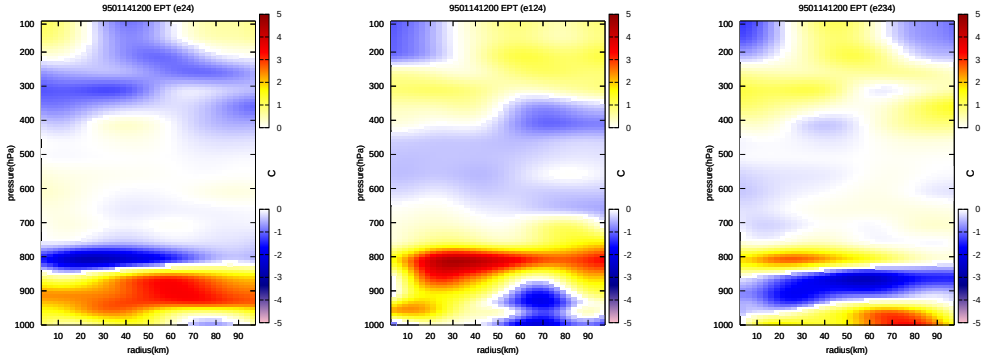

Figure 5.5.11: As in figure 5.5.10 but for e_{24} (SSHF and SST synergy, left), e_{124} (LHF, SSHF and SST synergy, middle) and e_{234} (SSHF, ULd and SST synergy, right)

complexity of non linear processes that are involved in the mutual interactions between factors.

Effects at mature phase

Mature state of the medicane (January 16th on 00 UTC, see left and middle plots in figure 5.5.12) is described as a cyclone with a height of 600 hPa and a radii about 100 km. Radii of the eye seems to be about 10 km with the base of the wall at 30 km (zone with the maximum wind speeds). In control simulation, at this moment, upper level disturbance and medicane are completely coupled, since upper level central minimum height (about 5470 gpm at 500 hPa) is located above the centre of the medicane (not shown). In comparison to the formation phase of the system, it is shown a more unstable structure of the storm according to the greater convective instable zone ($\partial_z EPT < 0$ in figure 5.5.12 top middle panel).

Surface fluxes preserve the same role that they have in the initial phase. However, LHF (e_1 effect at top right plot in figure 5.5.12) has increased significantly its influence to higher levels and it has a strong pressure fall role at low levels (not shown). e_3 drys the middle levels of the system and decreases (weaker than in the initial phase) pressure allover the vertical structure of the system (middle left plot in figure 5.5.12). SST warmed low levels and has it strongest deepening role in the selected moments (not shown).

Effects of the synergies between surface fluxes (middle middle plot in figure 5.5.12)

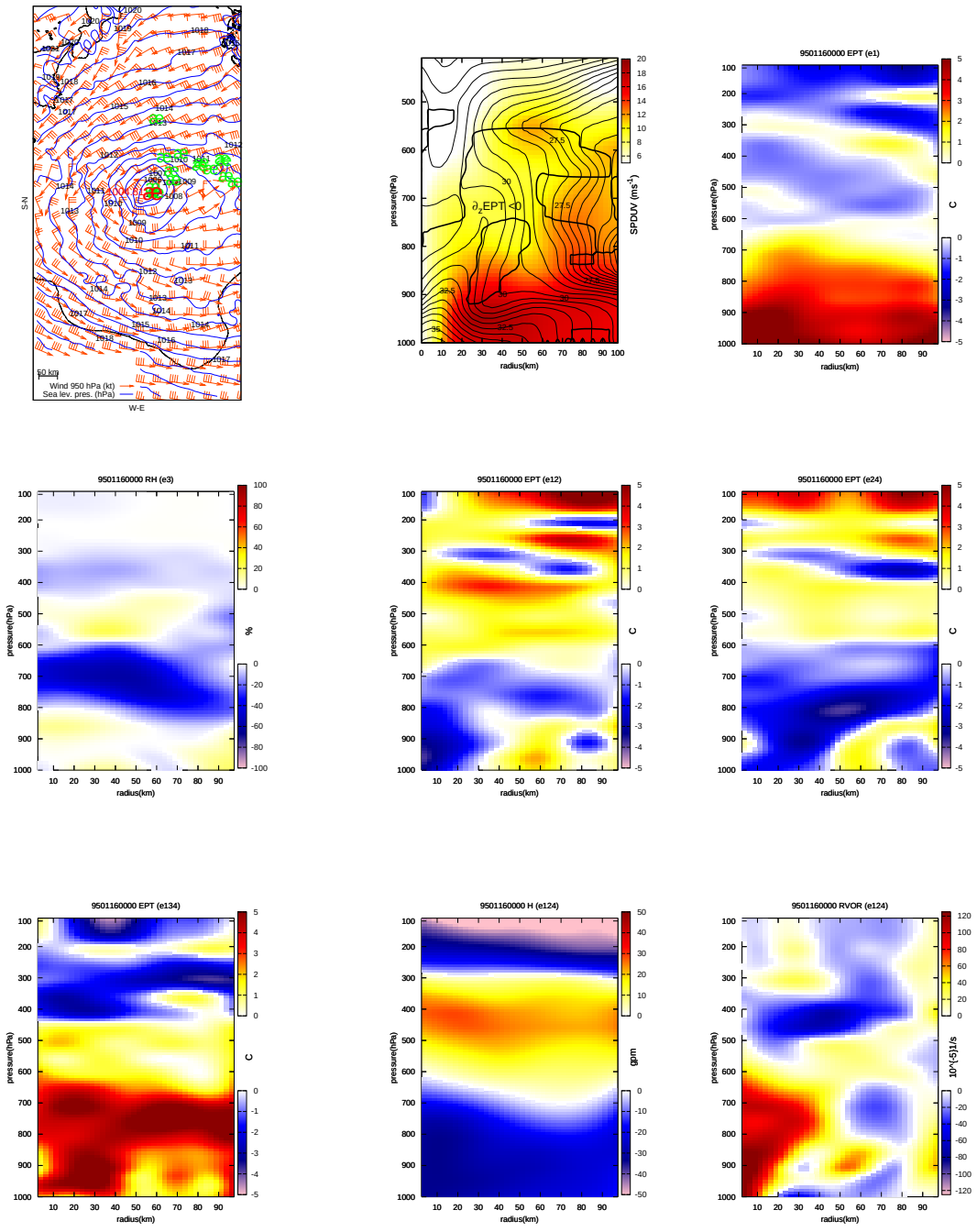

Figure 5.5.12: As in figure 5.5.10 and 5.5.11, but on January 16th at 00 UTC. Effects of e_1 on Equivalent potential temperature (EPT in $°C$, top right), e_3 on relative humidity (%, middle left), e_{12} on EPT ($°C$, middle middle), e_{24} on EPT ($°C$, middle right), e_{134} on EPT ($°C$, bottom left), e_{124} on geopotential Height (gpm, bottom middle) and of e_{124} on relative vorticity (s^{-1}, bottom right)

are most important in the core of the storm contributing to enhance its properties such as vertical low humidity profile, low wind speed velocities and low cloudiness (not shown). Synergy between LHF and ULd (e_{13}) has a dual role. It makes difficult the humidity flux following air trajectories of the air sea mechanism (middle level constant angular momentum surfaces structure as in figure 5.5.9), but deepened the system and enhanced the air-sea mechanism characteristics of the storm. Not only it helps to low the pressure, cloudiness and wind speed at the centre of the storm but it contributes to increase cloudiness, vorticity and humidity at outer region of the eye (not shown). SSHF and ULd mutual influences have a enhancing effect on the storm, since their mutual interaction reinforces their positive individual role. This synergy (e_{23}) moistened middle levels and dried the air at the top and weakened wind speed of the centre of the storm (not shown). e_{24} cooled and dried a wide zone within the storm that presents some similarities to the mid-level constant angular momentum surfaces (see middle right in figure 5.5.12). Must be noticed the antagonistic role of this effect in comparison to its role in the formation phase. It could be a reflect of the change in the dynamics of the system. During initial phase SSHF (factor 2), enhances storm reinforcing vertical transport of heat and moist to boundary layer and upper levels. However, at mature phase, SSHF enhance turbulence provoking a diminishing effect on the inward motion to the centre of the storm (maximum values of u_* are found at this phase, see figure 5.5.8).

e_{123} plays a dissipative effect (as it is shown in previous section), since it cooled and moistened the core of the system (not shown) at the same time that it decreased humidity and cloud formation in outer regions (not shown). Mutual interaction between LHF, ULd and SST plays an important enhancing role moistening and warming the air-sea mechanism trajectory pattern (e_{134}, bottom left) and promoting pressure fall and wind speed enforce at the base of the wall (not shown). Synergy between surface fluxes and SST (e_{124}) contributes strongly in the mechanical deepening (pressure fall and wind speed increasing) of the system (bottom middle, negative effect), but present other thermodynamic vanishing effects such us a cooling, moistening and enhancing cloud formation in the core (not shown). At the same time, at outer regions low level air is cooled and middle level is warmed meanwhile wind speed is increased as a result of it a strong increase of relative vorticity all over the centre of the storm is induced (see bottom right plot).

Effects during dissipation

During the dissipative phase of the storm (January 16th at 18 UTC see figure 5.5.13), control simulation (top left and middle plots in figure 5.5.13) shows a warm core structure with a radii about 50 km and a height of the vortex up to 750 hPa. At this moment the storm is not located below upper level disturbance (not shown). Simulated atmospheric conditions differ significantly among 16 simulations (see for example different lo-

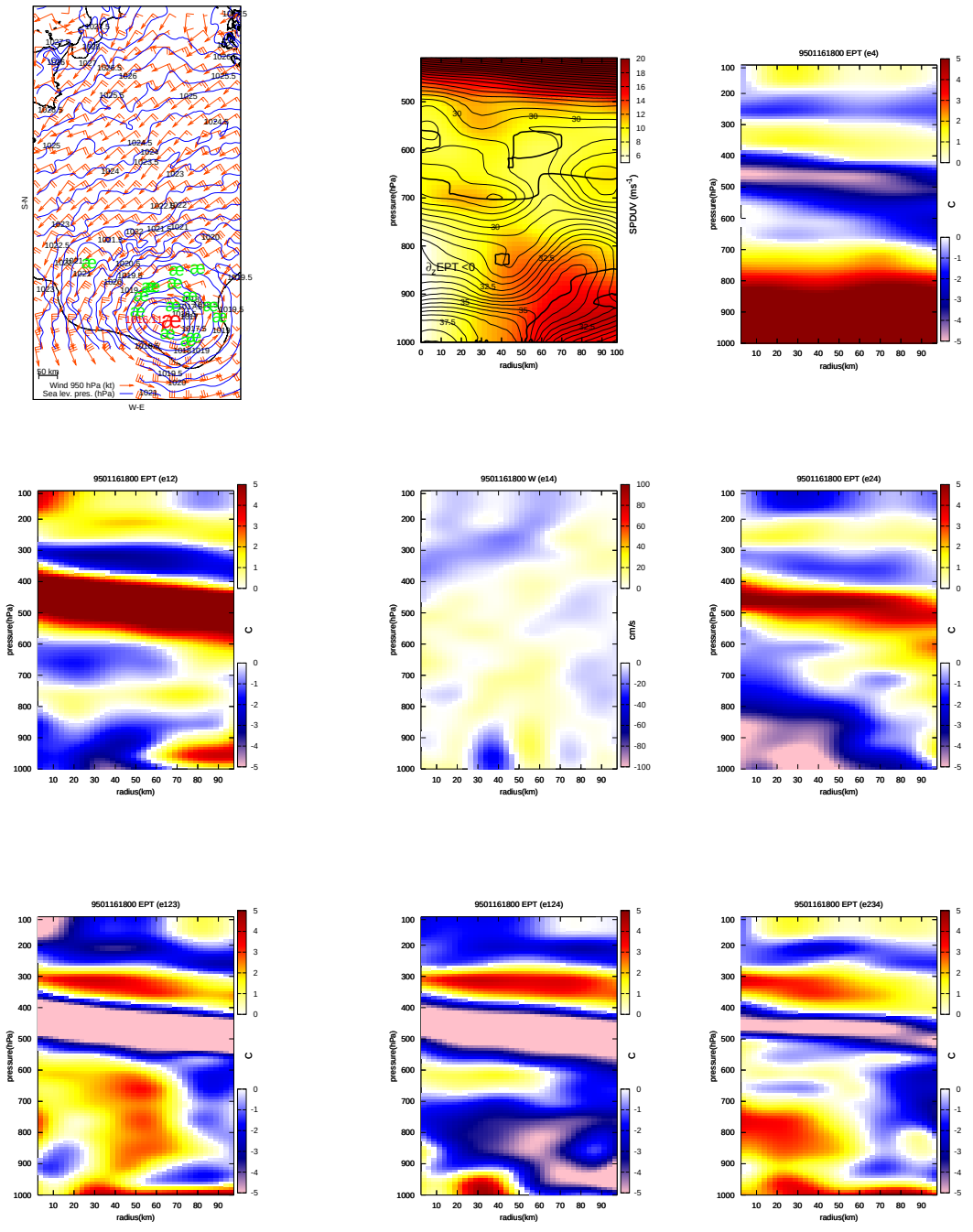

Figure 5.5.13: As in figure 5.5.10 and 5.5.11, but on January 16th at 18 UTC. e_4 on equivalent potential temperature (EPT, $°C$, top right), e_{12} on EPT ($°C$, middle left), e_{14} on Vertical velocity (cms^{-1}, middle middle), e_{24} on EPT ($°C$, middle right), e_{123} on EPT ($°C$, bottom left), e_{124} on EPT ($°C$, bottom middle) and e_{234} on EPT ($°C$, bottom right)

cations among simulated medicanes in top middle panel). Simulated tropopause heights at this time vary strongly. This is reflected in effects as strongly cooled(warmed) and decreased(increased) horizontal wind speed about 450 hPa (like in bottom left plot in figure 5.5.13). In simulations like f_{24}, f_0, simulated vortex is almost disappeared at this time (not shown). Tropopause is higher in those simulations that shown a vortex than in those that it is practically disappeared. Maximum tropopause height differences between simulations are about 150 hPa. However, in the simulations where the system is still simulated a weak structure is shown, and two differentiated patterns are separated at 40 km from the centre of the system (see top middle plot in figure 5.5.13). Keeping in main this description, effects will be only taking into account in middle and low levels.

Surface fluxes LHF and SSHF do not change their role in previous moments and they keep warming and moistening the low levels (not shown). Due to ULd the system is dried between 800-700 hPa (not shown). Due to SST low levels are warmed and moistened (top right panel in figure 5.5.13) meanwhile pressure is increased. According to the enlargement of the radius of the core, synergy between surface fluxes (e_{12}) increases and extends the same role at the mature state that it has at the centre of the storm (middle left plot in figure 5.5.13). LHF and ULd synergy (e_{13}) drys low levels and increase the horizontal wind at the centre of the storm (not shown). Synergy between SSHF and ULd e_{23} dries and diminishes horizontal wind speed at middle levels and the cyclonic rotation of the system (not shown). Effect e_{14} drys and cools low levels as such as diminishes up drafts at the base of the wall zone (middle middle plot in figure 5.5.13). As a result of the mutual interaction between SSHF and SST (e_{24}), low levels are strongly dried and cooled (middle right plot), and cloudiness in the wall zone is decreased. e_{34} dries low levels and characteristics of the wall such as wind speed, cloudiness and up drafts are diminished (not shown). Is notorious the vanishing role of the SST and its coupled interaction with surface fluxes at this phase. Must be said that this vanishing effect of the SST occurs in a region with the warmest SST (see figure 5.0.1), in contrast to previous studies (Emanuel, 1986; Rotunno and Emanuel, 1987; Homar et al., 2003b; Fita et al., 2007a) for which SST has an enhancing role. This is attributed to the vanishing phase of the storm. At this phase, low levels are almost saturated (see Q at 2m evolution in figure 5.5.8). Saturation of boundary layer has been described as a way from which dissipation of a hurricane might be done (Rotunno and Emanuel, 1987). Once boundary layer is saturated, heat and moisture transports capacity of the layer finishes and the storm loses its energy source. Thus, coupled interaction between a warmer SST and surface fluxes contributes to enhance moist into an almost saturated boundary layer favouring the dissipation of the storm.

Triple synergy e_{123} (bottom left plot in figure 5.5.13) plays an enhancing role deepening the system and enhancing the characteristics of the wall through an intensification of the wind speed, humidity and cloudiness in the zone in contradiction with the role in

previous section. It could be related to a diminishing of the saturation in the boundary layer allowing and enhance of its height (no clear ULd is shown at this position of all the storms). e_{124} cooled middle levels (bottom middle plot) but enforce the base of the wall increasing its humidity and up drafts from which more cloudiness is created (bottom middle). e_{134} moistened and cooled generally all the system (not shown) and decreased significantly the horizontal wind speed of the inner zone of the system (not shown). e_{234} moistens inner zone and cools low levels of the system. Moreover increases up drafts in the wall and also horizontal wind speed at high levels of the air-sea mechanism trajectories (bottom right plot in figure 5.5.13).

Comparison of results between point and 2-d effects

Previous to a comparison among azimuthal averaged effects and point effects some considerations should to be done. In the azimuthal averaged fields, 2-dimensional information is obtained, meanwhile the effects where obtained for an unique grid point at the centre of the storm. Due to 2-dimensional characteristics of the efectivities, simultaneous dissipating and enhancing role can be obtained, meanwhile point effects only give an unique behaviour at an individual grid point.

2-dimensional effects do not provide a clear baroclinic development at the beginning of the storm. Effects related to ULd do not have the strongest role in the baroclinic development role as it is reflected by point ones. Extratropical lows present a cold centre (Thorpe, 1986), but for example 2-dimensional e_3 and e_{23} warm the central part of the storm (see figure 5.5.10) promoting tropical-like warm core characteristics. e_{123} cyclolitc role is shown using both methodologies.

Cyclogenetic effects of the point effects on January 14th at 12 UTC such as e_{24}, e_{134} presented also an enhancing role as azimuthal averaged effects. In mature phase (January 16th at 00 UTC), point effects e_{124}, e_{24}, e_{134}, e_3 are revealed as cyclogenetic effects deepening centre of the storm, raising wind speed and relative vorticity at the centre of the storm. From vertical azimuthal averaged cross sections of the storm, effects show different enhancing/vanishing role: e_{124} shows an enhancing role in some aspects such as increasing vorticity at the centre or falling the pressure, but it cools and moistens the centre of the storm. e_{24} reduces the humidity on the theoretical trajectories (following constant angular momentum surfaces) of the particle of air. e_3 shows a vanishing effect due to the drying effect at middle levels, deepening at the same time the storm. Meanwhile e_{134} exhibited an enhancing role warming and moistening low-middle levels and decreasing the pressure of the system.

During the dissipating phase vanishing role of the synergies with the SST are obtained

with both methodologies. Punctual effects also change their role in later stages of the evolution.

Chapter 6

Assimilation of observational data in simulations

Articles on which this chapter is based:

L. Fita, R. Romero, A. Luque and C. Ramis, 2008: *Effects on numerical simulations of tropical-like Mediterranean storms of assimilating precipitation zones derived from satellite and lightning data*, Ann. Geophys., **submitted**

6.1 Effects of assimilating data in medicane simulations

Simulations of medicanes are an important challenge for the numerical models. These systems are usually small, short lasting in time and evolve above maritime areas. At the same time, maritime areas have sparse observations. Moreover, medicane formation and evolution is related to convective processes. There is a large variety of processes that trigger a convective process such as: mountain range, water source, upper level disturbance, shear, solar isolation. The lack of information of the real situation of the atmosphere could derive to a lost of a correct representation of the real conditions that will reproduce an incorrect simulation of the medicanes. Reed et al. (2001) show the sensitivity and beneficial effects on the numerical simulation when sea surface temperatures are corrected with observations. However, limited area mesoscale numerical models have shown a reasonable ability in simulating these storms (Lagouvardos et al., 1999; Pytharoulis et al., 2000; Reed et al., 2001; Homar et al., 2003b), in spite of the limited observational data given their maritime origin.

The modification of numerical simulations using observations from different sources has been shown as a successful way to improve the results (Stauffer and Seaman, 1990; Leslie et al., 1998; Zou and Xiao, 1999; Fan and Tilley, 2002; Ducrocq et al., 2002; Davolio and Buzzi, 2004; Orlandi et al., 2004; Lagouvardos and Kotroni, 2005). MM5 model (Grell et al., 1995) uses a four-dimensional data assimilation (FDDA) tool based on a Newtonian-relaxation or nudging (Stauffer and Seaman, 1990) applied on the prognostic equations.

A possible method for the improvement of medicane simulations is proposed using satellite derived information. Satellite-derived precipitation type (stratiform or convective) is used to modify humidity vertical profiles through FDDA in MM5 simulations. Lightning activity is used to mark convective points. The technique is applied in the simulation of the September 1996 case (studied by Homar et al. (2003b), see figure 5.1.4) and October 2003 (studied in Fita et al. (2007a), see figure 5.1.7).

6.1.1 Methodology

MM5 version 3.7 mesoscale model has been used to simulate these two cases. Two domains in two way interaction with a horizontal resolution of 15 and 5 km with 23 vertical levels have been defined. The domains have different dimensions and are centred at different points for each case. Initial and boundary conditions are derived from the European Center for Medium-range Weather Forecasts (ECMWF) global analyses (at 00, 06, 12, and 18 UTC). Analyses have been improved with Binary Universal Form for data Representation (BUFR) observations archived at ECMWF (in FM-94 BUFR format, see WMO

(2007)). Main MM5 physical configuration is graupel(reisner2) (Reisner et al., 1998) for moist microphysical scheme, Kain-Fritsch (Kain and Fritsch, 1993; Kain, 2004) cumulus scheme activated only in the coarse domain (5 km resolution is assumed to be high enough to resolve cumulus), and cloud scheme for radiation (Grell et al., 1995).

Three different planetary boundary layer (hereafter, PBL) schemes are used in this study in order to test the sensitivity of medicane simulations to the election of the PBL scheme. These PBL schemes are referred to as Blackadar, ETA and MRF (Grell et al., 1995). Blackadar scheme (Blackadar, 1979) computes PBL characteristics following bulk Richardson number. It does not use a Turbulent Kinetic Energy (TKE) equation and turbulent mixing is computed following an implicit vertical diffusion scheme. Eta scheme (Janjić, 1990, 1994) is 2.5 dimensional and it uses TKE with a local mixing dynamics. MRF scheme (Troen and Mahrt, 1986; Hong and Pan, 1996) which is an improvement of the Blackadar PBL scheme for higher horizontal resolutions.

Hong and Pan (1996) found that heavy rainfall events are better forecasted with MRF approximations than with a local PBL scheme (used in ETA model), due to a better representation of a well formed unstable PBL. Wisse and de Arellano (2004) show that MRF scheme produces a weaker PBL inversion with stronger vertical fluxes than ETA scheme. By this way heavier precipitation was obtained as a result of stronger transport of moist and heat to the free atmosphere. ETA scheme produces a lower vertical transport and helps to maintain a stronger inversion, as a result of it, higher values of CAPE are forecasted. Consequently ETA presents more extreme precipitation rates. These differences between vertical transports parametrised with different schemes were found more significant over maritime areas than over land (Wisse and de Arellano, 2004). Hurricane-like characteristics of the medicanes suggest that they should present a notable sensitivity to the strength of low-level transport of heat and moisture.

Satellite data from European Organisation for the Exploitation of Meteorological Satellites (EUMETSAT) and lightning datasets provided by Instituto Nacional de Meteorología (INM, Spanish Met. Office) show a deep convection (observed as cold cloud top pixels) and lightning activity during the formation phase of both storms (Luque et al., 2007). During their mature state, number of cold cloud top pixels decreased, as well as lightning activity (mostly located at these stages in warm cloud top pixels; see figures 6.1.1 and 6.1.2).

Infrared (11 μm) satellite images are used to depict stratiform or convective precipitation type. Lightning discharges are used to assist in the delineation of convective areas, assuming that all lightning activity is developed within convective cells. Once the precipitation type is obtained for each pixel, MM5 humidity vertical profile is modified according to two different vertical structures including a layer of saturated air (stratiform

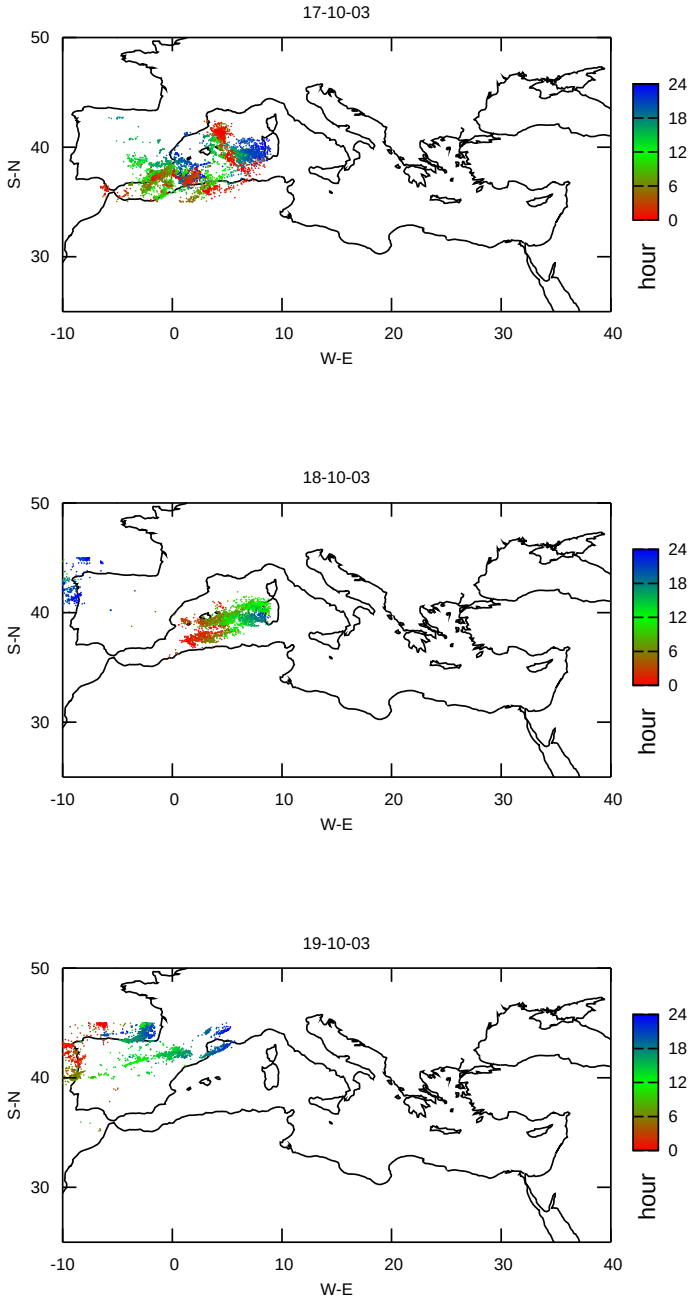

Figure 6.1.1: Lightning activity for the October 2003 case. During October 17th 2003 (top), Oct. 18th (middle) and 19th (bottom). Discharges are indicated as a point coloured according to the hour of hit (see color box). Source INM lightning detection net

or convective structure).

The Histogram Matching Technique (HMT) is used to derive rain characteristics (intensity of precipitation for a given cloud top infrared temperature value) from the satellite images (Turk et al., 2000; Kidd et al., 2003). HMT rainfall estimation curve is obtained by combining a set of simultaneous Meteosat infrared images with passive-microwave rainfall images (SSMI and AMSR sensors). In order to identify convective areas a cross-correlation methodology is applied for the tracking of cold cloud top pixels (cloud top Infrared-channel temperature lower than 239 K). Cloud pixels are tracked applying a cross-correlation method in 19 by 19 grid zones before the cloud pixel temperature change with time is calculated. Rainy points that are cooling in time are marked as convective according to the work of (Roberts and Rutledge, 2003), while the other rainy pixels are marked as stratiform. Lightning discharges (see evolution during October 2003 case in figure 6.1.1) are used to mark as convective pixels a 3x3 pixels zone centred at the discharge point even if these are outside the satellite convective area (see stratiform/convective distribution at two moments of the October 2003 episode in figure 6.1.2). Bear in mind that in the FDDA only the precipitation type will be used irrespectively of the amounts.

Following Davolio and Buzzi (2004) the humidity adjustment in the model is done following certain vertical structures associated with stratiform or convective precipitation types (see figure 6.1.3, and equation 6.1.3). By this way, it is ensured a relaxation (by factor $\mathcal{R}(\sigma)$) of the model grid point mixing ratio value ($\mathcal{Q}_m(i,j,k)$) to mid or low-level saturating mixing ratio ($\mathcal{Q}_s(i,j,k)$) consistent with the forcing, respectively, of stratiform or convective precipitation. The new humidity profiles are introduced in the simulations via analysis and observational nudging as implemented in the FDDA package of the MM5 model.

However, MM5 humidity field is expressed in terms of mixing ratio. Humidity profiles want to be saturated in some vertical levels according to a specific kind of precipitation. For that reason a computation of the saturated mixing ratio value at each grid point should be done with the model pressure and temperature values at that point (see equation 6.1.2).

$$e_s = 6.22 exp\left(\frac{17.67T}{T+243.5}\right) \tag{6.1.1}$$

$$\mathcal{Q}_s = 0.662\frac{e_s}{p-e_s} \tag{6.1.2}$$

e_s, saturated vapour pressure is given in Bolton's form (equation 6.1.1). T model temperature; p, model pressure, $\mathcal{Q}_s$ satured mixing ratio .

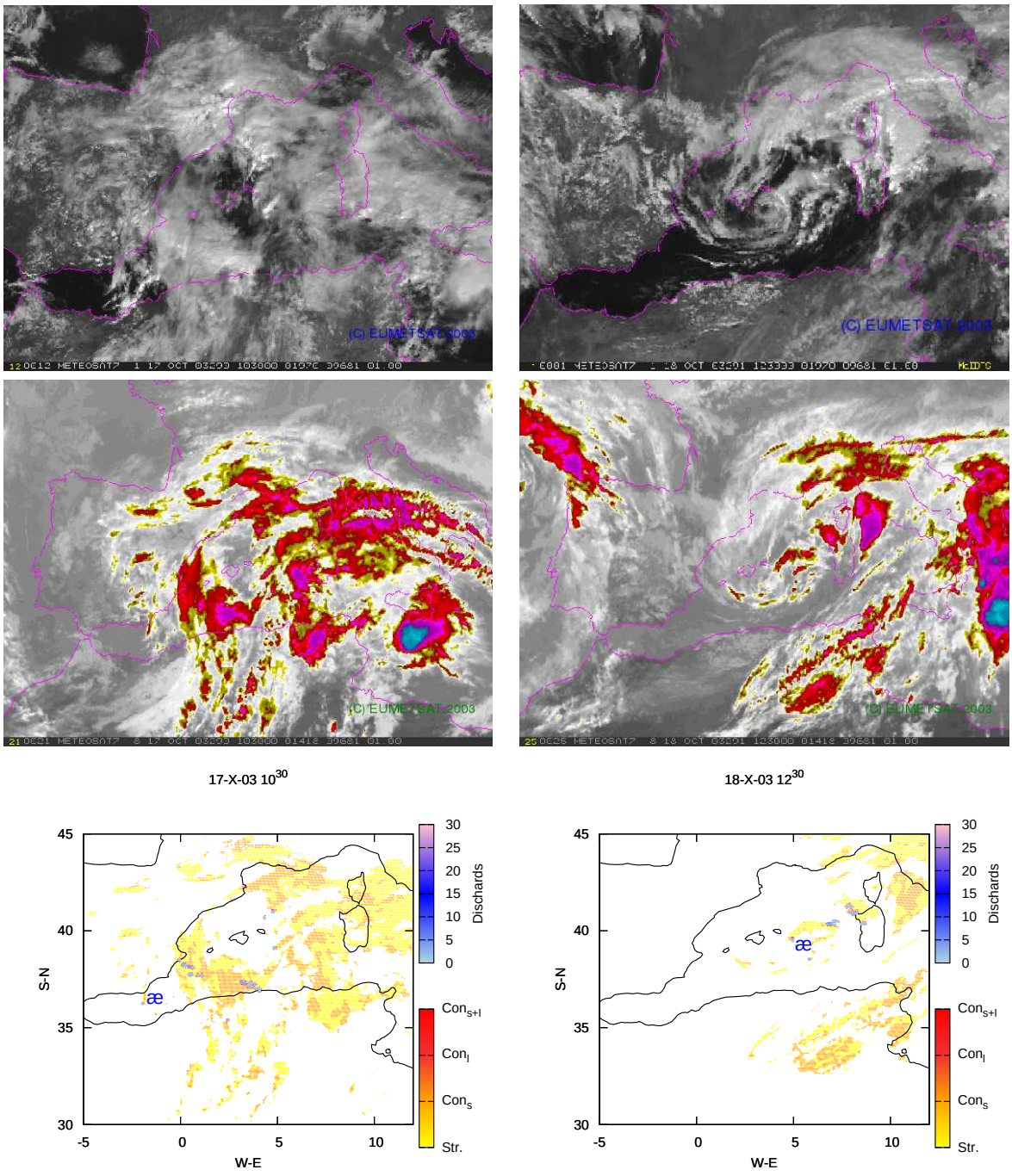

Figure 6.1.2: Visible channel (top) and coloured infrared (11 μm, bottom) images from METEOSAT-7 (Source EUMETSAT). Bottom panels: Stratiform (yellow colours), convective (orange-red colours; Con_s, satellite convective; Con_l, lightning convective; Con_{s+l}, satellite and lightning convective;) and number of discharges (blue dots). Blue æ indicates medicane position Left panels: on October 17th 2003 at 10^{30} UTC (left). Right panels: on October 18th at 12^{30} (maximum intensity)

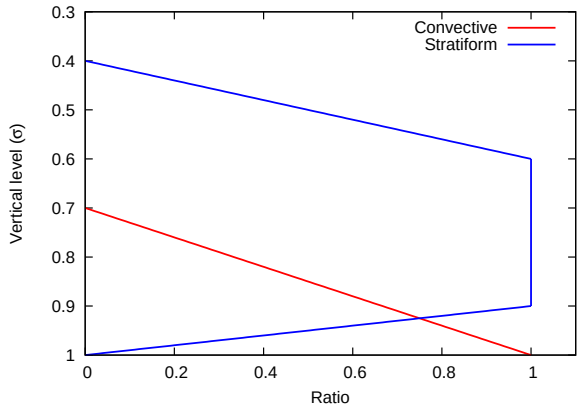

Figure 6.1.3: Vertical profile of factor $\mathcal{R}(\sigma)$ (used in equation 6.1.3) for the correction of the humidity profile in the convective precipitation (red) and stratiform (blue) precipitation areas.

$$\mathcal{Q}'(i,j,k) = \mathcal{Q}_m(i,j,k) + \mathcal{R}(\sigma)\left[\mathcal{Q}_s(i,j,k) - \mathcal{Q}_m(i,j,k)\right] \tag{6.1.3}$$

Nudging is only applied in the high resolution inner domain with a weight of 10×10^{-4} and a time window of 6 minutes from the time of the observation (full influence ± 3 minutes, linear decay ± 6 min further). Weight computation of nudging term is done every 2 model time-steps with a vertical influence of the observation between levels of 0.001 (Cressman-type).

Eight experiments are performed for each medicane case (see table 6.1.a). A control simulation (without humidity modification $\emptyset$ values). Two modifications of the MM5 simulations are done without FDDA technique, in which initial and boundary conditions for the humidity fields (i. e. analyses from ECMWF) are directly modified with the satellite derived information. First experiment applies the modifications only to the initial condition (REGRIDmod experiment). In the second experiment the procedure is carried out at each analysis time (00, 06, 12 and 18 UTC, REGRIDmod TOT experiment).

MM5 FDDA technique can be applied as analyses nudging. In this case, analyses grid point values drive tendencies of the model. Analysis nudging is done with the non-modified version of the analyses (FDDA AN exp.), and with analyses in which humidity vertical profile has been modified with satellite-based information (FDDA rhAN exp.).

Table 6.1.a: Complete set of experiments for the September 1996 case (left) and October 2003 case (right). $\Delta\vec{r}$ indicates horizontal resolution (km) of the satellite-derived information used. Δt indicates the frequency (hours) of assimilation into the simulations of the satellite-derived information. $\emptyset$ indicates no data assimilation. $\forall$, indicates maximum available resolution. t_0, indicates simulation start time

simulation	**960912**		**031018**	
	$\Delta\vec{r}$ (km)	Δt (h)	$\Delta\vec{r}$ (km)	Δt (h)
control	$\emptyset$	$\emptyset$	$\emptyset$	$\emptyset$
REGRIDmod	$\forall$	t_0	$\forall$	t_0
REGRIDmod TOT	$\forall$	6	$\forall$	6
FDDA AN	$\forall$	6	$\forall$	6
FDDA rhAN	$\forall$	6	$\forall$	6
OBS TOT	15	$\forall$	22.5	$\forall$
OBS 1h	3	1	15	1
OBS 3h	3	3	7	3

Satellite information is obtained every 30 minutes (i.e. operational frequency of METEOSAT-5 and METEOSAT-7 geostationary satellites) with a horizontal resolution about 5 km in the study zone. Modifications of vertical humidity profiles are done in the lowest 12 sigma-levels. Computational memory limitations do not allow to use together the maximum temporal and spatial resolution of the satellite information. Thus an observational nudging with full temporal resolution and reduced horizontal resolution (OBS TOT exp.) has been performed. Two additional experiments have been performed with the highest horizontal resolution that computational resources allow under a satellite information update frequency of 1h and 3h (OBS 1h and OBS 3h experiments). Table 6.1.a shows the specific configuration of each experiment. Figure 6.1.4 shows the resultant data included at the first time step of the October 2003 simulations according to each resolution.

The above experiments will be compared with respect to the control one with regard to the characteristics of the simulated medicanes and in terms of several meteograms. These meteograms are located at the genesis and evolution areas of each medicane and are drawn for different variables such as precipitable water, sensible surface heat flux, surface latent heat flux and convective available potential energy (CAPE).

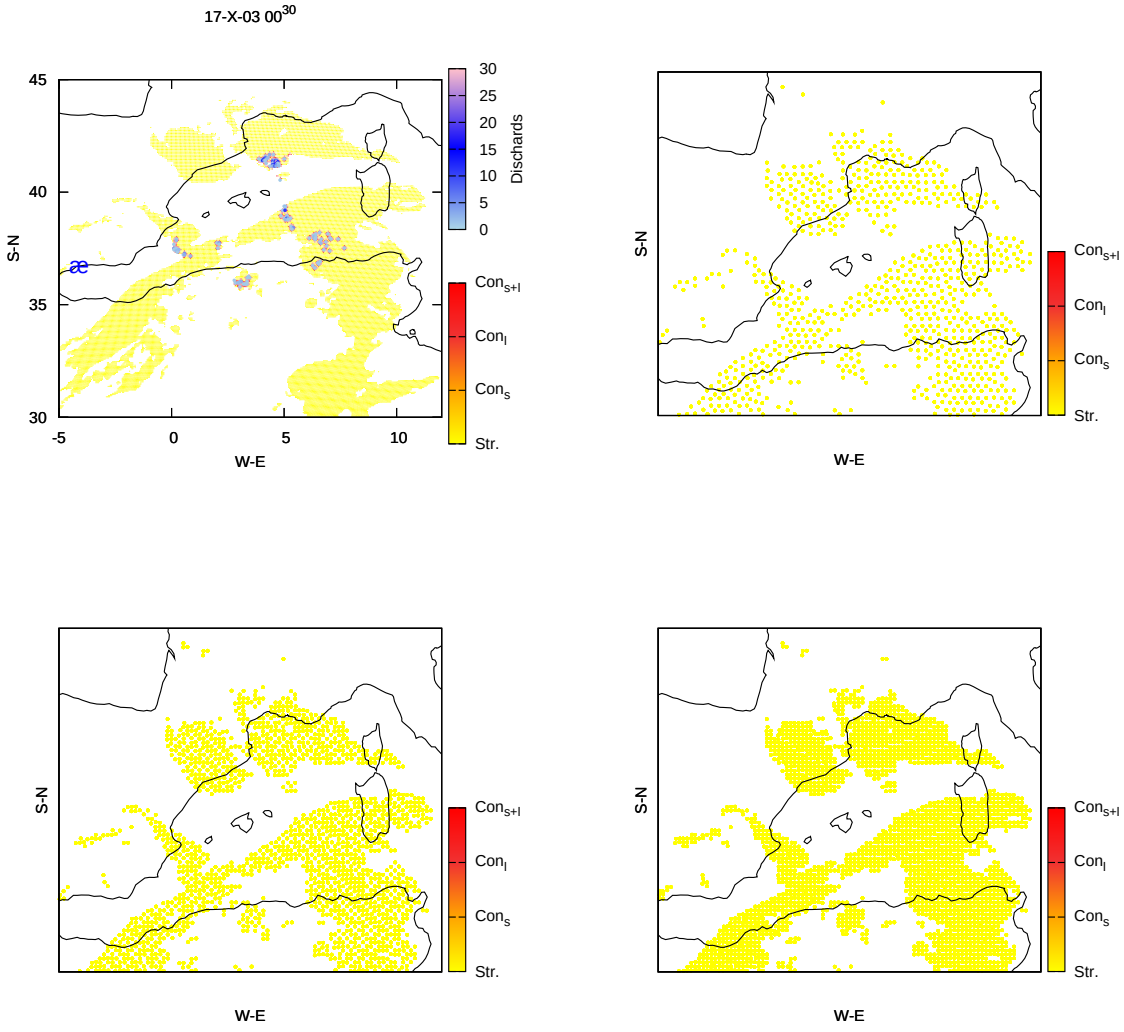

Figure 6.1.4: Rainy type of information that will be nudged (Domain 1 grid) on October 17th 2003 at 00^{00}. Original satellite-based information (top left, satellite grid), OBS TOT experiment (top right), OBS 1h 15k exp. (bottom left) and OBS 3h 7k exp. (bottom right). æ indicates position of medicane. Satellite information is from October 17th 2003 at 00^{30}, since no satellite image was available at starting simulation time

6.1.2 Results

Control simulations of the two cases with the three different PBL schemes show formation of the system but a poor agreement between simulated and observed trajectories (see figure 6.1.5). Both medicanes are formed under the western sector of an upper level trough (see figure 5.1.4 and 5.1.7 for the September 1996 and November 2003 cases respectively) characteristic of the baroclinic growing of disturbances (Hoskins et al., 1985). However, these two medicanes do not evolve closely related with the upper level disturbances since their trajectories differ with respect to the trajectory of the maximum vorticity centre of the upper level trough (see figure 6.1.6). Evolution of both medicanes is dominated by an upper level trough, but their trajectory is somewhat independent from the movement of the upper-level disturbance (at least of its vorticity maximum). It is also observed that in general, there is not a clear correspondence between low pressure values at the centre of the collection of the different simulated medicanes and maximum horizontal wind speeds (see figure 6.1.5).

Upper level disturbance exhibits sensitivity to the used PBL scheme (see figure 6.1.7). These differences between the evolutions of the upper level trough centre obtained with the three PBL schemes grow gradually in time. Changes on the characteristics of the low level peculiarities induced by the PBL processes influence the upper/low level baroclinic interaction, affecting the growing of the low level disturbance (e.g. sensible surface heat flux effect on Horvath et al. (2006)) and the diabatic behaviour of the upper level trough. Changes on the diabatic evolution of the upper level trough are also as consequence of changes on moisture content of the column of air as a reflect of different efficiencies on vertical transport from low levels induced by each pbl scheme. Less moisture content would weak convection and diabatic heating of middle levels due to latent heat release by cloud formation.

Meteograms at different locations along the medicanes path (see figures 6.1.8 and 6.1.9) show a variety of sensitivities to the selection of the PBL scheme (similar behaviour is observed for the meteograms at other points, not shown). Increase of the surface fluxes and precipitable water is a signature of the hurricane characteristics of the medicane (Emanuel, 1986). Accumulated potential energy would be used in the intensification of the system throughout convection, reflected as a decrease of CAPE values after the incoming of the medicane in the area. The strong surface winds increase surface fluxes and thus water vapour content in the lower troposphere from which cloud formation will be reinforced. Meteograms at other model grid points corresponding to later phases of the evolution of the medicanes show a similar behaviour (not shown).

Experiments involving assimilation of satellite and lightning activity information into the simulations (see table 6.1.a) produce significant modifications on the forecasts (see

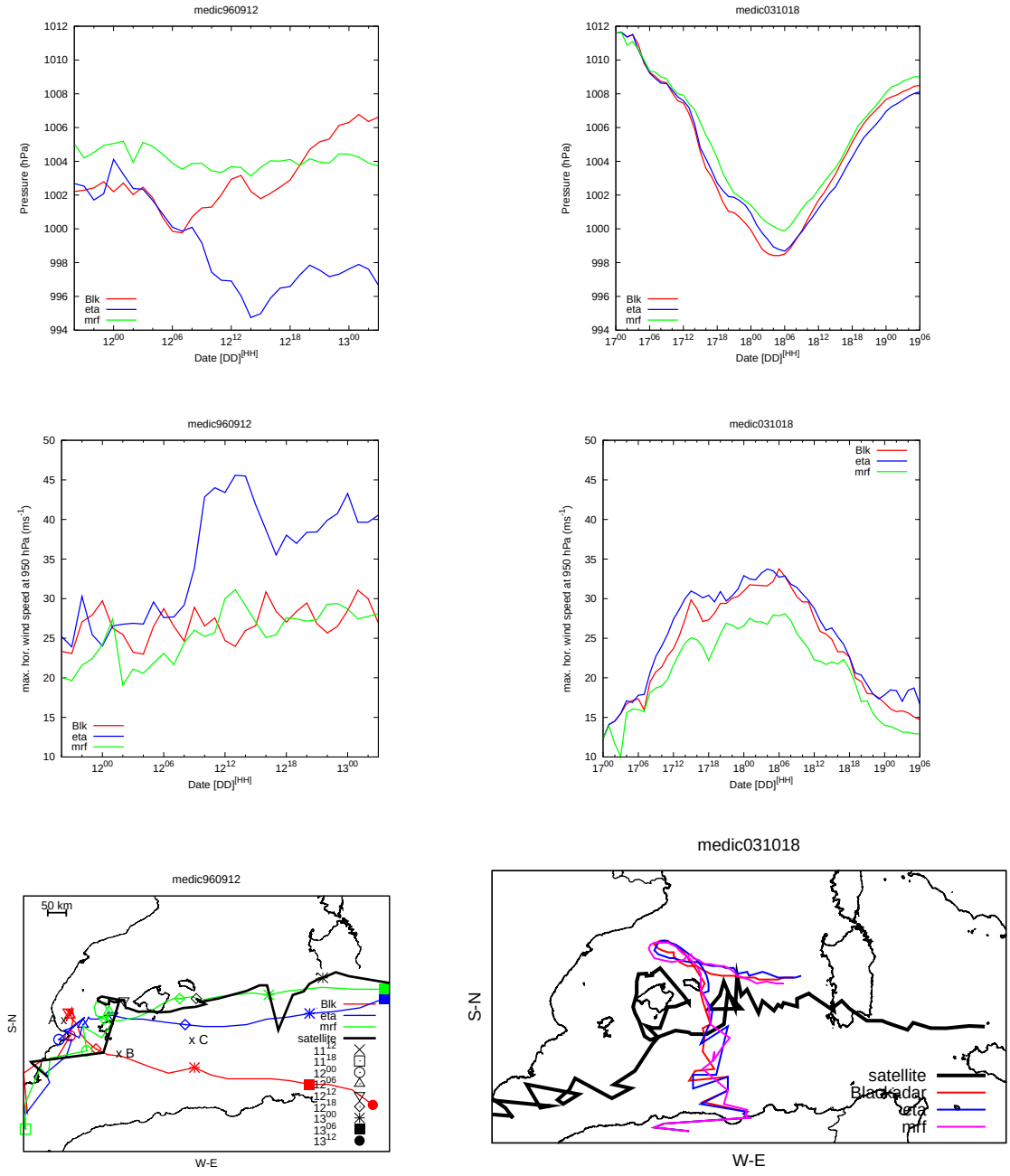

Figure 6.1.5: MM5 control simulation results with three different PBL schemes, Blackadar (red), eta (blue) and MRF (green). Evolution of the central pressure (hPa, top), maximum horizontal wind speed at 950 hPa (ms^{-1}, middle) and medicane trajectory (bottom, symbols along trajectories indicate simulation, time, see legend in graphs) compared with the satellite-based trajectory (thick black line). September 1996 case (left), October 2003 (right). A,B,C points indicate where meteograms have been obtained

figures 6.1.10 to 6.1.13). Simulated medicanes are deeper in almost all cases. According to the upper level influences previously discussed, trajectories of medicanes have changed significantly due to changes on the evolution of the upper level trough and changes in the medicane zone genesis that affected the relation between upper and low-level disturbances in the simulations (see figure 6.1.14). Regarding trajectories, these are generally worse for September 1996 case and better for October 2003 medicane, compared to the control ones.

Taylor diagrams (Taylor, 2001) of the simulated trajectories taking as reference the satellite-derived trajectory (with more than 30 values used in the statistics) are plotted (without overall bias correction) in figure 6.1.15. Taylor diagrams show higher sensitivity to the FDDA methods for the standard deviation than for the correlation. That means that the trajectories suffer a higher change in its morphology and zone of evolution than in their temporal sincrony with respect to the observed one. No smoothing of refilling techniques have been applied on the satellite-observed trajectories of the medicanes.

Experiments 'FDDA rhAN', 'OBS TOT', 'OBS 1h' and 'OBS 3h' imply a direct impact of the satellite/lightning information into the simulations. Only in these 4 experiments changes in the vertical humidity profiles are introduced at specific grid points and time steps, thus directly affecting the humidity tendency term in the model equations. In order to analyse the effect of data assimilation into the simulations, meteograms for these 4 experiments at one particular model grid point are drawn in figures 6.1.16 and 6.1.17.

Simulation results do not exhibit a significant improvement of the trajectories of the medicanes. In order to provide an objective way to compare simulated and satellite-derived trajectories and as an attempt to simplify the large amount of information, some statistical parameters are proposed (appendix A).

Simulated medicanes show slower translational speeds than the satellite observed ones (see control simulation results in figure 6.1.5). A new method to evaluate the temporal shift of two trajectories is here put in practice. The temporal shift between satellite-observed and simulated trajectories of the medicanes is objectively studied by means of the temporal dependence of bias and correlations (see $\mathcal{BIAS}^{min}_{dist}$ and PR^{max}_{bias} definitions in equations A.1.2 and A.3.15, respectively, of the appendix A). These statistical indices are iteratively recomputed using simulated trajectories that are positively or negatively displaced in time (e.g. an advanced trajectory is obtained when a simulated position at time t, $\vec{x}^t$, is changed to the position at time $t + n\Delta t$). Temporal shift between trajectories will correspond with that shift $n\Delta t$ ($\Delta t = 1$ hour) that minimises bias and maximises correlation scores. BIAS informs about the spatial proximity of the simulated and satellite-observed trajectories. Correlation is focused on the similarity between the morphologies of trajectories.

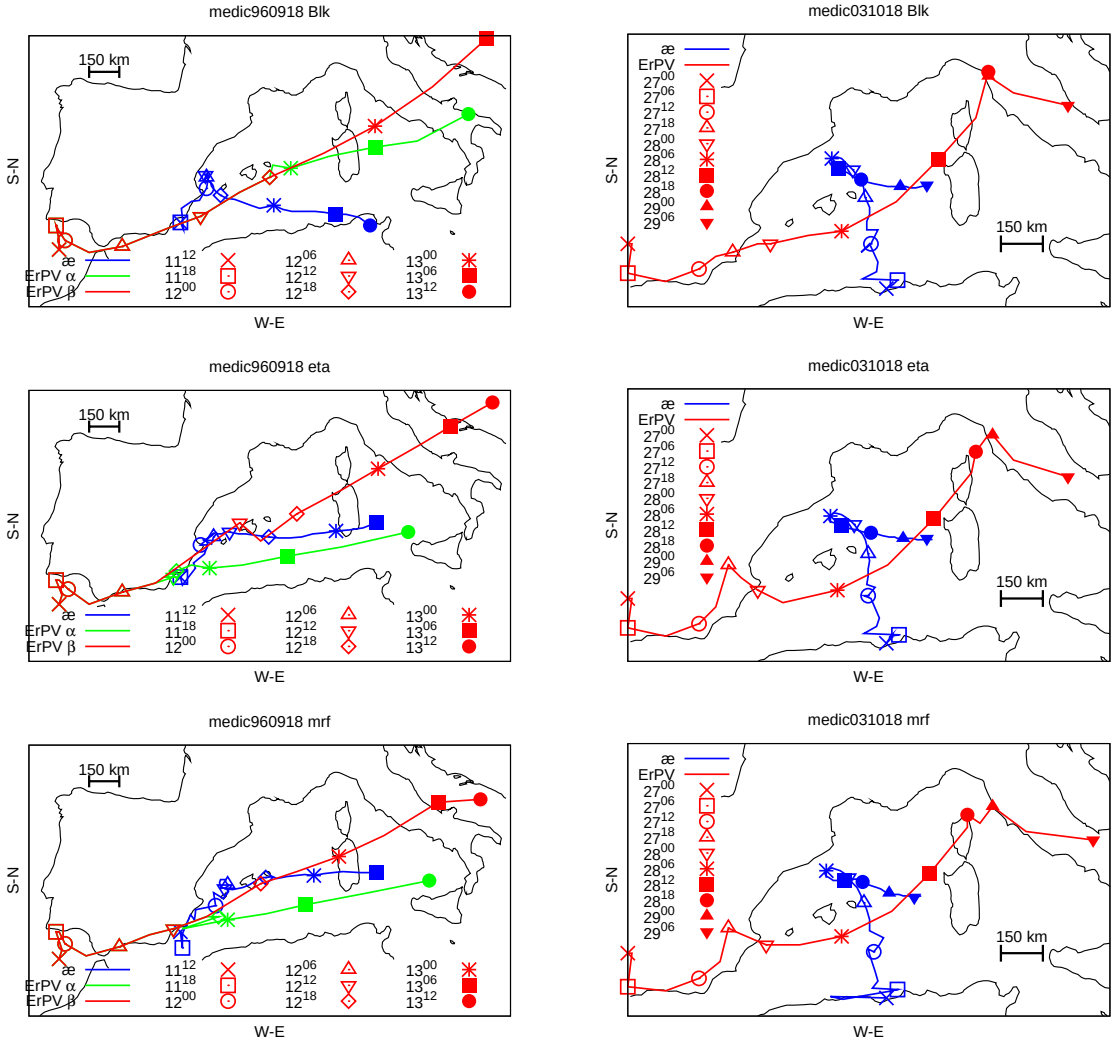

Figure 6.1.6: Evolution of Ertel PV maxima on the 330 K isentropic surface (red) related to the evolution of September 1996 (left) and October 2003 (right) medicane (blue) at different time steps (see legend). Simulations using Blackadar PBL scheme (top), ETA (middle) and MRF (bottom). In September 1996 simulation appear two maximals, α (green line), and β (red line)

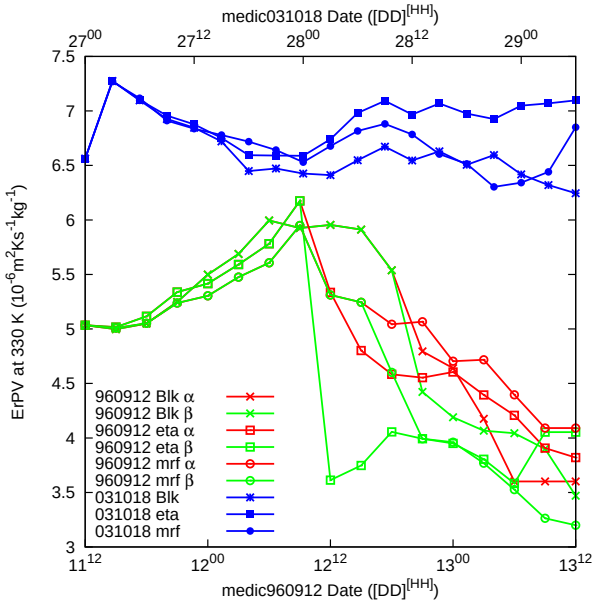

Figure 6.1.7: Temporal evolution of Ertel PV maxima on 330 K isentropic surface related to the evolution of medicanes 960912 (red) and 031018 (blue), for each PBL scheme: Blackadar (cross), ETA (square) and MRF (circle). Date/Time indicated at bottom axis for September 1996, and at top axis for October 2003 medicane. In September 1996 simulation appear two maximals, α (green line), and β (red line)

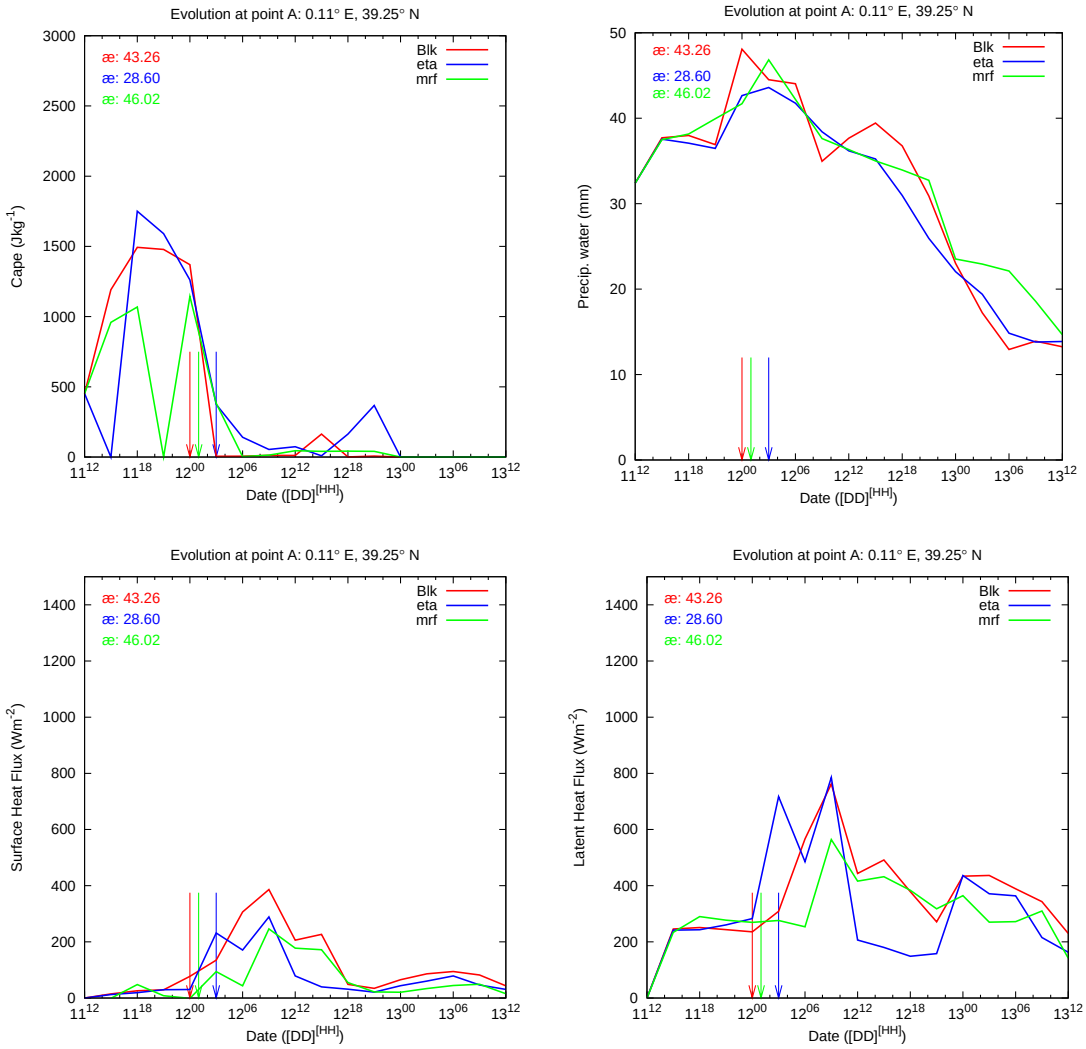

Figure 6.1.8: meteograms at point A (see left bottom panel of figure 6.1.5) for the simulation of September 1996 medicane, showing CAPE (Jkg^{-1}, top left), Precipitable water (mm, top right), surface sensible heat flux (Wm^{-2}, bottom left) and surface latent heat flux (Wm^{-2}, bottom right). Results obtained with each PBL scheme are included: Blackadar (red), ETA (blue) and MRF (green). Vertical arrows indicated the time at which the medicane simulated with each scheme passes closeliest to the point. Distances (km) of the medicane centre 'æ' to the point are indicated at the top left corner of the graphs

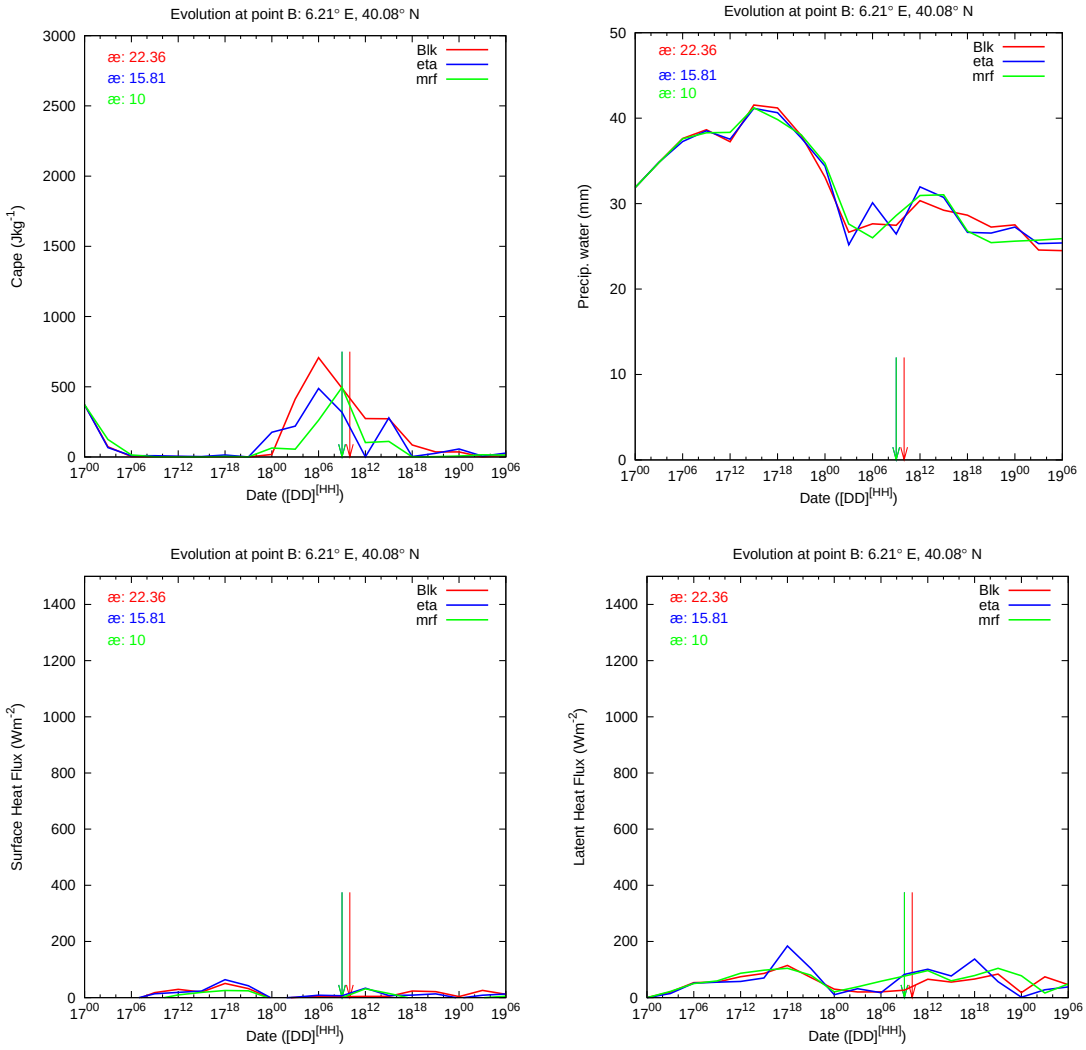

Figure 6.1.9: As in figure 6.1.8 but for the October 2003 medicane at point B (see bottom right panel of figure 6.1.5). ETA and MRF simulated medicanes arrows are superimposed since both medicanes reached the point B (right bottom panel of figure 6.1.5) at the same time, on 18th at 9 UTC

Simulated trajectories by the whole set of experiments have similar bias with respect to the satellite-based trajectory (see figure 6.1.18 as an example). It is shown how the satellite-derived information has mainly influenced the localisation in time of the medicane but it has basically left the morphology of the trajectories unchanged.

Similar dependence of $\mathcal{BIAS}_{dist}^{min}$ on temporal shift is obtained in each medicane for the group of experiments and PBL schemes (see figure 6.1.19).

Fort both cases, lowest correlation values are obtained for those simulations in which observational nudging has been applied, the best results being obtained with the 'FDDA AN' experiment. In general, larger similarity between simulated and observed trajectories are obtained in those simulations where observational nudging has not been applied (see figure 6.1.20).

For both studied medicanes, simulations with MRF scheme produce stronger systems than with Blackadar scheme. No significant differences between the nonlocal mixing schemes (Blackadar and MRF) on the evolution of the pressure at the centre, maximum wind speeds and the trajectory for each experiment are observed.

The larger differences with respect to the characteristics of simulated medicanes and meteograms among the simulations using the ETA model might be related to its local mixing characteristics. Satellite-derived information modifies vertical profiles of humidity at low levels (convective rain points) and middle levels (stratiform rain points). Blackadar and MRF PBL schemes produce a stronger vertical transport and more mixing at low levels than ETA scheme. Thus changes due to data assimilation might be weakened using the first two schemes (middle column panels in figure 6.1.17 show larger variations with respect to control ones).

September 1996

September 1996 medicane shows the strongest sensitivity on changes of the PBL scheme. In this case, last steps of the trajectory with Blackadar scheme show differences with the trajectories obtained with the other two schemes larger than 300 km. September 1996 medicane simulated with the Blackadar PBL scheme is deeper than the simulated with MRF scheme (maximum difference is about 4 hPa, see top and middle panels in figure 6.1.5) and maximum horizontal wind speeds for each simulated medicane differ also significantly (maximum differences about 10 ms^{-1}). Moreover, the deepest and strongest medicane is obtained when ETA scheme is used.

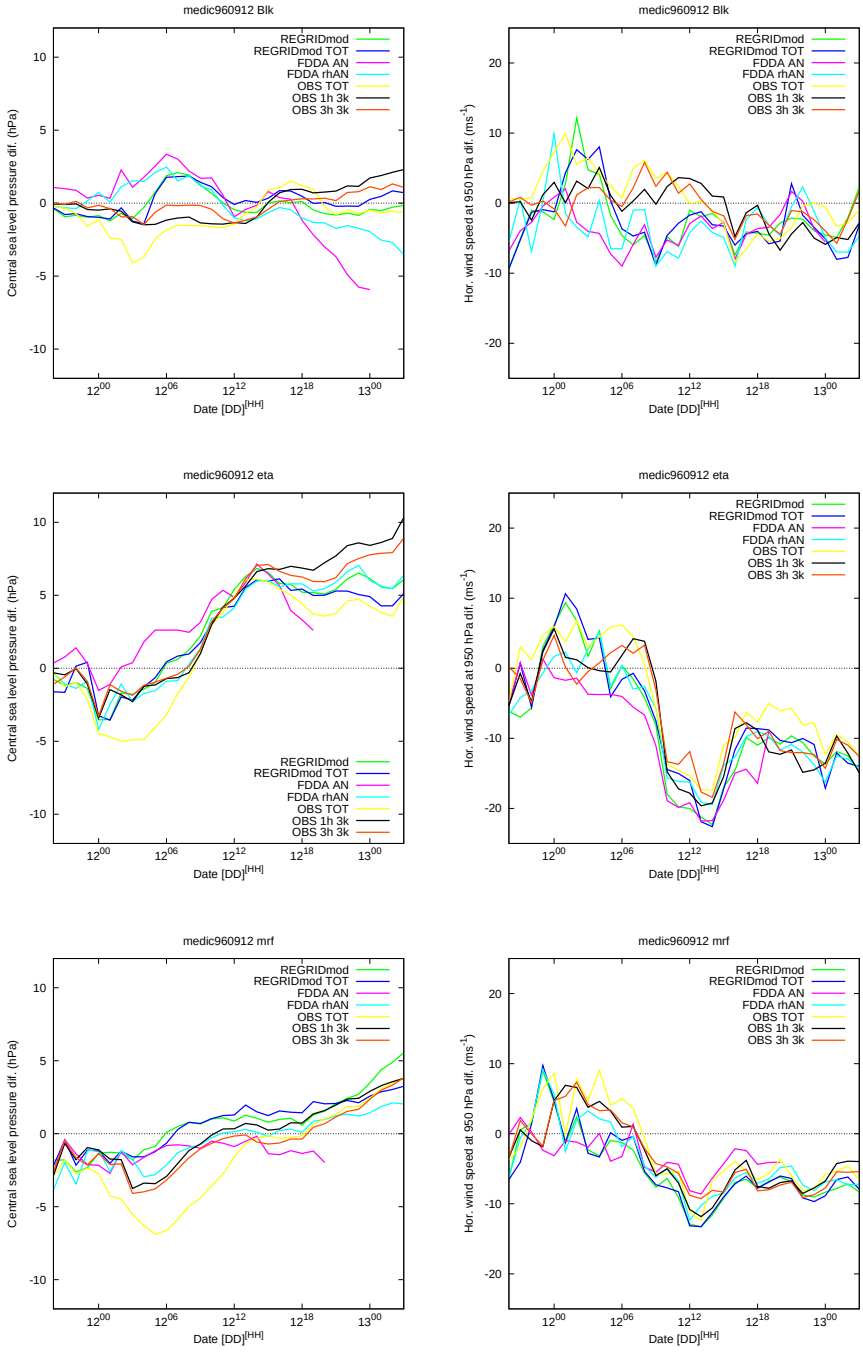

Figure 6.1.10: September 1996 medicane simulations. Left column: Central sea level pressure (hPa) referred to control value ($\mathcal{P}res_{sim} - \mathcal{P}res_{control}$). Middle column: Maximum horizontal wind speed (ms^{-1}) at 950 hPa within a radii of 200 km from the centre of the storm, referred to control value. Results are shown for the set of experiments with Blackadar PBL scheme (top), ETA (middle) and MRF (bottom). Lines colours are: Control simulation (red), REGRID mod (green), REGRID mod TOT (blue), FDDA AN (pink), FDDA rhAN (light blue), OBS TOT (yellow), OBS 1h 3k (black) and OBS 3h 3k (orange)

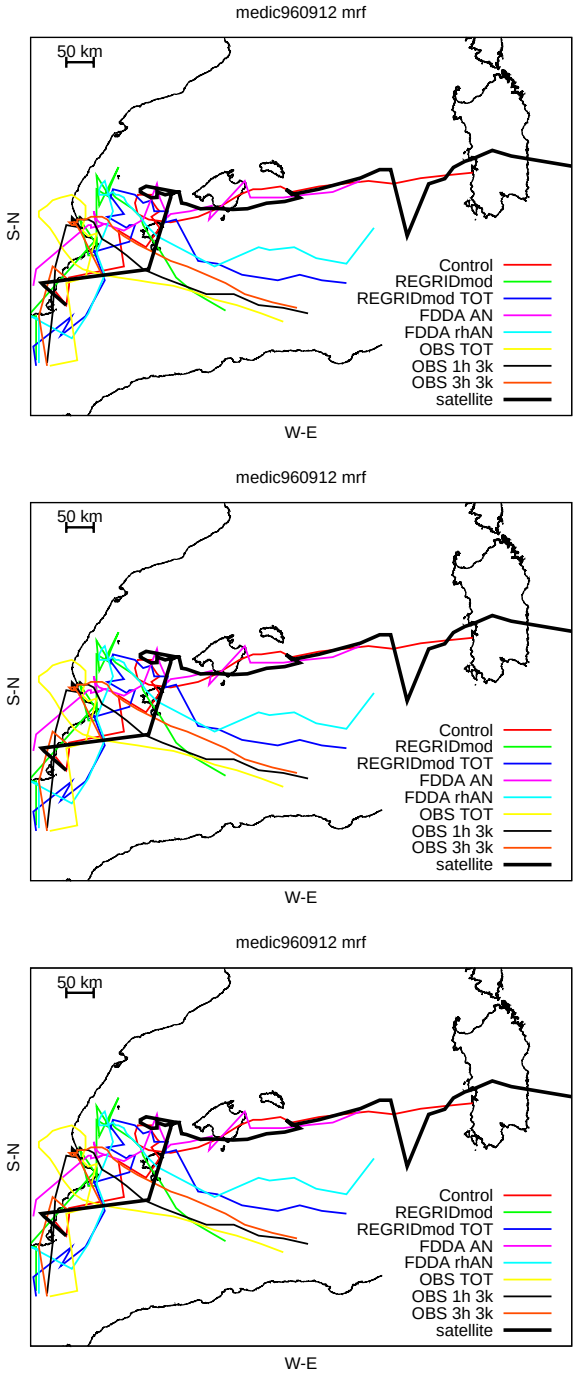

Figure 6.1.11: September 1996 medicane simulations. Trajectories of simulated medicanes. Results are shown for the set of experiments with Blackadar PBL scheme (top), ETA (middle) and MRF (bottom). Colour codification of the dots for each simulation is the same as in figure 6.1.10

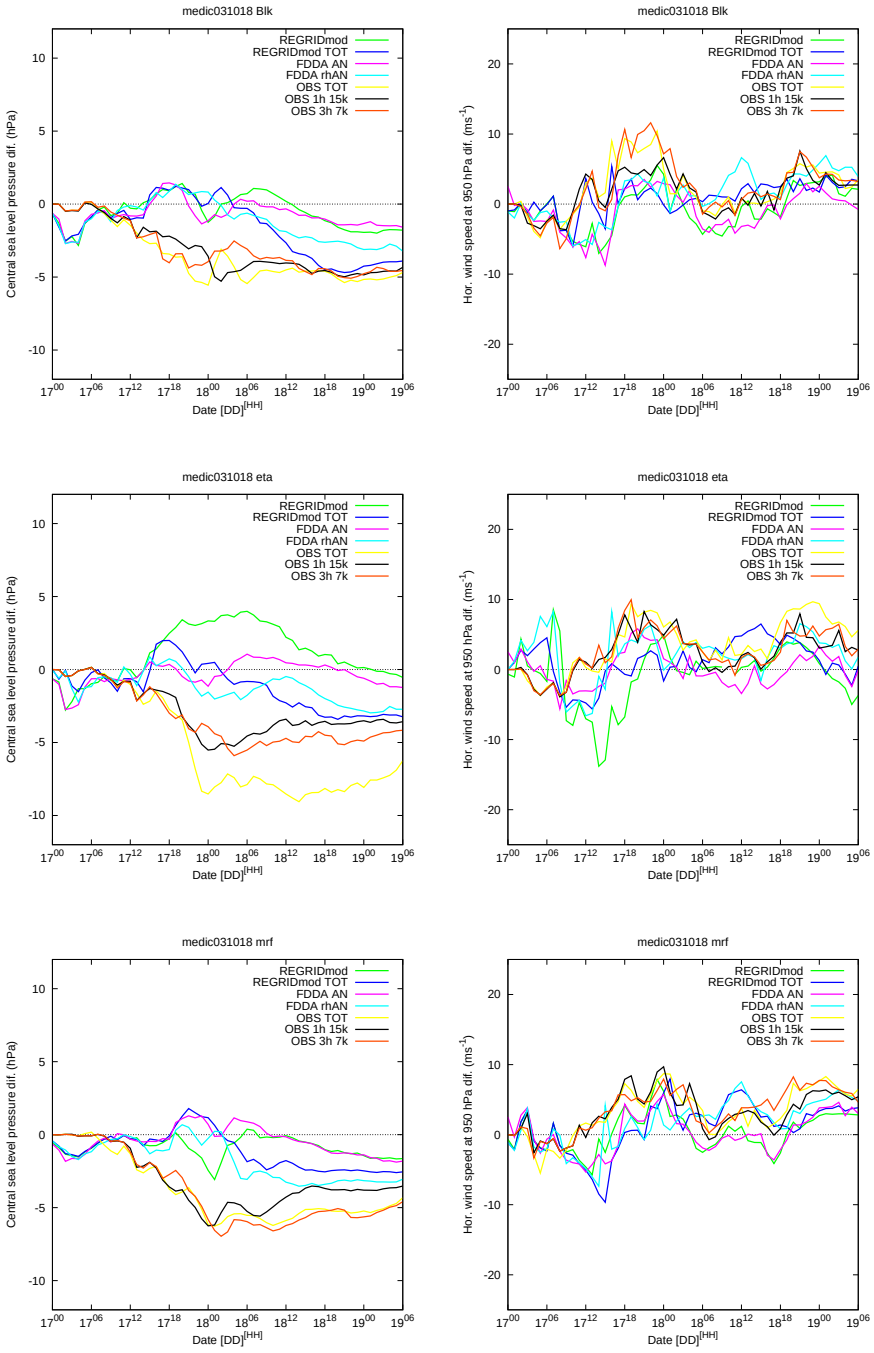

Figure 6.1.12: As in figure 6.1.10, but for the October 2003 case

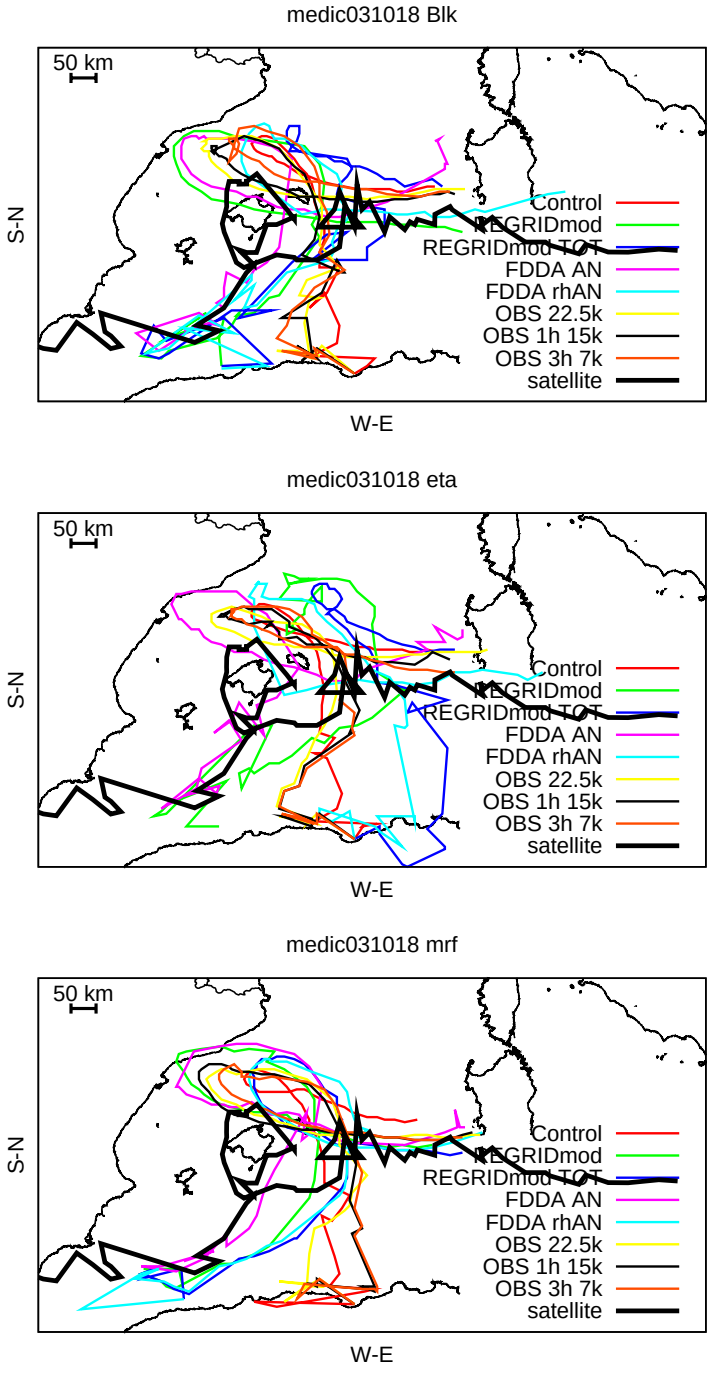

Figure 6.1.13: As in figure 6.1.11, but for the October 2003 case

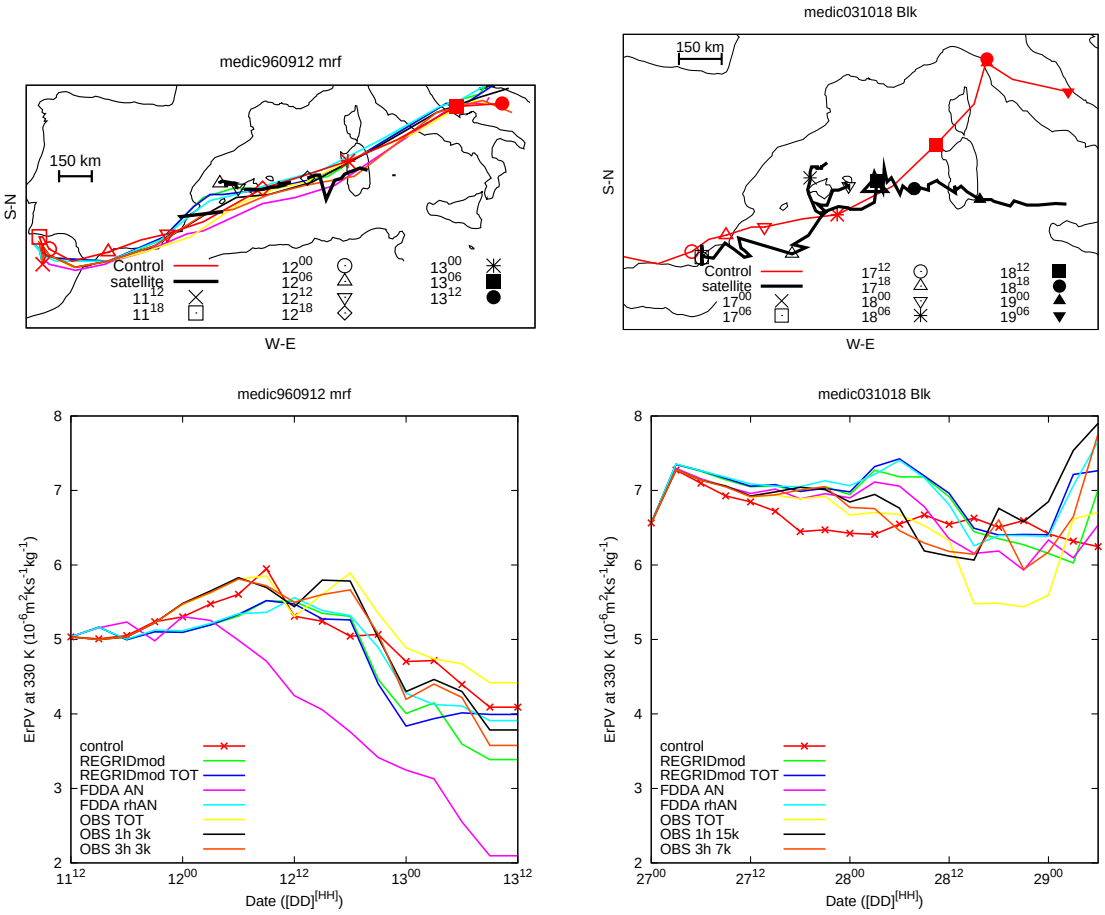

Figure 6.1.14: Top panels: Trajectories of the maximum Ertel PV closest with the medicane trajectory for each simulation. Satellite-based trajectory (thick solid line). Bottom panels: Temporal evolution of value maximum Ertel PV. For the September 1996 case with the MRF PBL scheme (left), for the October 2003 case with the Blackadar PBL scheme (right)

Evolution of September 1996 case (see left panels in figure 6.1.6) seems to exhibit a momentaneous strong relation with the upper level disturbance. The medicane is formed off the Eastern coast of the Iberian Peninsula. It grow in this region and starts to move eastwards at the same time that the centre of the trough enters over the zone (between Iberian peninsula and Balearic Islands). Associated flow to the upper level disturbance seems to drag the medicane from its genesis zone (see figure 6.1.6). The southernmost evolution of the upper level trough with Blackadar PBL scheme could explain the lower-latitude trajectory of the simulated medicane. Lower values of central pressure in ETA simulated medicane (see figure 6.1.5) could be explained by the strong overlap of the centre of the trough and the medicane (see left middle panel in figure 6.1.6) during which a mutual interaction through baroclinic development or the enhancement of the thermodynamic equilibrium between the Mediterranean Sea and the atmosphere (Emanuel, 2005) might contribute to increase the intensity of the storm.

September 1996 case shows strong sensitivity of central ErPV values of the trough to the PBL scheme. It is significant the large differences between the strength of simulated medicane with ETA PBL scheme and the other two simulations (see figure 6.1.14). During the simulation of the episode two vorticity maxima appeared (α, β, see green and red lines respectively in figures 6.1.6 and 6.1.7). Larger coupling between β upper and low level disturbances obtained with ETA pbl scheme contribute to generate a significantly deeper medicane. Maximum horizontal wind speed at 950 hPa reach hurricane intensity (over 33 ms^{-1}, see middle left panel in figure 6.1.5).

At the genesis zone of the September 1996 case (point A, figure 6.1.8), higher CAPE and Latent Heat Flux are obtained with the ETA scheme, but precipitable water is slightly lower. These results are in agreement with results of Wisse and de Arellano (2004) in which the lower magnitude of vertical transport in the ETA scheme compared with Blackadar and MRF nonlocal mixing schemes results in a less eroded capping inversion of the PBL, with higher CAPE values. Differences between PBL results are enhanced due to the maritime characteristics of the selected points where meteograms are drawn: high values of the Latent Heat Flux from sea areas and the nonlocal (Blk, MRF) vs. local (ETA) mixing properties of the schemes, result in significantly different moist vertical transport among the simulations. For a meteogram obtained at a land point (at the centre of Mallorca Island) lower differences between results are observed (not shown). Diurnal cycle at this land point is depicted with strongest signature (largest differences between day and night values) with MRF scheme. The genesis of the medicane (vertical arrows in figure 6.1.8) is accompanied by a decrease of CAPE, a transitory enhancement of precipitable water and a rise of the surface fluxes.

Simulations of September 1996 case with the satellite/lightning information show stronger medicanes than the control one during its mature phase (see figure 6.1.10), al-

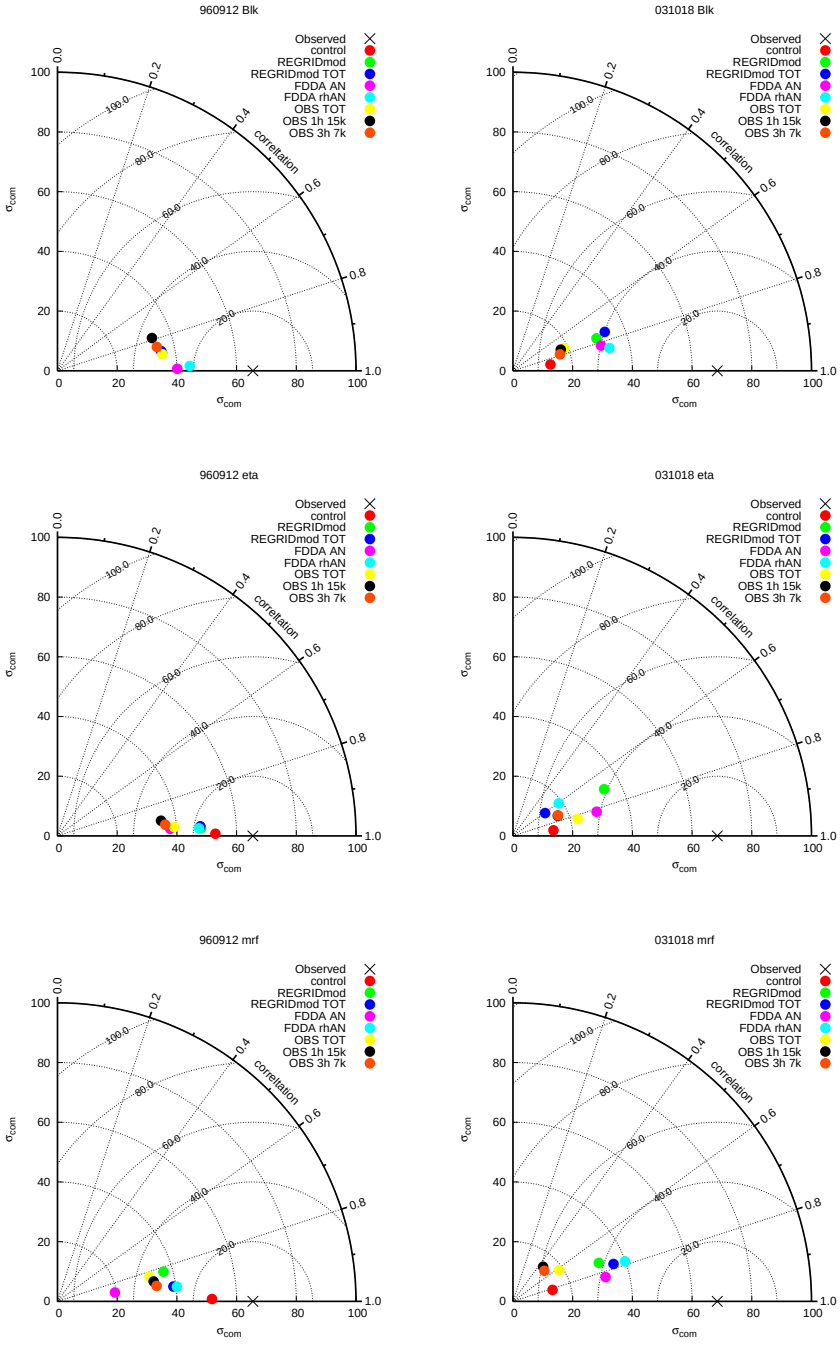

Figure 6.1.15: Taylor diagrams of simulated and satellite-observed trajectories, defined by the distances of trajectory vertices to the origin of coordinates of each domain of evolution. September 1996 (left) and October 2003 (right). With Blackadar (top), ETA (middle) and MRF (bottom) PBL schemes. σ_{com} standard deviation of the simulated trajectory (com) establishes the radius. $\mathcal{R}$, correlation between trajectories, establishes the angle respect to the abscissas. Root Mean Square Error (RMSE) is the distance between simulation dots and standard deviation of the observed trajectory (black cross). Colour codification of the dots for each simulation is the same as in figure 6.1.10

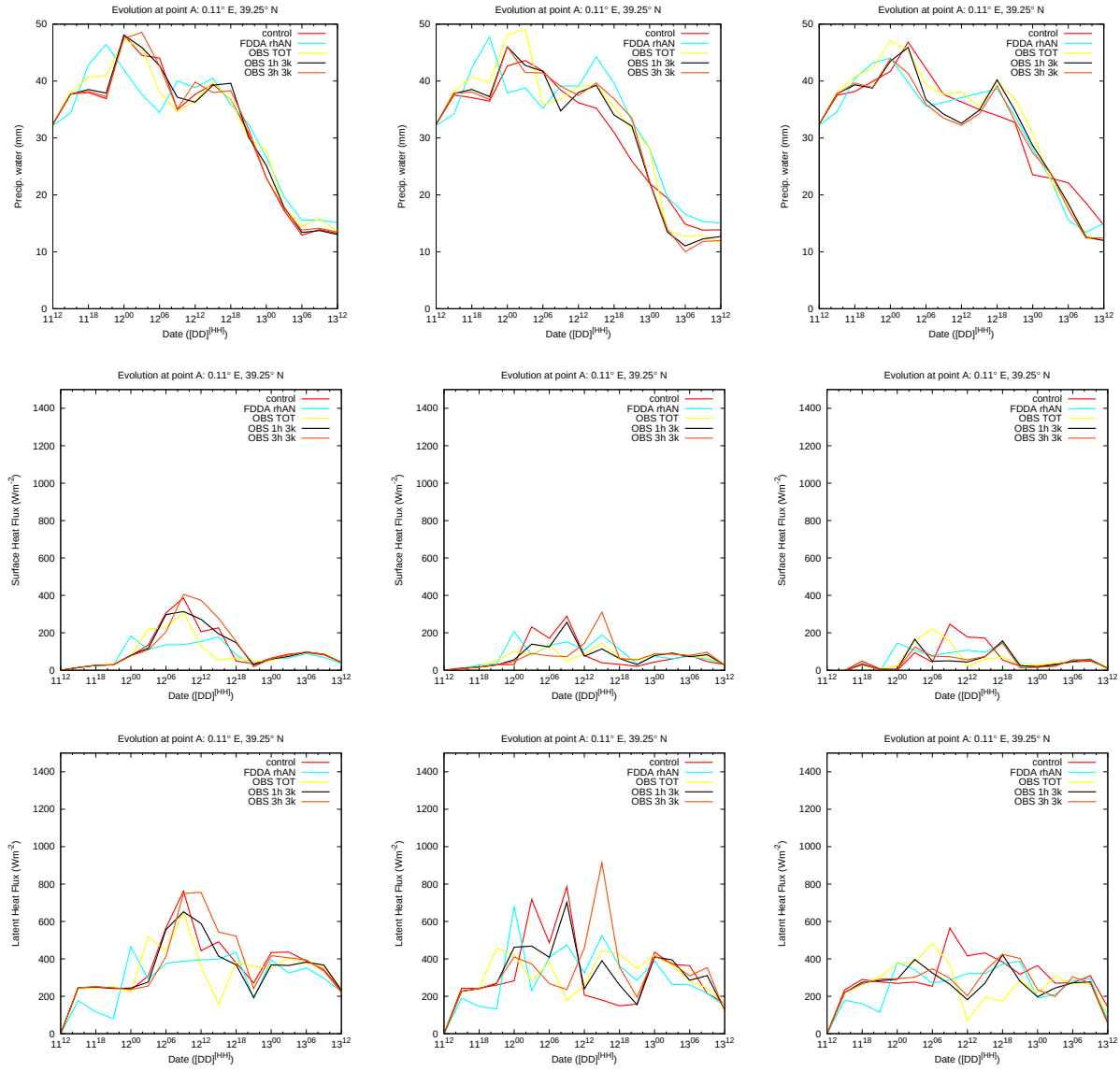

Figure 6.1.16: Evolution at point A (bottom left panel of figure 6.1.5) during September 1996 simulation of the Precipitable water (mm, top), surface sensible heat flux (Wm^{-2}, middle), latent heat flux (Wm^{-2}, bottom). For control simulation (red), OBS TOT (yellow), OBS 1h 3k (black) and OBS 3h 3k (orange), with the Blackadar (left), ETA (middle) and MRF (right) PBL schemes

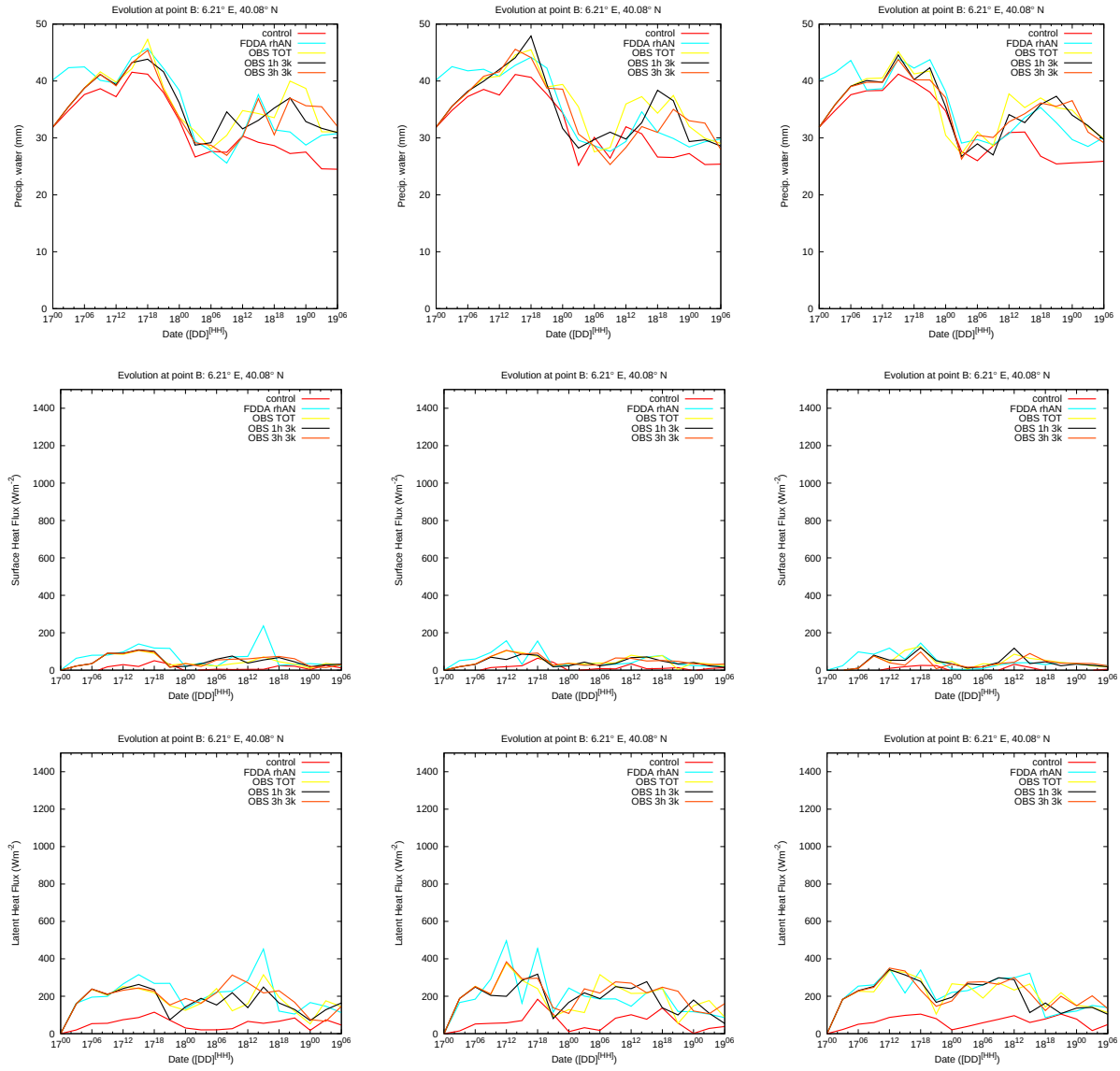

Figure 6.1.17: As in figure 6.1.16 but for the October 2003 case at point B (bottom right panel in figure 6.1.5)

though weaker medicanes are obtained at the later stages of the simulations. The largest differences on trajectory and central pressure value with respect to the control one (for all PBL schemes) are obtained with the experiment 'FDDA AN' (FDDA with unmodified ECMWF analyses). In these simulations (pink lines in figure 6.1.10), simulated medicanes are significantly weaker (they vanish before September 13th at 00 UTC) and their trajectory differ significantly from the other ones (figure 6.1.11). In these experiments, results are forced to be very similar to the ECMWF analyses, and ECMWF analyses do not fully capture the structure of the medicane owing to a poor horizontal resolution (ECMWF analyses at that time were truncated at T213, 0.5625° degrees of horizontal resolution). In FDDA AN experiment, MM5 simulated medicanes (for the three PBL schemes) present trajectories very similar to the upper level trough path (see figure 6.1.14 as an example of simulated trajectories of upper level maxima disturbance). Deepest simulated medicanes are obtained when the observational nudging is applied (experiments labelled OBS TOT, OBS 1h 3k, OBS 3h 3k; yellow, black, and orange lines in figure 6.1.10). OBS TOT experiment (coarse spatial resolution of observations that allows the highest temporal resolution of satellite information) produces the deepest medicane.

September 1996 deepest medicane is obtained by experiment 'OBS TOT' (humidity modification at every time step with the maximum computer[1] allowed spatial resolution, in this case 15 km; yellow line in figure 6.1.10). Similar tendencies of central pressure, maximum horizontal wind speed and trajectories of the simulated medicanes are obtained in the experiments using the same horizontal resolution but different temporal frequencies (experiments labelled 'OBS 1h 3k' and 'OBS 3h 3k', orange and black lines respectively in figure 6.1.10). However, experiment 'OBS 1h 3k' presents a bit stronger dissipation rate of the medicane than the lower temporal resolution experiment.

Taylor Diagrams show how the implementation of FDDA on 960912 case worsens trajectories (lower correlation and lower standard deviations). Simulated trajectories for September 1996 medicane are much closer to the satellite observed (lower Root Mean Square Error, RMSE, of the distance between simulation points and reference point in the diagrams) than October 2003. Data assimilation in September 1996 simulations modify both indexes, correlation and standard deviation, with a higher impact on the standard deviation.

No significant differences among the evolutions of precipitable water and sensible and latent heat fluxes from meteogram at the genesis zone of September 1996 are obtained with the assimilation of satellite/lightning information (see figure 6.1.16) with respect to the control one.

[1] On a PC Linux cluster with central and auxiliary nodes all with 4Gb of memory

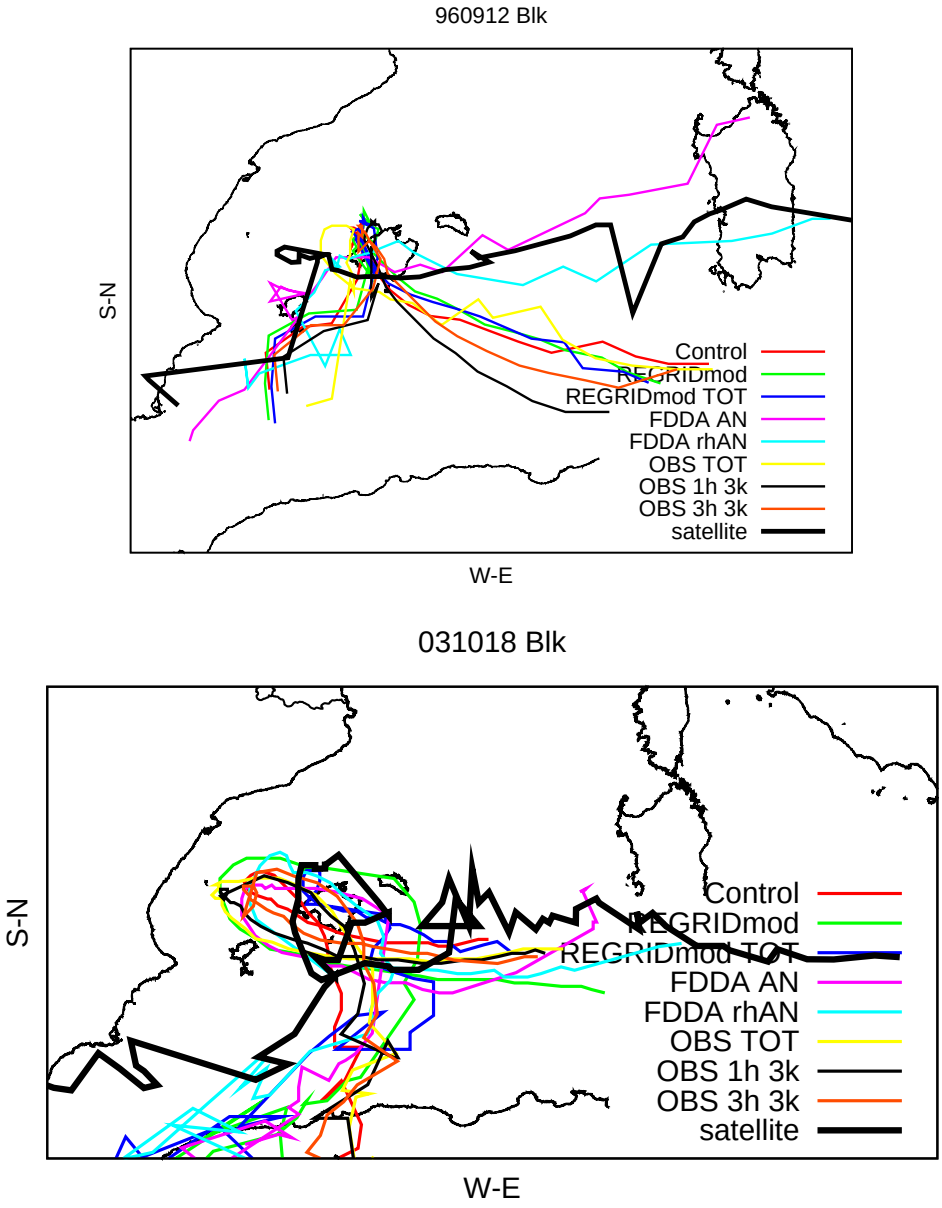

Figure 6.1.18: BIAS corrected simulated trajectories (i.e. bias is removed by traslation of the trajectories according to the spatial satellite-derived path) simulated trajectories with the Blackadar PBL scheme for each experiment. Solid black line is the satellite trajectory. For the September 1996 case (top) and October 2003 case (bottom). Colour codification of the lines is the same as in figure 6.1.10

September 1996 episode has a stronger sensitivity of $\mathcal{BIAS}_{dist}^{min}$ to the temporal shift than the October 2003 case. September 1996 episode has a symmetric response to advances/delays of the simulated trajectories. The lowest $\mathcal{BIAS}_{dist}^{min}$ values for almost all the experiments are obtained without the addition of a temporal shift in the simulated trajectories. Clearer results for the 960912 case can be attributed to the simplicity of the trajectory of the medicane in comparison to the 031018 case, in which the trajectory presents a loop. For September 1996 medicane, lowest $\mathcal{BIAS}_{dist}^{min}$ values are obtained in the experiments that do not use observation nudging (labelled REGRIDmod, REGRIDmod TOT, FDDA AN, FDDA rhAN).

No significant improvements of the BIAS corrected 'pure coordinate correlation' ($\mathcal{PR}_{bias}^{max}$) are obtained when simulated trajectories are temporally advanced or delayed (see figure 6.1.20). The introduction of a positive/negative temporal displacement in the September 1996 simulations produces a clear decrease of the correlation. None experiment or temporal shift gives better correlation results than the correlation attained by the control simulation without BIAS correction (horizontal solid black line in figure 6.1.20).

FDDA experiments with ETA PBL scheme simulate a stronger medicane, dissipation of the system occurs faster than in the control simulation using the same ETA PBL scheme (an abrupt change on 12th September 1996 at 09 UTC in middle panels of figure 6.1.10 is observed). It was shown how in the control simulation a long-lasting interaction occurs between the upper level trough β maxima and the medicane (see middle left panel in figure 6.1.6). Different trajectories of the upper level and low level centres simulated in the FDDA experiments seem to produce a reduction in the interaction between disturbances (not shown).

For September 1996, better skills (higher correlations, lower bias) are generally obtained when experiments are done with ETA PBL scheme.

October 2003

Blackadar simulation of October 2003 medicane is deeper than that one simulated with ETA scheme. However, medicane simulated with ETA scheme presents, during some periods of the evolution, the highest wind speed values.

October 2003 medicane evolution does not seem to follow so clearly the upper level disturbance as the previous case. There are not significant differences among the trajectories obtained with the different PBL schemes (see figure 6.1.5). Medicane and centre of the trough do not evolve simultaneously in this case. The closest approach between both systems does not reach 200 km (see right panels in figure 6.1.6). Therefore, October 2003 medicane might be more influenced by the general flow pattern associated with the

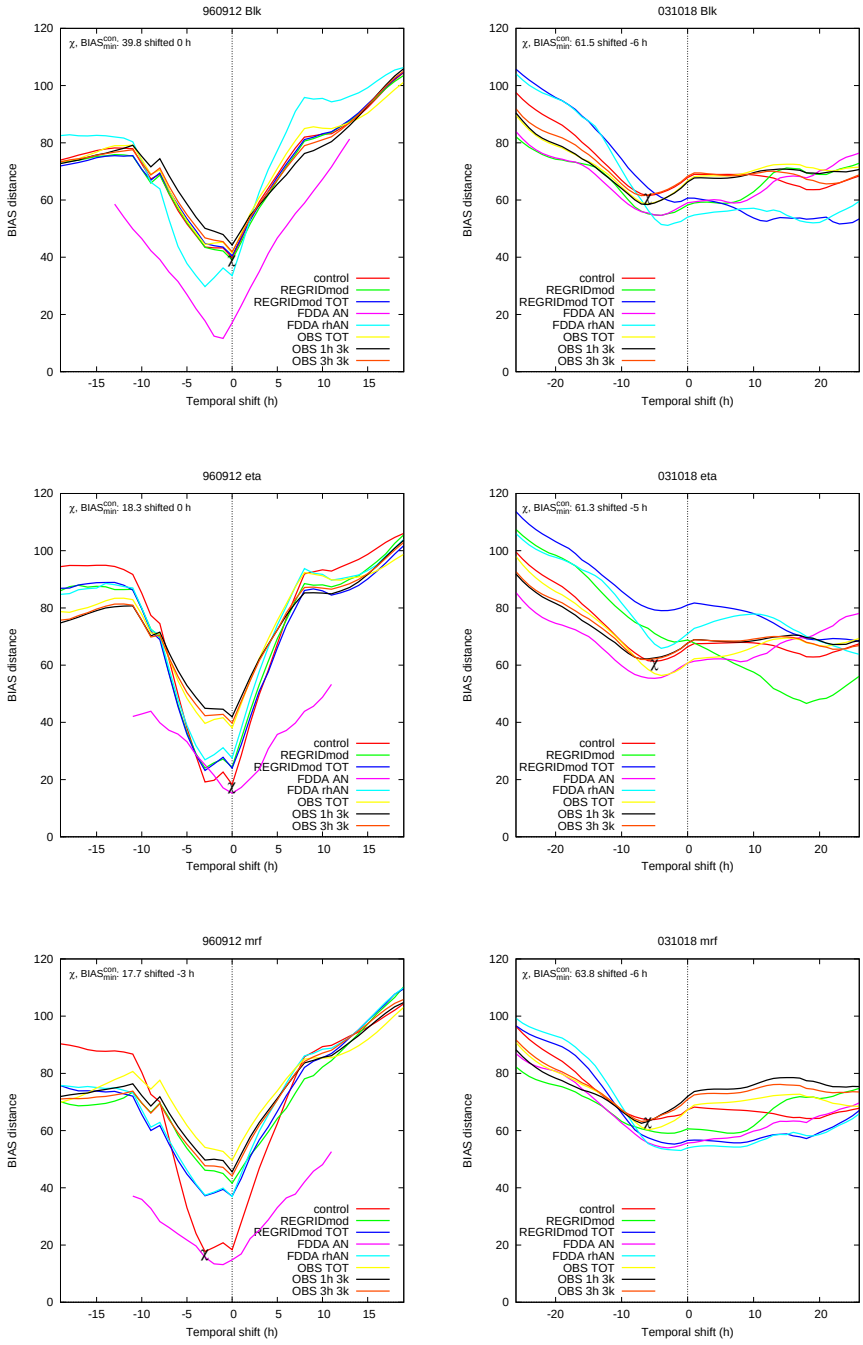

Figure 6.1.19: Dependence of the $\mathcal{BIAS}^{min}_{dist}$ of the distance between satellite-derived trajectory and simulated trajectories on temporal shift for the September 1996 (left) and October 2003 (right) cases. With the Blackadar (top), ETA (middle) and MRF (bottom) PBL schemes. Negative values mean temporal advances of the simulated trajectory and positive values mean delays. χ is the value of the minimum $\mathcal{BIAS}^{min}_{dist}$ for the control trajectory obtained for a given temporal shift. Colour reference of the lines is the same as in figure 6.1.10

upper level trough rather than by the precise movement of its centre of maximum vorticity.

October 2003 evolution of the upper level disturbances seems to be more adiabatic than September 1996 event, as a reflect of the independence between the upper-level maximum vorticity centre and medicane, for which a lower interaction between lower and upper level disturbances is established.

October 2003 case does not exhibit large differences between meteograms at formation zone (point B, figure 6.1.9) and presents lower values for all selected variables than the previous case. The intrusion of the growing medicane in the zone is also observed as a decrease of CAPE, a transitory maximum of precipitable water and an increase of surface fluxes. Larger differences in precipitable water amounts and surface fluxes intensities with respect to ETA simulation values are shown by the Blackadar and MRF meteograms in later stages of October 2003 simulations (see figure 6.1.17).

In comparison to September 1996 episode, October 2003 case reflects a lower influence of the the FDDA technique on the simulations (see figures 6.1.12 and 6.1.13).However, this case presents the strongest sensitivity of the characteristics of simulated medicane on the FDDA technique. Differences between the set of eight experiments for a given PBL scheme are larger than in previous case. There are differences between experiments for the same PBL scheme larger than 10 hPa in the central pressure value and 10 ms^{-1} for the maximum horizontal wind speeds. Upper level trough trajectories do not differ significantly, these differences becoming larger at later stages of the episode (see figure 6.1.14). This result would confirm the aforementioned low dependency of the medicane evolution on the upper level evolution, since changes in the trajectories and characteristics of the upper level maximum are weak. Deepest medicanes are related to the experiments where observational nudging is applied. In these cases, deeper pressure at the centre of the storm is also associated with stronger horizontal wind speeds.

October 2003 episode presents the strongest simulated medicanes with experiments 'OBS TOT' and 'OBS 3h 7k' (see table 6.1.a). These results, in agreement with the results obtained in the previous case, show that observational nudging for the two presented cases is more sensitive to the horizontal resolution of the data than to the temporal frequency with which the data is incorporated in the simulations.

FDDA methodology improves the trajectories of the October 2003 simulations (see figure 6.1.15) according to the decrease of the RMSE between simulated and observed trajectories, having a low impact on the correlation in contrast to its significant effect on the standard deviation.

Meteograms of precipitable water, sensible and latent heat surface fluxes at the genesis

zone of October 2003 case show higher values than in control simulation (see figure 6.1.17) when satellite/lightning data is used (similar behaviour of the variables is observed in the meteograms at other points, not shown). Bearing in mind the low sensitivity in previous case, this would mean that the humidity field is better represented in the ECMWF analyses of the September 1996 case, than in the October 2003 analyses.

October 2003 presents a clear decrease of $\mathcal{BIAS}_{dist}^{min}$ when simulated trajectories are temporally advanced with respect to the satellite one, while both increasing/decreasing effects when they are delayed. Bias results for the 2003 medicane are case dependant. A general advance about 6 hours reduces the bias ($\mathcal{BIAS}_{dist}^{min}$) between simulated and observed trajectories.

Some of the October 2003 simulations improve the pure coordinate correlation between trajectories, but temporal shift makes the results worse, even produces negative correlation values (see figure 6.1.20). Strong differences for a specific PBL with respect to the experiments are a reflect of the strong sensitivity of the October 2003 case on the FDDA technique.

For October 2003 episode the best simulation is not determined by an unique PBL scheme or experiment.

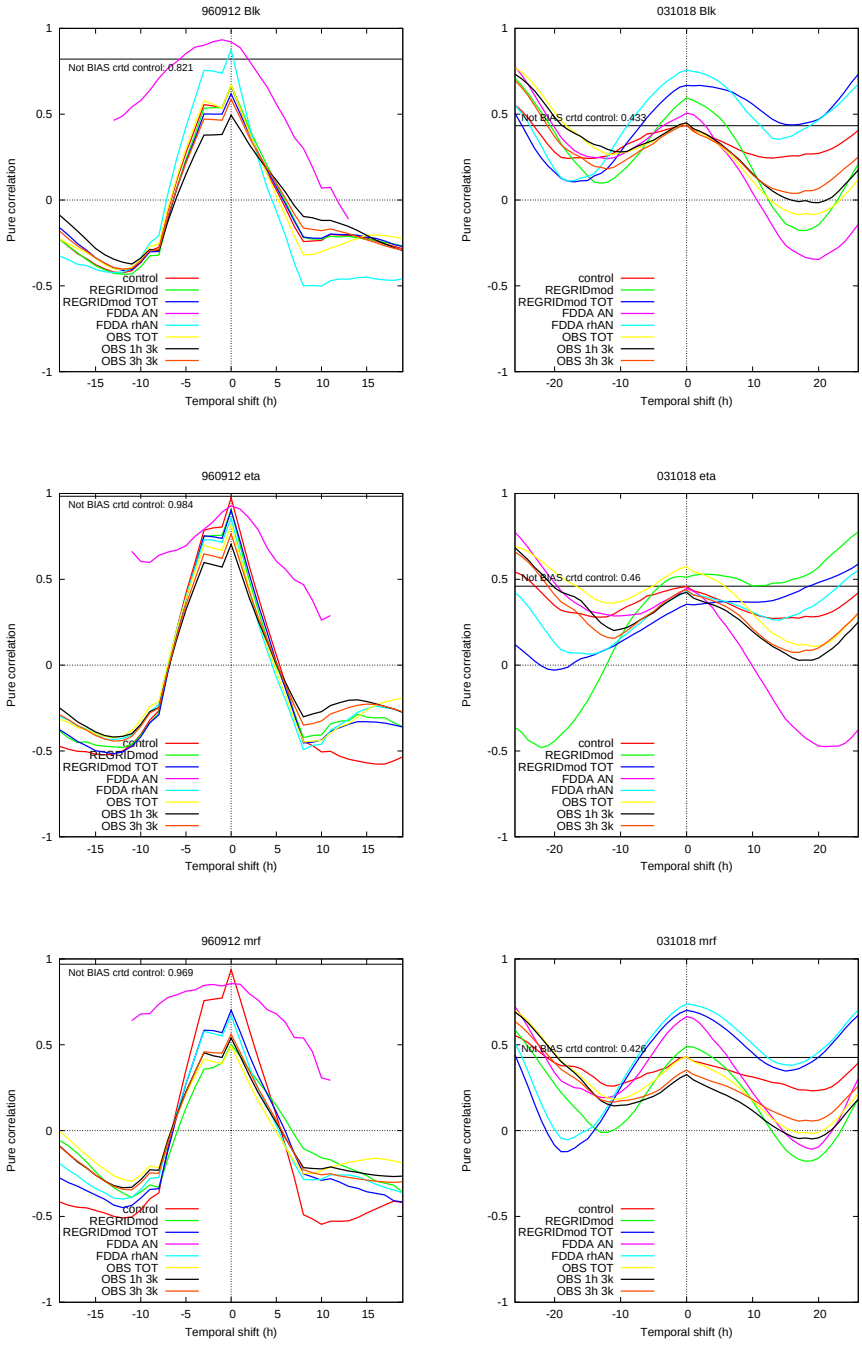

Figure 6.1.20: Dependence of the pure coordinate correlation $\mathcal{PR}^{bias}$ (bias corrected) for each experiment as function of temporal shift, for the September 1996 case (left panels) and October 2003 (right panels). With the Blackadar (top), ETA (middle) and MRF (bottom) PBL schemes. Solid black line is the correlation for the control simulation without BIAS correction. Colour codification of lines is the same as in figure 6.1.10

Chapter 7

Conclusions

A variety of Mediterranean cyclogenesis has been analysed. Although they evolved within the same environment a relative important number of different mechanisms and processes responsible for their genesis, maintenance and dissipation have been found. Three main numerical techniques: atmospheric numerical model, piecewise PV inversion and Factor Separation have been used to analyse the cyclogenesis in the Mediterranean basin. Each one provides different information from the processes allowing a robust and global view of the topic.

Conclusions obtained as result of all the developed studies are referred to two aspects: dynamical description of Mediterranean intense cyclogenesis and limitations and improvements of used numerical methodologies. It must be recognised that these conclusions have two main limitations: case dependence and numerical origin.

The non-linearity of the atmosphere limits its comprehension. Similar initial conditions might derive in different situations and phenomena. By this way, in order to obtain a wide and general perspective of the dynamics of the atmosphere a wide number of cases must be studied. Even after the study of a large number of similar episodes, due to the non linearity, a new case could be completely different. Thus, results must be seen as the particular response of the 'atmosphere' at the specific situation.

Almost all the results are based in numerical models and/or numerical techniques. Observations have only been used in some cases as a way to make, in some manner, more realistic the initial conditions of the representation of the atmosphere. Although atmospheric observations are sparse and contain errors, they constitute the most accurate and close description of the real atmosphere that we can have. Numerical methodologies constitute a well developed labour that allows: a complete description and evolution of the atmosphere based on equations and the repetition of the experiments. However without the use and validation of observations one can not be sure of the degree of nu-

merical/method artifice of its results.

Keeping in mind the previous limitations in relation to the results, the author is pretty confident in his results. A selection of different cases when it was possible has been tried in order to widen the scope of the results. In the piecewise PV inversion study of the November 2001 episode, results for a unique case are obtained. But in this study, two objectives were searched: analysis of the case and the practice of an improvement of the piecewise PV inversion numerical technique. The use of observations has been very limited, and it has been reduced to a general comparison with satellite-based trajectories or radar reflectivities. This can limit the accuracy of the results, however, there is any way to verify, contrast or validate some of the objectives of the studies, like the effects of factors or piecewise PV inversions with measurements or observations.

7.1 Strong cyclogenesis: November 2001

The 912 November 2001 Mediterranean cyclone has been studied in terms of its sensitivity to changes in the initial conditions due to three PV anomalies: the surface thermal anomaly related to the origin of the cyclone and the baroclinic initial conditions of the environment; the upper level trough related to the baroclinic growth mechanism of the cyclone; the upper level North Atlantic high pressure zone related to the environmental conditions of the upper troposphere. The anomalies show different morphologies and intensities, but since the energy-quantification of the initial modification has been applied, sensitivity results might be only attributed to the dynamical role of the anomalies. The surface thermal anomaly is revealed as the most important feature of the initial conditions for the cyclogenesis. A significant effect on the initial central pressure of the cyclone and a weak effect on its initial position are shown. Both have a strong effect on the resultant evolution of the case. The sensitivities to changes in the initial conditions due to the upper level disturbances are also important. Nevertheless, the initial impact on the structure of the cyclone is lower than for the thermal anomaly, but in later stages of the episode the impact becomes the strongest. The effects of changes in the initial conditions associated with the North Atlantic high are weak. However, in the last phase of the cyclone evolution, the initial perturbations show a notorious impact on the trajectory of the cyclone.

The sensitivity results are strongly affected by the baroclinic mechanism. It is illustrated that the diversity of simulated cyclones can be mainly explained as a function of the changes in the vertical tilt between the upper level trough and the surface disturbance. The sensitivity test to the increase(decrease) in the surface thermal anomaly shows that with similar values of the upper level disturbance, changes in the relative position and central pressure value of the surface disturbance generates deeper(weaker) and faster(slower) evolution of the simulated cyclone. This case also emphasises the mutual

interaction between anomalies, in the sense that the thermal anomaly perturbation does not affect the initial structure and intensity of the upper level disturbance, but during the simulated period, the upper level disturbance strength clearly differs between both experiments. The upper level disturbance perturbations modify both the initial central value of the cyclone and the upper level trough, but only slightly modify the relative distance between both features. These variations generate a strongly varied evolution of the cyclone. Finally, the North Atlantic high does not exhibit a significant role on the upper level disturbance, on the surface cyclone strength or on the relative position between disturbances. However, the small perturbations on the relative position between the upper and low level disturbances seem to be enough to originate significantly different final cyclones.

7.2 Intercomparison of 11 Mediterranean cyclogenesis

The results for 11 Mediterranean cyclones have been presented. Must be studied much more cases in order to obtain a much representative climatology of the Mediterranean cyclogenesis.

The effectiveness of the studied factors does not show many similarities between cases and only weak generalisations can be done, however the baroclincity of the Mediterranean basin is shown by the importance of the upper level PV anomaly. It is detectable the presence of an upper-level low in almost all the cases. Secondary role is played by dry low-level anomaly and its interaction with the upper level one. It is obtained the importance of the low-level positive PV mainly in some cases related to the baroclinic development process and/or to the thermal low genesis due to solar insolation over the North African plateau or other regions. Finally, background flow appeared to be responsible of the cyclone movement.

Moist low-level PV has been considered as a factor. The sensitivity of the 11 cases to this factor has been shown very poor. It should keep in mind that this factor only marks the moist low-level PV of the cyclone, trying by this way to deal with the diabatic aspects of the cyclogenesis. However, small sensitivity results of the factor might reflect it as an inadequate way to capture the importance of the moist-induced diabatic processes. A new approach considering directly the diabatic terms of the equations is proposed as a more correct way to capture the moist induced diabatic processes.

Factors are often cyclogenetic and cyclolitic as a probable signature of the complexity of the Mediterranean topography and the large number of factors that are reproduced in

a cyclogenesis and they have not been taking into account such as: upper level-low level interaction sensitivity on the relative position between disturbances, cyclone position relative to the orography and background flow.

Geographical differences between dynamics of cyclones can be make. Western & Central Mediterranean cyclones seem to be mainly dominated by upper and low PV anomalies and their synergy. A variety of principal factors is shown by eastern Mediterranean cyclones. This could be also related to the variety of typologies of the Eastern selected cyclones. Since Western and Central cases are generally African or Alpine lee cyclones. In contrast, Eastern cyclones have different genesis and trajectories.

Dynamical group of the cyclones show some differences. 'African' cyclones are principally driven by by Upper level disturbances or its synergy with low level PV. 'Maritime' cyclones are mainly dominated by upper level disturbances and weakly by the background flow. The selected 'Alpine Lee' cyclones shows a first phase dominated by the Upper level disturbance and a second one driven by low level disturbances. It is also shown big compensations between strong cyclolitic and cyclogenetic effects.

This methodology allow to an objective classification of the Mediterranean cyclogenesis rather that other classification based on society impacts or geographical affected areas (e.g. MEDEX database, see `http://medex.inm.uib.es`). The derived climatology is based in dynamical concepts that after an improvement of the technique can apport a general scope of the main processes related to the Mediterranean cyclogenesis. Results are not very precise, but is hoped that a significant increase of the number of cases and the appropriate selection of factors will provide significant results.

7.3 Thermal influences

This study is focused on a numerical study of a severe storm event that occurred on August 16th 2003 in Northeastern Spain. Maximum precipitation amounts of 115 mm were registered in the rain gauges of Alcañiz, the most affected town. Hailstones of up to 12 cm were registered and the town was declared a disaster zone, claiming losses of over 10 M. A C-band radar with a high temporal resolution made it possible to follow up the storm activity.

The event was characterised by a trough at mid to upper tropospheric levels. The arrival of a cold front from the NW of the Iberian Peninsula moving eastward caused high-altitude cooling. Numerical simulations were performed to examine the accuracy of the model in reproducing the severe storm of Alcañiz. The control run shows the presence of a thermal mesolow favouring the entrance of warm and humid air from the Mediter-

ranean Sea all the way up the Ebro Valley. The total precipitation field indicates that the most intense precipitation fell in the study zone, coinciding to a great extent with the radar data. The radar simulation carried out with the model proves that, even though MM5 underestimates the maximum precipitation registered, it does reproduce the spatial and temporal evolution of the storm quite closely. On a convective scale, the result of the simulation can be considered to be very satisfactory.

Besides, a numerical sensitivity study was carried out as well to analyse the factors contributing to the localisation of the intense precipitation. The roles played by topography and solar radiation were also examined, since these factors have previously been identified as relevant in severe storms in Northeastern Spain. In fact, the experiment carried out with no solar radiation shows a weakening effect on the mesolow and a reduction of the instability in the low troposphere. This hinders the activity of mechanisms triggering convection and inhibits precipitation, limiting it to small areas of the Pyrenees and the Mediterranean coast. In the experiment with flat terrain the corridor effect of the Ebro Valley on the mesolow disappears, as well as the low-level warm inflow from the Mediterranean Sea. The results conclude that the separate effects of either solar radiation or topography are not decisive by themselves in accounting for the intense precipitation caused by the severe storm of Alcañiz. However, the synergic effect of the two factors combined is fundamental for the spatial and temporal localisation of the storm, and has an inhibiting effect in other areas of Northeastern Spain.

7.4 Lee influences

This numerical sensitivity study investigated the initial phase of a deep Mediterranean cyclone that took place in the lee of the Atlas Mountains in November 2004 and caused a range of severe weather events throughout the Mediterranean region. In this numerical study, a factor separation method was applied to investigate the influences of orography, upper-level potential vorticity and surface sensible heat flux on the Atlas lee cyclone initiation and development, focused on the period until the cyclone left the lee area and entered the Mediterranean Sea.

Orography proved responsible for the first phase of the lee cyclogenesis, where a shallow cyclone was formed over a barotropic area in the lee of the High Atlas, due to frontal retardation and creation of an associated thermal anomaly. Although the orographic influence resembled the first stage of Alpine lee cyclogenesis, the orographically induced pressure drop reached 5 hPa during 24 hours and was not so rapid like in cases of Genoa cyclogenesis.

The second phase of the deepening was characterised by the cyclogenetic influence of

the upper-level potential vorticity perturbation (a part of the upper-level PV anomaly). Indeed, with a total upper-level PV anomaly removed from the initial conditions, the cyclone did not form in the lee of the Atlas, that proves that the upper-level dynamical factors are a necessary ingredient of Atlas lee cyclogenesis, in accordance with some idealised studies on Sharav lee cyclones (Egger et al., 1995). In simulations with the PV perturbation included, the low-level air was colder, resulting in the creation of a stronger thermal anomaly and associated baroclinic zone. Furthermore, the upper-level PV perturbation showed responsible for a vertical (downward) propagation of cyclonic circulation, as indicated by the increased cyclonic winds in the lower atmosphere. In other words, the influence of positive PV advection contributed to the stronger low-level convergence and more rapid cyclone initiation.

It seems that the most pronounced feature of surface sensible heat flux contribution was an afternoon cyclolysis. Namely, SSHF was accompanied with increased vertical mixing in the afternoon PBL and associated weakening of the baroclinic (and barotropic) zone, inducing less intensive cyclone deepening. Secondly, heat exchange between the ground and the surface air reduced the horizontal surface air baroclinicity, as the horizontal air temperature gradient of the baroclinic zone was bigger then the horizontal ground temperature gradient in the arid Atlas lee. And finally, it is proposed that the exclusion of surface sensible heat flux enhanced the long-wave earth radiation that tended to act as a heat supply to the moist areas (associated with the cyclone) in the free troposphere.

The synergy between orography and upper-level PV perturbation was at first cyclolytic, followed by the cyclogenetic contribution towards the end of the analysed period. The cyclolytic influence existed probably due to the fact that in the simulation with orography and upper-level PV included, the cyclone experienced filling over the terrain obstacle on the way to the Mediterranean Sea. The subsequent cyclogenetic contribution of the synergy had some potential for comparison with the low-level-upper-level vortex interaction in the second stage of Alpine lee cyclogenesis. However, at the end of the analysed period the cyclone centre positions differed significantly, not allowing a resolute conclusion.

The spread of the cyclone centres in the model simulations was shown to be a powerful tool in understanding the effect of different factors on the cyclone evolution. For instance, orography moved the cyclone initiation closer to the mountain and the favourable lee area where the thermal anomaly was the strongest and tended to keep the cyclone more stationary. On the other hand, the upper-level potential vorticity perturbation moved the cyclone formation location away from the mountain and was responsible for the faster advection of the cyclone to the Mediterranean Sea. It seems that the intensity of the upper-level PV anomaly has an influence on the subsequent cyclone movement and possibly has some potential to account for the seasonal cyclone path variability.

Another sensitivity experiment was performed to try to account for the influence of a thermal anomaly on the generation of a low-level vortex in the first stage of lee cyclogenesis. However, the simulation shown that the thermal anomaly in the lee of the Atlas built up rather quickly. It almost reached the intensity of the thermal anomaly of the control run in 24 hours since the start of the simulation, just before the cyclogenesis started. Thus, little reliance could be made on the separation of low-level PV and thermal anomaly influences on the intensity of cyclone initiation. However, it seems that the location of the slightly weaker cyclone initiation showed sensitivity to a thermal anomaly positioning in the mountain lee.

So far, the very area of the Atlas lee was subjected neither to a significant number of numerical or theoretical studies, nor to observational field campaigns like MAP. However, the arid lee area of the Atlas Mountains has some potential to attribute more precisely the influence of dynamical processes to the lee cyclogenesis due to the lack of moist processes at play. Furthermore, the vertical and horizontal scales of the High Atlas Mountains are reasonably comparable to the Alpine dimensions.

It is one of the goals of the planned MEDEX special field campaign to better monitor Mediterranean cyclones and storms, which are often not well detected by observation networks. In addition, this effort should be accompanied by an increased number of numerical and theoretical studies, specially the ones that investigate the life cycles of the high-impact deep Mediterranean cyclones.

7.5 Medicane environments

An analysis of the characteristics and behaviour of the tropical-like Mediterranean storms has been presented. The study applied a nonhydrostatic, cloud-resolving model used previously to simulate tropical cyclones in order to analyse the potentiality of seven environments in which a tropical-like Mediterranean storm occurred. Observations show that the seven analysed Mediterranean systems are of tropical storm strength. From satellite imagery, a similar morphology to the tropical cyclone systems is also obtained for the medicanes: a clear rounded cloud system, in the centre of which a free cloud zone, like an eye, is formed. Satellite imagery showed different trajectories and speeds for the movements of the medicanes.

Mediterranean systems exhibit notable differences from the tropical ones. Sea surface temperature did not play as significant role as in hurricanes. As noticed in previous work (Emanuel, 2005), high values ($> 26°C$) of sea surface temperature are not essential, in contrast to hurricanes. Thus, the vertical profile of the atmosphere, defined from the

combination of a mid-upper level cold low and a SST-controlled boundary layer, has been shown as one important aspect of medicane formation. Generally, analysed synoptic situations during medicane formation showed significant instability and high precipitable water quantities in the atmospheric column.

The cloud model simulates a 'theoretical' storm derived from an initial environment. Some assumptions and simplifications are implicit in the model. A main point is related to the energy source. It is assumed that the storm will only obtain the energy from the sea surface and related surface fluxes. The axisymmetric cloud-resolving model demonstrates that medicanes can be developed and sustained at least partially by surface enthalpy fluxes, especially if the initial environment is moist. However results showed stronger and larger potential storms in comparison to the observed ones. Simulated wind speeds were significantly stronger, and simulated cloud-eye dimensions were wider. Simulated storms are formed more slowly (mainly 3-4 days) than the 'real' ones as revealed by satellite images (mainly 1-2 days). Moreover, Mediterranean observed storms dissipated mainly in 2-3 days. Meanwhile, simulated storms were maintained for a longer period (mainly 4-5 days) and some cases did not show any weakening process. These significant differences are considered to be a sign of the complex atmospheric processes operating in the Mediterranean systems that the simplified numerical model is not able to resolve. The complex orography, the small dimensions of the basin and the continental influences from the neighbouring European and African lands are particular aspects of the Mediterranean which are not present in the largely homogeneous tropical environments. These aspects will of course modify and limit the evolution of the tropical-like systems in the Mediterranean basin. Besides, the assumptions of the cloud-resolving model do not allow one to take into account baroclinic influences which are prominent in the Mediterranean. In some cases, ECMWF analyses showed a significant horizontal thermal gradient in the region of the storm evolution, (e.g.: 950115 case). Tropical-like Mediterranean storms grow and evolve from a combination of deep convection and typical mid-latitude baroclinic processes. The axisymmetric cloud-resolving model assumes a homogeneous atmosphere. This assumed background atmosphere is also temporally invariant during the period of simulation. Spatial homogeneous and temporal invariant assumptions are inappropriate in the Mediterranean basin (Reiter, 1975). Thus, a less restrictive cloud resolving model, in which either a baroclinic environment or a time-evolving environment could be introduced, is at least necessary in order to produce realistic tropical-like storms in Mediterranean air masses. The MM5 three-dimensional numerical model was applied on two of the events to confirm that hypothesis. The results reflected a good agreement with observations and know aspects of these systems, such as warm core, the eye-wall structure and the subsidence at the centre of the storm.

The main results of the sensitivity tests of the environments, which have been computed with the tropical cloud model, showed similar results as the tropical cases. The

value of the SST is clearly important for the formation and evolution of medicanes. In the simulations, colder SST inhibited the formation of the medicanes while, warmer SST accelerated and enforced the medicane formation. The results of the simulations in which the size of the vortex was changed were significantly different from the control ones. Stronger and faster systems were formed when the initial vortex was enlarged. The importance of the vertical profile of the atmosphere for the medicane formation has been described. The sensitivity tests on the moisture content of the air column showed a deep impact on the formation and the evolution of the storm. Drier air made the formation and the evolution of the storm more difficult, while moister air enforced and accelerated the formation of the storm. Thus, the characteristics of the initial vertical profile of the atmosphere have been shown to be important influences on the evolution and formation of the medicanes. Finally, a warmer initial vortex produced a faster and stronger evolution of the simulated storms. This reflects the impact of a faster(slower) organisation of the convection induced by a stronger(weaker) rotation of the initial vortex (Rotunno and Emanuel, 1987). The good results obtained with MM5, encourages authors to use this kind of primitive equation model simulations in order to complete a more adequate model-based sensitivity test of the medicanes.

Moreover, due to the maritime characteristics of the systems, the lack of observations and records of medicanes impedes research on their development. More observations are needed for a correct understanding of medicanes.

7.6 Medicane sensitivity

High resolution simulations and the Factor Separation analysis of three tropical-like storms has give some relevant information about the role of the air-sea interaction mechanism in these systems.

Temporal and group dependences of the synergies of the cases show significant differences, as a reflection of the different behaviours of the three cases. Two phase distinctions can be made for each case. During these phases principal effects change. Instead the differences between cases, some general aspects of these kind of systems are obtained.

Beginning phases of the systems are dominated by the upper level disturbances and the interaction between surface fluxes and Sea Surface Temperature. Upper level vorticity effect at low level would contribute to the reinforce of an initial weak vortex, around which the medicane will be formed. At the same time, upper level disturbances coupled with the moistened and warm air above sea established a vertical thermodynamic disequilibrium, that is necessary for medicanes formation. In contrast, its interaction with surface fluxes

have a cyclolitc role due to a diminishing of the baroclinic conditions and the energy budget at the top of the outer region of the medicane boundary layer. Boundary layer and its high sensitivity on SST constitutes the initial source of moist and heat from which the constitution of the storm will be done.

Once the storm is well formed, air-sea interaction mechanism is revealed as a mechanism from which the system is reinforced, maintained and dissipated, as it is shown by the major importance of the multiple synergies rather than individual effects. January 1995 case has a significant different dynamics than the May 2003 case. September 1996 case shows an intermediate behaviour between the two cases, that is a reflection of a short period of tropical-like development. January 1995 case presents a dynamics mainly dominated by multiple synergies related to the SST. Meanwhile, principal effects of May 2003 case are principally related to pure effects or coupled synergies.

Group analysis dependence of the effects allows to make a relative study of that factors and they hidden synergies with that one are not taken into account in the study. From this methodology are obtained signatures of different possible strong effects not considered. Even though hidden synergies are not revealed. These various not considered factors are like: latent heat release from strong cloud formation and orography. These unresolved effects are not reflected in all the cases and effect group-dependences varies respect factors and cases. September 1996 case shows the strongest not well resolved group-dependence of the synergies for the central sea level surface pressure variable. The large number of unresolved synergies exhibited by the storm could be attributed to the short period of tropical-like behaviour and to the proximity to Eastern-Iberian coastal line, orography and islands, that are not present in the other cases and might influence its evolution.

Principal effects of each forecasted field are pretty similar for each case. It is shown that factors act in the same sense for the studied variables. Thus, cyclogenetic (cyclolitic) factors also accelerated (slow downed) and increased (weakened) the vorticity of the system. Principal deepen factors for the three cases are the upper level disturbances, SSHF and SST synergy, LHF and SST synergy, triple synergy between LHF, SSHF and SST and finally triple synergy between SSHF, Upper level disturbances and SST. Major weakening effects are triple synergy of LHF, SSHF and upper level disturbances. Differences between cases are also shown by the different computed effects. A clear temporal phased effect is shown by the effects on the relative vorticity at the centre of the storm at 950 hPa. This phased based effect is shown more clearly by 960912 and 030527 rather than by 950116 case where a mixing of effects is shown. All the obtained dynamical differences revealed January 1995 case as a system much more close to a tropical-like system than strong convective case of a small baroclinic cyclone like May 2003 case.

Air-sea mechanism was developed to describe the dynamics of a mature tropical storm. It is well known that Mediterranean characteristics are quite different from the tropical ones. MM5 simulations attempt to be a more realistic simulation of an atmospheric system. By this way, some differences respect to a theoretical model may be expected. In spite of the differences of size, strength and environment of evolution of the medicanes with respect to the hurricanes and tropics some similarities between medicanes and air-sea mechanism have been found. In the medicanes, sea surface has an important role in the heat and moist source. At the same time, a precursor role of a weak vortex has also been detected in the Mediterranean cases. Warm cores, strong inflow fluxes and strong updrafts are also obtained. However, in medicanes an upper level cold low is a key element for the formation of the systems, and in their movement. The importance of this element is shown in the SST temperatures of the medicanes (15.7, 24.3 and 17.1 °C that are significantly cooler than the threshold temperature for a tropical storm (26°C).

Results have shown a large variety of dynamics. A similar dynamical study should be done with other clear cases of tropical-like storms in order to obtain a much more concrete scope of the dynamics of the system. FS has the ability of give information about the effects of factors and synergies. A deeper knowledge of these synergies is needed in order give a better understanding and explanation of the results that provide the technique. However, some of these synergies involve complex diabatic processes that evolved in a very complex environment with a large number of uncertainties and non-linear coupled features.

7.6.1 Sensitivity of January 1995

Deep examination of the air-sea mechanism in the 950116 medicane case revealed the complexity and multiple dependences of the air-sea mechanism. Azimuthal averaged effects show different behaviour of each factor at different zones and stages of the medicane evolution. Factors can affect different regions of the structure of the storm and can reach its complete structure, be clearly focused in the central part of the storm or be important in the up-outward constant angular-momentum surfaces region. At the same time, wide differences can be found between effects that only differ in one factor with similar characteristics (like strong differences between e_{23} and e_{234} during the formation phase).

Pure effects (effects without synergies) do not change their role during the entire evolution of the system. Surface fluxes and SST basically moisten and warm the base of the storm (promoting an environment with convective instability $\partial_z EPT < 0$), meanwhile upper level disturbance cooled and dried the air beneath. No clear signature of a baroclinic development has been obtained with vertical cross sections at the formation phase of the storm. However, synergy between SSHF and ULd and triple synergy between SSHF, LHF

and SST exhibit a role from which the system acquires the tropical-like characteristics.

During mature state, almost all factors play an enhancing role. It is show how practically all the synergies and factors contributed to enhance and enforce the characteristics of the medicane. However, due to dry characteristics of the air of upper level, a vanishing role can be attributed to this factor, from which middle level air is dried. But at the same time, it contributes to maintain cold upper level air from which the medicane can close properly its energy budged.

Dissipation is characterised by a vanishing role of the synergies related to the SST, meanwhile other factors and synergies maintain in general their previous exhibited role. Moreover change of effect of the coupled SST synergies occurred in a zone where environmental conditions of growing can occur since SST presented its warmest values. This should indicate changes in the dynamics of the system that stopped the mutual reinforce interaction predicted in the tropical storms due to a saturation of the boundary layer.

In order to make an intercomparison between point and 2-dimensional effects of the study should bear in mind that the effects are calculated on different forecasted fields and in different ways. Moreover 2-dimensional effects have a spatial dependence that difficult the intercomparison, since they can present enhancing and vanishing role at the same time. No clear correspondences are obtained during the formation phase, since point effect shows a cyclogenetic development of the storm, meanwhile 2-dimensional effect upper level disturbances and synergy between sea and surface fluxes plays a deepening role with tropical characteristics. At mature state the correspondence between effects is not clear due to dual role of some effects. Meanwhile vanishing role of the synergies with SST obtained in 2-dimensional effect is partially detected by the point effect of the study.

Air-sea interaction has been studied in the particular scope of the Mediterranean tropical-like storms. In order to generalise the results for the air-sea mechanism, a similar study to the sensitivity on the same four factors could be reproduced with tropical or hurricane storms. By this way, structure and dynamics of the air-sea interaction could be better understand due to a stronger and clearer characteristics of these systems. Moreover, a deeper and more detailed study of the meaning of each factor and synergy should be done, in order to make more comprehensive the diabatic and strong nonlinear processes that reflect each synergy.

7.7 Assimilation of observational data in numerical simulations

Significant sensitivity to the choose of PBL scheme has been found for both medicanes. Nonlocal mixing PBL schemes lead to larger precipitable water quantities and more intense sensible and latent heat surface fluxes, but weaker available energy for the development of the system. Accordingly, simulations with a local-mixing scheme like ETA generated a deeper and stronger system. In September 1996 episode a notable system reaching wind hurricane intensity was obtained. No clear conclusions on which scheme is better for simulating these episodes can be obtained, since observations of the characteristics of the medicane are not available. However, deeper systems seem to be in better agreement with barograph measurements of September 1996 medicane at Palma de Mallorca (Homar et al., 2003b).

Satellite-derived images is a powerful way to obtain information at high temporal and spatial resolution over maritime areas. In this work images have been used as a method to derive precipitation type, in combination with lightning information which provides a precise way to determine convective grid points. These tools are then used to constrain MM5 vertical humidity profiles to the observed precipitation type. Medicane simulations show a high sensitivity to the representation of the humidity profile. Almost all the experiments with a modified humidity field simulated a deeper and stronger medicane. More available energy for convection and medicane growth is obtained when humidity correction is applied owing to the increase of potential instability. However, trajectories of simulated systems differ significantly from observed ones. Other satellite-based information like water-vapour channel wind speed estimations could also be retrieved and incorporated into the simulations (Leslie et al., 1998). It has not been done since the main interest of the study is to obtain the sensitivity only to changes on the humidity profile.

September 1996 medicane's trajectory is worsened when satellite information is used, meanwhile in October 2003 case it is improved. Basically, trajectories are only modified in their morphology and genesis zones. No modification of the movement speed of the medicanes is obtained with the technique. As simple modification of the initial and boundary conditions (experiments 'REGRIDmod' and 'REGRIDmot TOT') is significant enough as to generate modifications in the simulated systems. Implementation of satellite-derived information worsens both BIAS and correlation characteristics of September 1996 simulated trajectories. Best results are obtained with the 'FDDA AN' experiments (for the three PBL schemes) in which ECMWF analyses nudging is applied. Only for these experiments, simulated medicane trajectories of October 2003 event have better correlations than control simulation, although these analyses nudging experiments provide the weakest systems. No experiment is able to reduce the temporal shift between observed and

simulated medicanes. October 2003 simulated medicane reflects a delay of 6 hours with respect to the observed one from satellite.

Simulations with ETA PBL scheme seem to have a better response to the application of the observational nudging technique.

Different statistical coefficients have been presented for an objective intercomparison of simulated and observed trajectories. However, a robust object-oriented methodology appears to be necessary. This approach should be able to compare more efficiently basic aspects of the trajectories such as: morphology, genesis and evolution zone and speed of evolution.

7.8 Numerical methodologies

As a result of the objectives of some studies some modifications or new applications were done on the selected numerical techniques: MM5 numerical model, piecewise PV inversion technique and Factor separation.

7.8.1 MM5 numerical model

Presented studies show sensitivities to the SSHF. In order to make it possible, a modified version of the Blackadar PBL scheme has been made by the author. This modification cancels SSHF PBL scheme computations. This modification was made following a previous one used in the *Grup de meteorologia* of the *Universitat de les Illes Balears* in which LHF from the see was annulled.

Sensitivity studies on the SST has also been carried out. A modification on the MM5 module in which boundary conditions are acquired is made. This modification allows directly the modification of the value of the SST provided by the global analyses.

BUFR files has been used in order to improve the global analyses used as the boundary conditions of the simulations. In order to make it possible with the use of ECMWF emos libraries, a new program has been prepared. This program allows the conversion of the binary codified BUFR file to specific ascii format that MM5 module comprises.

In order to apply FDDA technique in MM5 simulations two different modifications has been made. First one consists on the modification of the boundary conditions of the simulations. In this case, the rainy type provided by satellite information was used to modify directly the vertical humidity profile of the boundary conditions. Second modification has been made in the observational nudging. MM5 humidity prognostic variable

is the mixing ratio. A modification of various subroutines of the MM5 model have been done in order to transform satured satellite-based information to the correspondent mixing ratio value into the model grid-point.

At the same time, Vis5d userfuncs have been prepared such as: azimuthal averaged vertical cross sections following a given trajectory, meteograms, soundings and grid-volume energy computations.

MM5 model is able to simulate the medicane cases as a small, strong vortex related to strong winds and precipitation. Simulation of 950116 case presents the most similar structure to a tropical-like storm. On verticals profiles of the storm, one can see patterns such as an eye-wall structure as a moist saturated area close to the centre characterised by strong up-drafts; warm core and vertical structure. However, due to the lack of observations in the maritime areas, a validation of the simulations can not be properly done. Moreover, MM5 model trajectory simulations of the cases differ significantly from the satellite-based observed ones and also exists an important delay between simulated and satellite-based observed evolutions. These significant differences between simulations and observed cases could be related to the difficult to obtain a more realistic representation of important fields like relative humidity profiles and SST over maritime areas as initial conditions in the simulations.

MM5 model is able to simulate a medicane structure in both September 1996 and October 2003 environments. Simulated tropical-like storms, however, present some differences from the observed path in satellite imagery. Simulated systems evolve more slowly, and for the October 2003 case, the storm is generated in a wrong zone. Medicanes have been shown as a meteorological feature able to increase significantly surface heat and moisture fluxes.

In order to avoid computational limitations, MM5 FDDA code should be modified to allow the nudging of higher amount of data independently of computer characteristics. Other modelling analyses such as the sensitivity to other parametrisation schemes (cumulus, explicit rain) and nudging parameters (time-window, radius of influence) should also be carried out in further steps of the study. The sensitivity of the assimilation technique to different convective/stratiform vertical humidity profiles as well as different temporal and spatial resolutions of the ingested satellite-derived data should also be established. Satellite based observational nudging could be applied in the initial steps of operational forecasts at national weather services or research centres. For the selected cases, FDDA technique has a higher sensitivity on horizontal spatial resolution of the assimilated satellite/lightning data rather than on its temporal resolution.

7.8.2 Piecewise PV inversion

Piecewise PV Inversion techniques, combined with perturbed numerical simulations, have been used as a tool to dynamically study various features of atmospherics systems. These techniques can offer useful information about mechanisms and roles of a wide range of features involved in the life cycle of the disturbances. Although numerical solutions to well-defined inversion equations are determined, some uncertainties and subjectivities arise in its application. Some of these case-dependent aspects are: computation of a reference state from which to define the PV anomalies (zonal mean, temporal mean, number of members to establish an average, etc.), morphology and magnitude of the anomalies, and degree of modification of the initial conditions. In the present study an objective procedure has been proposed as a method to quantify the latter aspect of the technique. In this way, one can diminish the ambiguity on the use of the PV Inversion technique applied to modify the initial conditions of numerical simulations.

It is proposed to use the total Mean Absolute Variation (MAV) of energy introduced, due to the modification of the initial conditions. The Root Mean Square Variation (RMSV) could have been proposed, but by squaring the values, contributions of big and small energetic variation values are differently, weighted in the RMSV calculation. The partition of the energy into mechanical, internal and kinetical energies can be useful information from which a deeper understanding of the role of the collection of features can be obtained.

Finally, the proposed quantification method of the piecewise PV inversion derived perturbations can be applied as a general methodology in dynamic meteorology. The application to various events would allow an objective intercomparison between cases, independent of the morphology, characteristics and origin of the selected anomalies. This method of quantification could contribute to the PV study and analysis based on the most important features involved in the evolution of the cyclones or other atmospheric phenomena.

7.8.3 Factor Separation

The Lagrangian application of the FS gives the opportunity to study the system as itself, since computations of values are made from grid points located within a similar dynamical environment. At the same time, it allows the study of specific spatial-correlated dynamics like air-sea interaction. However, a Lagrangian FS does not give any information related to spatial effects of the factors. For that reason, in order to complete the study, Lagrangian FS results should be accompanied with some information about the simulated trajectories.

At the same way, azimuthal averaged cross sections has been shown as a possible way

to obtain a wide and deep view of the three-dimensional processes that are involved in an atmospheric system following a Lagrangian application of the FS technique.

7.9 Final remarks by the Author

Use of new approaches, different applications and/or daring use of numerical techniques bring some success and more challenge. In presented studies, according to the knowledge of the author, different scopes of known problems have been provided such us: objective quantification of the modification throughout piecewise PV inversion technique, Lagrangian application of the factor separation, four factor separation sensitivities, satellite rain derived information on MM5 simulations and statistical tools to compare trajectories. However, new perspectives give different or modified questions that they have not been completely solved.

Author recognises that some of the directions, towards which the presented studies appointed, keep partially unsolved. Limited base of knowledge of the author is the main reason of these undetermined, not physical reason given and/or not deeply analysed aspects. This is certainly a big disillusion and something important to make notice. But in contrast, this aims the author to: keep acquiring more knowledge that should allow the explanation of unsolved aspects, follow a creative scientific way from which 'new' methodologies are proposed and provide new open questions to the scientific community.

Author also recognises the positive fact that is intrinsic of the *Grup de Meteorologia del departament de física de la Universitat de les Illes Balears*. Due to the wide, deep and solid experience of the research team in which the research has been done, author has been able to deal and propose the studies here presented. Discussions, revisions and base of knowledge has been essential to properly develop the research of the Author.

The Portland group compiler is the only licensed software used in all the presented studies. All graphics produced by the author have been drawn with the open source gnuplot tool. All documents and presentations during the period of research have been designed with LaTeX(one presentation was made in html). Computational resources, scripts and work have been based on PC-Linux platform, self-made Fortran programs and distinct shell and AWK self-made modules.

Appendix A

Statistics of trajectories

A.1 Minimum BIAS

The $\mathcal{BIAS}_{dist}$ between satellite-derived medicane trajectory $\mathcal{TRJ}_{ref}$ and trajectory of simulation used to compare $\mathcal{TRJ}_{com}$ is given by:

$$\mathcal{BIAS}_{dist} = \frac{1}{n}\sum_{t=1}^{n}\delta r(t) \tag{A.1.1}$$

where $\delta r(t) = \sqrt{\delta x(t)^2 + \delta y(t)^2}$ is the distance at time t between $\mathcal{TRJ}_{ref}$ and $\mathcal{TRJ}_{com}$. In the expression $\delta æ(t) = æ_{ref}(t) - æ_{com}(t)$, difference between $æ = [x, y]$ coordinates of the trajectories. Assuming morphological differences and different evolving zones of the trajectories, as well as different speeds of evolution of the compared medicanes, $\mathcal{BIAS}_{dist}$ would generally present a dependence on temporal shift of $\mathcal{TRJ}_{com}$. Temporal shift τ for which $\mathcal{BIAS}_{dist}$ becomes minimum (see equation A.1.2), provides an idea of this difference between translational speeds. Temporal range $\tau = [-n/2, n/2]$ is used (n number of total time-steps of length Δt) for the inspection for the adequate τ that minimise $\mathcal{BIAS}_{dist}$. Taking as inspection limits of $\pm n/2$, it is ensured a minimum number of trajectories values (n) for the statistical computation:

$$\mathcal{BIAS}^{min}_{dist} = min\left[\frac{1}{n}\sum_{t=1}^{n}\sqrt{\delta x(t,\tau)^2 + \delta y(t,\tau)^2}\right] \tag{A.1.2}$$

where $\delta æ(t,\tau) = æ_{ref}(t) - æ_{com}(t \pm \tau)$, differences between coordinates $æ = [x, y]$ of trajectory $\mathcal{TRJ}_{ref}$ at time t and trajectory $\mathcal{TRJ}_{com}$ shifted $\pm\tau = n\Delta t$, n time steps of Δt length.

A.2 Distance Correlation

Correlation (classical definition, or Pearson correlation) between satellite-derived trajectory and simulated one is given by:

$$\mathcal{R} = \frac{< \mathcal{D}_{ref}\mathcal{D}_{com} > - < \mathcal{D}_{ref} >< \mathcal{D}_{com} >}{\sigma_{\mathcal{D}_{ref}}\sigma_{\mathcal{D}_{com}}} \tag{A.2.3}$$

where $\sigma_{\mathcal{D}_\chi} = \sqrt{< \mathcal{D}_\chi^2 > - < \mathcal{D}_\chi >^2}$, standard deviation of trajectory χ, and $< \mathcal{D}_\chi >$ average position of trajectory $\chi = [ref, com]$ (equation A.2.4), and $< \mathcal{D}_\chi^2 >$, averaged quadratic distance of trajectory χ

$$< \mathcal{D}_\chi >= \frac{1}{n}\sum_{t=1}^{n} \mathcal{D}_\chi = \frac{1}{n}\sum_{t=1}^{n} \sqrt{x(t)_\chi^2 + y(t)_\chi^2} \tag{A.2.4}$$

$$< \mathcal{D}_\chi^2 >= \frac{1}{n}\sum_{t=1}^{n} \mathcal{D}_\chi^2 = \frac{1}{n}\sum_{t=1}^{n} x(t)_\chi^2 + y(t)_\chi^2 \tag{A.2.5}$$

$$< \mathcal{D}_{ref}\mathcal{D}_{com} >= \frac{1}{n}\sum_{t=1}^{n} \mathcal{D}_{ref}\mathcal{D}_{com} \tag{A.2.6}$$

A.3 Pure coordinate Correlation

It is a classical or Pearson correlation (see equation A.2.3) between observed and simulated trajectory coordinate series is computed as the correlation of two vectors ($\mathcal{R}$) made of the (x, y) coordinate series of both trajectories. With the statistics $\sigma_{\mathcal{R}_\chi} = \sqrt{< \mathcal{R}_\chi^2 > - < \mathcal{R}_\chi >^2}$, Standard deviation of trajectory χ, and $< \mathcal{R}_\chi >$ average value of trajectory $\chi = [ref, com]$ (equation A.3.8), and $< \mathcal{R}_\chi^2 >$, quadratic average value of trajectory χ

$$\mathcal{R}_\chi = \frac{1}{2n}\sum_{t=1}^{2n} R(t)_\chi \tag{A.3.7}$$

$$\mathcal{R}_\chi^2 = \frac{1}{2n}\sum_{t=1}^{2n} R(t)_\chi^2 \tag{A.3.8}$$

$$\mathcal{R}_{ref}\mathcal{R}_{com} = \frac{1}{2n}\sum_{t=1}^{2n} R(t)_{ref}R(t)_{com} \tag{A.3.9}$$

$$\tag{A.3.10}$$

where

$$R_\chi = (\mathcal{X}_{com}, \vec{\mathcal{Y}}_{com}) = (x_\chi^{t=1}, \cdots, x_\chi^{t=n}, y_\chi^{t=1}, \cdots, y_\chi^{t=n}) \tag{A.3.11}$$

A.3.1 Bias correction

The total bias $\mathcal{BIAS}^{com}_{ref}$ between compared and reference trajectories is defined as:

$$\mathcal{BIAS}^{com}_{ref} = \mathcal{BIAS}(x)^{com}_{ref} + \mathcal{BIAS}(y)^{com}_{ref} \tag{A.3.12}$$

where $\mathcal{BIAS}(æ)^{com}_{ref}$, BIAS of coordinate $æ = [x, y]$ is given by:

$$\mathcal{BIAS}(æ)^{com}_{ref} = \frac{1}{n}\sum_{t=1}^{n} æ(t)_{ref} - æ(t)_{com} \tag{A.3.13}$$

Trajectory of comparison $\mathcal{TRJ}_{com} = \left(\mathcal{X}_{com}, \vec{\mathcal{Y}}_{com}\right)$ is corrected with the $\mathcal{BIAS}(æ)^{com}_{ref}$ according to:

$$\tilde{\mathcal{TRJ}}_{com} = \left(\vec{\mathcal{X}_{com}} - \mathcal{BIAS}(\mathcal{X})^{com}_{ref}\ ,\ \vec{\mathcal{Y}_{com}} - \mathcal{BIAS}(\mathcal{Y})^{com}_{ref}\right) \tag{A.3.14}$$

A.3.2 BIAS temporal lack correction

Following $\mathcal{BIAS}^{com}_{ref}$ correction of trajectory $\tilde{\mathcal{TRJ}}_{com}$, a set of temporal shifts are performed in the trajectory ($\tilde{\mathcal{TRJ}}_{com}(\pm\tau)$) in order to obtain the τ value from which the pure coordinate correlation $\mathcal{PR}$ becomes the highest one ($\mathcal{PR}^{max}_{bias}$, see expression A.3.15). The obtained τ value provides a guidance of the temporal shift between simulated and observed trajectories:

$$\begin{aligned} \mathcal{PR}^{max}_{bias} &= max\left(\mathcal{PR}\right)[\pm\tau] = \\ max\Big([&< \mathcal{X}_{ref} > - < \tilde{\mathcal{X}}(\pm\tau)_{com} >] + \\ [&< \mathcal{Y}_{ref} > - < \tilde{\mathcal{Y}}(\pm\tau)_{com} >]\Big) \end{aligned} \tag{A.3.15}$$

Bibliography

Aebishcer, U. and Schär, C., 1998: *Low-Level Potential Vorticity and Cyclogenesis to the Lee of the Alps*, J. Atmos. Sci., **55**, 186207.

Alonso, S., Portela, A., and Ramis, C., 1994: *First considerations on the structure and development of the Iberian thermal low-pressure system*, Ann. Geophys., **12**, 457–468.

Alpert, P. and Ziv, B., 1989: *The Sharav cyclone - Observations and some theorethical considerations*, J. Geophys. Res., **94**, 18 49518 514.

Alpert, P., Neeman, B. U., and Shay-El, Y., 1990: *Climatological analysis of Mediterranean cyclones using ECMWF data*, Tellus, **42A**, 65–77.

Alpert, P., Tsidulko, M., Kirchak, S., and Stein, U., 1995: *A multi-stage evolution of an ALPEX cyclone*, Tellus, **48A**, 209–220.

Alpert, P., Ben-gai, T., Baharad, A., Benjamini, Y., Yekutieli, D., Colacino, M., Diodato, L., Ramis, C., Homar, V., Romero, R., Michaelides, S., and Manes, A., 2002: *The paradoxical increase of Mediterranean extreme daily rainfall in spite of decrease in total values*, Geophys. Res. Lett., **29**, 1–4, doi:10.1029/2001GL013554.

Amengual, A., Romero, R., Gómez, M., Martn, A., and Alonso, S., 2007: *A hydrometeorological modeling study of a flash flood event over Catalonia, Spain*, J. Hydrometeorol., **8**, 282–303.

Arfken, G., 1985: Mathematical Methods for Physicists, 3rd ed., Orlando, FL: Academic Press.

Argence, S., Lambert, D., Richard, E., Söhne, N., Chaboureau, J.-P., Crépin, F., and Arbogast, P., 2006: *High resolution numerical study of the Algiers 2001 flash flood: sensitivity to the upper-level potential vorticity anomaly*, Adv. in Geosci., **7**, 251–257.

Barker, D., Huang, W., Guo, Y.-R., and Bourgeois, A., 2003: *A three-dimensional Variational (3DVAR) Data Assimilation System for use with MM5*, NCAR Technical Note, **NCAR/TN-453+STR**, 68pp.

Barrett, R., Berry, M., Chan, T. F., Demmel, J., Donato, J., Dongarra, J., Eijkhout, V., Pozo, R., Romine, C., and Van der Vorst, H., 1994: Templates for the Solution of Linear Systems: Building Blocks for Iterative Methods, SIAM (http://www.netlib.org/linalg/html_templates/Templates.html).

Bender, M. A., Tuleya, R. E., and Kurihara, Y., 1987: *A numerical study of the effect of island terrain on tropical cyclones*, Mon. Weather Rev., **115**, 130–155.

Bister, M. and Emanuel, K. A., 1998: *Dissipative Heating and Hurricane Intensity*, Meteorol. Atmos. Phys., **50**, 2662–2682.

Blackadar, A., 1979: *High resolution models of the planetary boundary layer*, Advances in Environmental Science and Engineering 1, **1**, 5085.

Bleck, R., 1990: *Depiction of upper/lower vortex interaction associated with extratropical cyclogenesis*, Mon. Weather Rev., **118**, 573–585.

Bluestein, H. B., 1992: Synoptic-Dynamic Meteorology in Midlatitudes. Volume 1, Oxford university press, Inc.

Bretherton, F. P., 1966: *Critical layer instability in baroclinic flows*, Q. J. Roy. Meteor. Soc., **92**, 325–334.

Businger, S. and Reed, R. J., 1989: *Cyclogenesis in cold air masses*, Weather Forecast., **4**, 133–156.

Buzzi, A. and Speranza, A., 1983: *Cyclogenesis in the lee of the Alps*, Mesoscale meteorology - Theories, observations and models; Proceedings of the Advanced Study Institute, **1**, 55–142.

Buzzi, A. and Tibaldi, S., 1978: *Cyclogenesis in the lee of Alps: A case study*, Q. J. Roy. Meteor. Soc., **104**, 271–287.

Campins, J., Genovés, A., Jansà, A., Guijarro, J. A., and Ramis, C., 2000: *A catalogue and a classification of surface cyclones for the western Mediterranean*, Int. J. Climatol., **20**, 969–984.

Campins, J., Jansà, A., and Genovés, A., 2006: *Three-dimensional structure of western Mediterranean cyclones*, Int. J. Climatol., **26**, 323–343.

Charney, J. G., 1955: *The use of primitive equations of motion in numerical prediction*, Tellus, **7**, 22–26.

Charney, J. G. and Eliassen, A., 1964: *On the Growth of the Hurricane Depression*, J. Atmos. Sci., **21**, 68–75, doi:10.1175/1520-0469(1964)021⟨0068:OTGOTH⟩2.0.CO;2.

Cucurull, L., Vandenberghe, F., Barker, D., Vilaclara, E., and Rius, A., 2004: *Three-Dimensional Variational Data Assimilation of Ground-Based GPS ZTD and Meteorological Observations during the 14 December 2001 Storm Event over the Western Mediterranean Sea*, Mon. Weather Rev., **132**, 749–763, doi:10.1175/1520-0493(2004)132⟨0749:TVDAOG⟩2.0.CO;2.

Davis, C. A. and Emanuel, K. A., 1991: *Potential vorticity diagnostics of cyclogenesis*, Mon. Weather Rev., **119**, 1929–1953.

Davolio, S. and Buzzi, A., 2004: *A nudging scheme for the assimilation of precipitation data into a mesoscale model*, Weather Forecast., **19**, 855–871.

Doswell, C. A., Ramis, C., Romero, R., and Alonso, S., 1997: *A Diagnostic Study of Three Heavy Precipitation Episodes in the Western Mediterranean Region*, Weather Forecast., **13**, 102–124.

Ducrocq, V., Ricard, D., Lafore, J., and Orain, F., 2002: *Storm-Scale Numerical Rainfall Prediction for Five Precipitating Events over France: On the Importance of the Initial Humidity Field*, Weather Forecast., **17**, 1236–1256, doi:10.1175/1520-0434(2002)017⟨1236:SSNRPF⟩2.0.CO;2.

Dudhia, J., 1989: *Numerical Study of Convection Observed during the Winter Monsoon Experiment Using a Mesoscale Two-Dimensional Model*, J. Atmos. Sci., **46**, 3077–3107, doi:10.1175/1520-0469(1989)046⟨3077:NSOCOD⟩2.0.CO;2.

Dudhia, J., 1996: *A multi-layer soil temperature model for MM5*, Preprints.from the Sixth PSU/NCAR Mesoscale Model Users'Workshop 22-24, p. http://www.mmm.ucar.edu/mm5/lsm/soil.pdf.

Egger, J., Alpert, P., Tafferner, A., and Ziv, B., 1995: *Numerical experiments on the genesis of Sharav cyclones: Idealized simulations*, Tellus, **47A**, 162174.

Emanuel, K., 2003: *Tropical Cyclones*, Annu. Rev. Earth. Pl. Sc., **31**, 75–104.

Emanuel, K. A., 1983: *On Assessing Local Conditional Symmetric Instability from Atmospheric Soundings*, Mon. Weather Rev., **111**, 2016–2033, doi:10.1175/1520-0493(1983)111⟨2016:OALCSI⟩2.0.CO;2.

Emanuel, K. A., 1986: *An Air-Sea Interaction Theory for Tropical Cyclones. Part I: Steady-State Maintenance*, J. Atmos. Sci., **43**, 585–604.

Emanuel, K. A., 1995: *The Behavior of a Simple Hurricane Model Using a Convective Scheme Based on Subcloud-Layer Entropy Equilibrium*, J. Atmos. Sci., **52**, 3960–3968.

Emanuel, K. A., 2005: *Genesis and maintenance of "Mediterranean hurricanes"*, Adv. in Geoscie., **2**, 217–220.

Ernst, J. A. and Matson, M., 1983: *A Mediterranean tropical storm?*, Weather, **38**, 332–337.

Ertel, H., 1942: *Ein neuer hydrodynamischer wirbelsatz*, Meteor. Z., **59**, 271–281.

Evensen, G., 2003: *The Ensemble Kalman Filter: theoretical formulation and practical implementation*, Ocean Dynamics, **53**, 343367, doi:10.1007/s10236-003-0036-9.

Fan, X. and Tilley, J. S., 2002: *The impact of assimilating satellite-derived humidity on MM5 forecasts*, MM5 forecasts. Preprints, 15th Conference on Numerical Weather Prediction, AMS, 12-15 August, San Antonio, TX, pp. 47–50.

Fita, L., Romero, R., and Ramis, C., 2006: *Intercomparison of intense cyclogenesis events over the Mediterranean basin based on baroclinic and diabatic influences*, Adv. in Geosci. (Proccedings PLINIUS 2006), **7**, 333–342.

Fita, L., Romero, R., Luque, A., Emanuel, K., and Ramis, C., 2007a: *Analysis of the environments of seven Mediterranean tropical-like storms using an axisymmetric, non-hydrostatic, cloud resolving model*, Nat. Hazard. Earth Sys., **7**, 1–16.

Fita, L., Romero, R., and Ramis, C., 2007b: *Objective quantification of perturbations produced with a piecewise PV Inversion technique*, Ann. Geophys., **25**, 2335–2349.

Fita, L., Romero, R., Luque, A., and Ramis, C., 2008a: *Effects on numerical simulations of tropical-like Mediterranean storms of assimilating precipitation zones derived from satellite and lightning data*, Ann. Geophys., **submitted**.

Fita, L., Romero, R., and Ramis, C., 2008b: *Sensitivity study of tropical-like storms. part I: Sensitivity of air-sea mechanism in three storms*, Ann. Geophys., **submitted**.

Fita, L., Romero, R., and Ramis, C., 2008c: *Sensitivity study of tropical-like storms. part II: Air-sea mechanism in the muter phase of January 1995 medicane*, Ann. Geophys., **submitted**.

Font, L., 1983: Climatología de España y Portugal., Instituto Nacional de Meteorologa.

Gaertner, M. A., Jacob, D., Gil, V., nguez, M. D., Padorno, E., and Sánchez, E., 2007: *Tropical cyclones over the Mediterranean Sea in climate change simulations*, Geophys. Res. Lett., **34**, L14 711, doi:10.1029/2007GL029977.

García-Ortega, E., Fita, L., Romero, R., López, L., Ramis, C., and Sánchez, J., 2007: *Numerical simulation and sensitivity study of a severe hail-storm in northeast Spain*, Atmos. Res., **83**, 225–241, doi:10.1016/j.atmosres.2005.08.004.

Gayà, M., Homar, V., Romero, R., and Ramis, C., 2001: *Tornadoes and waterspouts in the Balearic Islands: Phenomena and environment characterization*, Atmos. Res., **56**, 253–267.

Grell, G., Dudhia, J., and Stauffer, D., 1994: *A description of the fifth-generation Penn State/NCAR mesoscale model (MM5)*, NCAR Technical Note, **NCAR/TN-398+STR**, 117pp.

Grell, G. A., Dudhia, J., and Stauffer, D. R., 1995: *A description of the Fifth-generation Penn State/NCAR Mesoscale Model (MM5)*, NCAR Technical Note, **NCAR/TN-398+STR**, 122pp.

Grell, G. A., Emeis, S., Stockwell, W. R., Schoenemeyer, T., Forkel, R., Michalakes, J., Knoche, R., and Seidl, W., 2000: *Application of a multiscale, coupled MM5/chemistry model to the complex terrain of the VOTALP valley campaign*, Atmospheric Environment, **34**, 1435–1453, doi:10.1016/S1352-2310(99)00402-1.

Gyakum, J. R., 1983a: *On the Evolution of the QE II Storm. I: Synoptic Aspects*, Mon. Weather Rev., **111**, 1137–1155.

Gyakum, J. R., 1983b: *On the Evolution of the QE II Storm. II: Dynamic and Thermodynamic Structure*, Mon. Weather Rev., **111**, 1156–1173.

Hakim, G. J., Keyser, D., and Bosart, L. F., 1996: *The Ohio valley wave-merger cyclogenesis event of 25-26 january 1978. Part II: Diagnosis using quasigeostrophic potential vorticity inversion*, Mon. Weather Rev., **124**, 2176–2205.

Holton, J., 1979: An introduction to dynamic meteorology, Academic Press Inc.

Homar, V., Ramis, C., Romero, R., Alonso, S., a Moya, J. G., and Alarcón, M., 1999: *A case of convection development over the western Mediterranean sea: A study through numerical simulations*, Meteorol. Atmos. Phys., **71**, 169–188.

Homar, V., Ramis, C., and Alonso, S., 2002a: *A deep cyclone of African origin over the Western Mediterranean: diagnosis and numerical simulation*, Ann. Geophys., **20**, 93–106.

Homar, V., Romero, R., Ramis, C., and Alonso, S., 2002b: *Numerical study of the October 2000 torrential precipitation event over eastern Spain: Analysis of the synoptic-scale stationarity*, Ann. Geophys., **20**, 2047–2066.

Homar, V., Gayà, M., Romero, R., Ramis, C., and Alonso, S., 2003a: *Tornadoes over complex terrain: An analysis of the 28th August 1999 tornadic event in eastern Spain*, Atmos. Res., **67-68**, 301–317, doi:10.1016/S0169-8095(03)00064-4.

Homar, V., Romero, R., Stensrud, D., Ramis, C., and Alonso, S., 2003b: *Numerical diagnosis of a small, quasi-tropical cyclone over the western Mediterranean: Dynamical vs. boundary factors*, Q. J. Roy. Meteor. Soc., **129**, 1469–1490.

Hong, S.-Y. and Pan, H.-L., 1996: *Nonlocal boundary layer vertical diffusion in a medium-range forecast model*, Mon. Weather Rev., **124**, 2322–2339.

Horvath, K., Fita, L., Romero, R., and Ivancan-Picek, B., 2006: *A numerical study on the first phase of a deep Mediterranean cyclone: Cyclogenesis in the lee of the Atlas Mountains*, Meteorologische Z. 1, **15**, 133–146, doi:10.1127/0941-2948/2006/0113.

Hoskins, B. J., McIntyre, M. E., and Robertson, A. W., 1985: *On the use and significance of isentropic potential vorticity maps*, Q. J. Roy. Meteor. Soc., **111**, 877–946.

Houssos, E. E., Lolis, C. J., and Bartzokas, A., 2007: *The atmospheric conditions over Europe and the Mediterranean, favoring snow events in Athens, Greece*, Adv. in Geoscie., **12**, 127–135.

Huo, Z., Zhang, D.-L., Gyakum, J. R., and Stainforth, A. N., 1995: *A diagnostic analysis of the superstorm of march 1993*, Mon. Weather Rev., **123**, 1740–1761.

Huo, Z., Zhang, D.-L., and Gyakum, J., 1998: *An Application of Potential Vorticity Inversion to Improving the Numerical Prediction of the March 1993 Superstorm*, Mon. Weather Rev., **126**, 424–436, doi:10.1175/1520-0493(1998)126⟨0424:AAOPVI⟩2.0.CO;2.

Huo, Z., Zhang, D.-L., Gyakum, J. R., and Stainforth, A. N., 1999: *Interaction of potential vorticity anomalies in extratropical cyclogenesis. Part II: Sensitivity to initial perturbations*, Mon. Weather Rev., **127**, 2563–2575.

Ikawa, M. and Saito, K., 1991: *Description of a nonhydrostatic model developed at the forecast research department of the MRI*, Technical Reports of the Meteorological Research Institute, **28**.

IPCC, 2007: Climate Change 2007: The Physical Science Basis. Contribution of Working Group I to the Fourth Assessment Report of the Intergovernmental Panel on Climate Change, [Solomon, S., D. Qin, M. Manning, Z. Chen, M. Marquis, K.B. Averyt,M. Tignor and H.L. Miller (eds.)] Cambridge University Press, Cambridge, United Kingdom and New York, NY, USA.

Janjić, Z. I., 1990: *The Step-Mountain Coordinate: Physical Package*, Mon. Weather Rev., **118**, 1429–1443.

Janjić, Z. I., 1994: *The Step-Mountain Eta Coordinate Model: Further Developments of the Convection*, Mon. Weather Rev., **122**, 927–945.

Jordan, C. L., 1958: *Mean Soundings for the West Indies Area*, J. Meteorol., **15**, 91–97.

Kain, J. S., 2004: *The Kain-Fritsch Convective Parameterization: An Update*, K. Appl. Meteorol., **43**, 170–181.

Kain, J. S. and Fritsch, J. M., 1990: *A one-dimensional entraining/detraining plume model and its application in convective parameterization*, J. Atmos. Sci., **47**, 2748–2802, doi:10.1175/1520-0469(1990)047⟨2784:AODEPM⟩2.0.CO;2.

Kain, J. S. and Fritsch, J. M., 1993: *Convective parameterization for mesoscale models: The Kain-Fritsch scheme*, The Representation of Cumulus Convection in Numerical Models, Meteor. Monogr., **No. 24**, 165–170.

Kidd, C., Kniveton, D. R., Todd, M. C., and Bellerby, T. J., 2003: *Satellite Rainfall Estimation Using Combined Passive Microwave and Infrared Algorithms*, J. Hydrometeorol., **4**, 1088–1104.

Krichak, S. O. and Alpert, P., 2002: *A fractional approach to the factor separation method*, J. Atmos. Sci., **59**, 2243–2252.

Krichak, S. O., Tsidulko, M., and Alpert, P., 2004: *Monthly Synoptic Patterns Associated with Wet/Dry Conditions in the Eastern Mediterranean*, Theo. Appl. Climatolo., **65**, 215–229.

Kuo, Y. A., Shapiro, M. A., and Donall, E. G., 1991a: *The interaction between baroclinic and diabatic processes in a numerical simulation of a rapidly intensifying extratropical marine cyclone*, Mon. Weather Rev., **119**, 368–384.

Kuo, Y.-H., Reed, R. J., and Low-Nam, S., 1991b: *Effects of surface energy fluxes during the early development and rapid intensification stages of seven explosive cyclones in the western Atlantic*, Mon. Weather Rev., **119**, 457–476.

Lagouvardos, K. and Kotroni, V., 2005: *Improvement of high-resolution weather forecasts through humidity adjustment based on satellite data*, Q. J. Roy. Meteorol. Soc., **131**, 2695–2712.

Lagouvardos, K., Kotroni, V., Nickovic, S., Jovic, D., and Kallos, G., 1999: *Observations and model simulations of a winter sub-synoptic vortex over the central Mediterranean*, Meteorol. Appl., **6**, 371–383.

Leslie, L. M., LeMarshall, J. F., Morison, R. P., Spinoso, C., Purser, R., Pescod, N., and Seecamp, R., 1998: *Improved Hurricane Track Forecasting from the Continuous Assimilation of High Quality Satellite Wind Data*, Mon. Weather Rev., **126**, 1248ˇ20131 258, doi:10.1175/1520-0493(1998)126⟨1248:IHTFFT⟩2.0.CO;2.

Lilly, D. K., 1962: *On the numerical simulation of bouyant convection*, Tellus, **14**, 148–172.

Liu, Y., Zhang, D., and Yau, M. K., 1997: *A Multiscale Numerical Study of Hurricane Andrew (1992). Part I: Explicit Simulation and Verification*, Mon. Weather Rev., **125**, 3073–3093.

Lorenc, A. C., Ballard, S. P., Bell, R. S., Ingleby, N. B., Andrews, P. L. F., Barker, D. M., Bray, J. R., Clayton, A. M., Dalby, T., Li, D., Payne, T. J., and Saunders, F. W., 2000: *The Met. Office global three-dimensional variational data assimilation scheme*, Q. J. Roy. Meteor. Soc., **126**, 2991–3012.

Lorenz, E. N., 1963: *Deterministic Nonperiodic Flow*, J. Atmos. Sci., **20**, 130–141.

Lorenz, E. N., 1991: *Dimension of weather and climate attractors*, Nature, **353**, 241–244.

Louis, J.-F., 1979: *A parametric model of vertical eddy fluxes in the atmosphere*, Bound.-Lay. Meteorol., **17**, 187–202, doi:10.1029/2004GL019821.

Luque, A., Fita, L., Romero, R., and Alonso, S., 2007: *Tropical-like Mediterranean Storms: An Analysis from satellite*, Proceedings. 2007 Joint EUMETSAT/AMS Conference – Amsterdam, pp. 1–7.

Maheras, P., Flocas, H. A., Patrikas, I., and Anagnostopoulou, C., 2001: *A 40 year Objective climatology of Surface Cyclones in the Mediterranean Region: Spatial and Temporal Distribution*, Int. J. Climatol., **21**, 109–130.

Mak, M., 1997: *Influence of Surface Sensible Heat Flux on Incipient Marine Cyclogenesis*, J. Atmos. Sci., **55**, 820–834.

Martín, A., Romero, R., Homar, V., de Luque, A., and Alonso, S., 2007: *Sensitivities of a Flash Flood Event over Catalonia: A Numerical Analysis*, Mon. Weather Rev., **135**, 651–669, doi:10.1175/MWR3316.1.

Mellor, G. L. and Yamada, T., 1982: *Development of a turbulence closure model for geophysical fluid problems*, Rev. Geophys., **20**, 851–875.

Molteni, F., Buizza, R., Palmer, T. N., and Petroliagis, T., 1996: *The ECMWF Ensemble Prediction System: Methodology and validation*, Q. J. Roy. Meteor. Soc., **122**, 73–119, doi:10.1002/qj.49712252905.

Monserrat, S., Vilibić, I., and Rabinovich, A. B., 2006: *Meteotsunamis: atmospherically induced destructive ocean waves in the tsunami frequency band*, Nat. Hazard. Earth Syst. Sci., **6**, 1035–1051.

Montgomery, M. T. and Farrell, B. F., 1992: *Polar Low Dynamics*, J. Atmos. Sci., **49**, 2484–2505.

Ooyama, K., 1964: *A dynamical model for the study of tropical cyclone development*, Geofis. Int, **4**, 187–198.

Orlandi, A., Ortolani, A., Meneguzzo, F., Levizzani, V., Torricella, F., and Turk, F. J., 2004: *Rainfall assimilation in RAMS by means of the Kuo parameterisation inversion: method and preliminary results*, J. Hydrol., **288**, 20–35.

Pettersen, S. and Smebye, S. J., 1971: *On the development of extratropical cyclones*, Q. J. Roy. Meteor. Soc., **97**, 457–482.

Phillips, N. A., 1954: *Energy transformations and meridional circulations associated with simple baroclinic waves in a two-level, quasi-geostrophic model*, Tellus, **6**, 273–286.

Picornell, M. A., Jansà, A., Genovés, A., and Campins, J., 2001: *Automated database of mesocyclones from the Hirlam(INM)-0.5° analyses in the Western Mediterranean*, Int. J. Climatol., **21**, 335–354.

Pytharoulis, I., Craig, G. C., and Ballard, S. P., 2000: *The hurricane-like Mediterranean cyclone of January 1995*, Meteorol. Appl., **7**, 261–279.

Rabier, F., Thépaut, J.-N., and Courtier, P., 1998: *Extended assimilation and forecast experiments with a four-dimensional variational assimilation system*, Q. J. Roy. Meteor. Soc., **124**, 1861–1887.

Rabier, F., Järvinen, H., Klinker, E., Mahfouf, J.-F., and Simmons, A., 2000: *The ECMWF operational implementation of four-dimensional variational assimilation. I: Experimental results with simplified physics*, Q. J. Roy. Meteor. Soc., **126**, 1143–1170.

Ramis, C. and Jansà, A., 1983: *Condiciones meteorológicas simultáneas a la aparicioón de oscilaciones del nivel del mar de amplitud extraordinaria en el Mediterráneo occidental*, Rev. Geofísica (in spanish), **39**, 3542.

Ramis, C., Romero, R., Homar, V., Alonso, S., and Alarcón, M., 1998: *Diagnosis and Numerical simulation of a Torrential Precipitation Event in Catalonia (Spain)*, Meterol. Atmos. Phys., **69**, 1–21.

Ramis, C., López, J., and Arús, J., 1999: *Two cases of severe weather in Catalonia (Spain): a diagnostic study*, Meteorol. Appl., **6**, 11–27.

Rasmussen, E. and Zick, C., 1987: *A subsynoptic vortex over the Mediterranean with some resemblance to polar lows*, Tellus A, **39**, 408–425.

Reed, R. J., Stoelinga, M. T., and Kuo, Y.-H., 1992: *A model-aided study of the origin and evolution of the anomalously high potential vorticity in the inner region of a rapidly deeping marine cyclone*, Mon. Weather Rev., **120**, 893–913.

Reed, R. J., Kuo, Y.-H., Albright, M. D., Gao, K., Gua, Y.-R., and Huang, W., 2001: *Analysis and modeling of a tropical-like cyclone in the Mediterranean Sea*, Meteorol. Atmos. Phys., **76**, 183–202.

Reiser, H. and Kutiel, H., 2007a: *The rainfall regime and its uncertainty in Valencia and Larnaca*, Adv. in Geosci., **12**, 101106, doi:10.1029/2004GL019821.

Reiser, H. and Kutiel, H., 2007b: *Rainfall uncertainty in the Mediterranean: definition of the rainy season a methodological approach*, Theor. Appl. Climatol., pp. 65–+, doi: 10.1007/s00704-007-0343-z.

Reisner, J., Rasmussen, R., and Bruintjes, R., 1998: *Explicit Forecasting of Supercooled Liquid Water in Winter Storms Using the MM5 Mesoscale Model*, Q. J. Roy. Meteor. Soc., **124**, 1071–1107, doi:10.1002/qj.49712454804.

Reiter, E. R., 1975: Handbook for Forecasters in the Mediterranean: Weather Phenomena of the Mediterranean Basin, Environmental Prediction Research Facility, Naval Postgraduate School, Monterey, CA.

Roberts, R. D. and Rutledge, S., 2003: *Nowcasting Storm Initiation and Growth Using GOES-8 and WSR-88D Data*, Weather Forecast., **18**, 562–584.

Robinson, W. A., 1989: *On the structure of potential vorticity in baroclinic instability*, Tellus, **41A**, 275–284.

Romero, R., 2001: *Sensitivity of a Heavy Rain producing Western Mediterranean cyclone to embedded Potential Vorticity anomalies*, Q. J. Roy. Meteor. Soc., **127**, 2559–2597.

Romero, R., 2008: *A method for quantifying the impacts and interactions of potential vorticity anomalies in extratropical cyclones*, Q. J. Roy. Meteor. Soc., **in press**.

Romero, R. and Emanuel, K., 2006: *Space-time probability density of Mediterranean hurricane genesis in the light of an empirical tropical index*, 5a Assamble Hispano-Portuguesa de Geodesia y Geofisica, **(Spanish)**, 4.

Romero, R., Ramis, C., and Alonso, S., 1997: *Numerical simulation of an extreme rainfall event in Catalonia: Role of orography and evaporation from the sea*, Q. J. Roy. Meteor. Soc., **123**, 537–559.

Romero, R., Guijarro, J. A., Ramis, C., and Alonso, S., 1998: *A 30-year (1964 1993) Daily Rainfall data base for the Spanish Mediterranean regions: first exploratory study*, Int. J. Climatol., **18**, 541560.

Romero, R., Sumner, G., Ramis, C., and Genovés, A., 1999: *A classification of the atmospheric circulation patterns producing significant daily rainfall in the Spanish Mediterranean area*, Int. J. Climatol., **19**, 765–785.

Romero, R., Doswell, C. A., and Ramis, C., 2000: *Mesoscale Numerical Study of Two Cases of Long-Lived Quasi-Stationary Convective Systems over Eastern Spain*, Mon. Weather Rev., **128**, 3731–3751.

Romero, R., Doswell, C., and Riosalido, R., 2001: *Observations and fine-grid simulations of a convective outbreak in northeastern Spain: importance of diurnal forcing and convective cold pools*, Mon. Weather Rev., **129**, 2157–2182.

Rotunno, R. and Emanuel, K., 1987: *An Air-Sea Interaction Theory for Tropical Cyclones. Part II: Evolutionary Study Using a Nonhydrostatic Axisymmetric Numerical Model*, J. Atmos. Sci., **44**, 542–561.

Sánchez, A. C. J. and Fraile, R., 1992: *Statistical comparison of the properties of thunderstorms in different areas around the Ebro Valley (Spain)*, Atmos. Res., **28**, 237–257.

Sánchez, J., García, E., Marcos, J., and Dessens, J., 1999: *Formation of big and giant drops inside Mediterranean convective cells*, Proceedings of the EGS Plinius Conf. Maratea, Italy., **1**, 57–65.

Sanders, F., 1986: *Explosive cyclogensis in the West-central North Atlantic ocean, 1981-84. Part I: Composite structure and mean behavior*, Mon. Weather Rev., **114**, 1781–1794.

Sanders, F. and Gyakum, J. R., 1980: *Synoptic-Dynamic climatology of the 'Bomb'*, Mon. Weather Rev., **108**, 1589–1606.

Schulz, J., Jeans, M., stefan, E., and Schlussel, P., 1996: *Evaluation of satellite derived latent heat flux*, J. Climate, **10**, 2782–2795.

Smagorinsky, J., 1963: *General circulation experiments with the primitive equations.I: The basic experiment*, Mon. Weather Rev., **91**, 99–164.

Stauffer, D. R. and Seaman, N. L., 1990: *Use of Four-Dimensional Data Assimilation in a Limited-Area Mesoscale Model. Part I: Experiments with Synoptic-Scale Data*, Mon. Weather Rev., **118**, 1250–1277, doi:10.1175/1520-0493(1990)118⟨1250:UOFDDA⟩2.0.CO;2.

Stein, U. and Albert, P., 1993: *Factor Separation in Numerical Simulations*, J. Atmos. Sci., **50**, 2107–2115.

Stull, R. B., 1988: An introduction to boundary layer meteorology, Kluwer Academic Publishers.

Tayanç, M., Karaca, M., and Dalfes, H., 1998: *March 1987 Cyclone (Blizzard) over the Eastern Mediterranean and Balkan Region Associated with Blocking*, Mon. Weather Rev., **126**, 3036–3047, doi:10.1175/1520-0493(1998)126⟨3036:MCBOTE⟩2.0.CO;2.

Taylor, K. E., 2001: *Summarizing multiple aspects of model performance in a single diagram*, J. Geophys. Res., **106**, 7183–7192.

Thorpe, A. J., 1986: *Synoptic scale disturbances with circular symmetry*, Mon. Weather Rev., **114**, 1384–1389.

Toth, Z. and Kalnay, E., 1993: *Ensemble Forecasting at NMC: The Generation of Perturbations*, B. Am. Meteorol. Soc., **74**, 2317–2330.

Toth, Z. and Kalnay, E., 1997: *Ensemble Forecasting at NCEP and the Breeding Method*, Mon. Weather Rev., **125**, 3297–3319, doi:10.1175/1520-0493(1997)125⟨3297:EFANAT⟩ 2.0.CO;2.

Tous, M. and Romero, R., 2006: *Towards a European climatology of meteorological parameters associated to the genesis of severe storms*, Tethys, **3**, 9–17, doi:10.3369/tethys. 2006.3.02.

Trigo, I. F., Davies, T. D., and Bigg, G. R., 1999: *Objective Climatology of Cyclones in the Mediterranean Region*, J. Climate, **12**, 1685–1696.

Trigo, I. F., Bigg, G. R., and Davies, T. D., 2002: *Climatology of Cyclogenesis Mechanisms in the Mediterranean*, Mon. Weather Rev., **130**, 549–569.

Tripoli, G. J., Medaglia, C. M., Dietrich, S., Mugnai, A., Panegrossi, G., Pinori, S., and E. A. Smith, E. A., 2005: *The 9-10 November 2001 Algerian Flood: A Numerical Study.*, B. Am. Meteorol. Soc., **86**, 1229–1235.

Troen, I. and Mahrt, L., 1986: *A Simple Model of the Atmospheric Boundary Layer: Sensitivity to Surface Evaporation*, Bound-Lay Meteorol., **37**, 129–148.

Tsidulko, M. and Alpert, P., 2001: *Synergism of upper-level potential vorticity and mountains in Genoa lee cyclogenesisA numerical study*, Meteorol. Atmos. Phys., **78**, 261285.

Tudurí E. and Ramis, C., 1997: *The Enviromments of Significant Convective Events in the Western Mediterranean*, Weather Forecast., **12**, 294–306.

Tudurí E., Romero, R., López, L., Garcia, E., Sánchez, J., and Ramis, C., 2003: *The 14 July 2001 hailstorm in northeastern Spain: diagnosis of the meteorological situation*, Atmos. Res., **67-68**, 541–558.

Turk, F. J., Rohaly, G., Hawkins, J. D., Smith, E. A., Grose, A., Marzano, F. S., Mugnai, A., and Levizzani, V., 2000: *Analysis and assimilation of rainfall from blended SSMI, TRMM and geostationary satellite data*, 10th AMS Conference on Satellite Meteorology and Oceanography, Long Beach CA, 15 Jan 2000, pp. 66–69.

Uccelini, L. W., Keyser, D., Brill, K. F., and Wash, C. H., 1985: *The Presidents' Day Cyclone of 18-19 February 1979: Influence of upstream trough amplification and associated Tropopause folding on rapid cyclogenesis*, Mon. Weather Rev., **113**, 962–987.

Uppala, S., Kallberg, P., Simmons, A., Andrae, U., da Costa Bechtold, V., Fiorino, M., Gibson, J., Haseler, J., Hernandez, A., Kelly, G., Li, X., Onogi, K., Saarinen, S., and (...), 2005: *The ERA-40 re-analysis*, Q. J. Roy. Meteor. Soc., **131**, 2961–3012.

Whitaker, J. S., Uccellini, L. W., and Brill, K. F., 1988: *A Model-Based diagnostic study of the rapid development phase of the Presidents' Day cyclone*, Mon. Weather Rev., **116**, 2337–2365.

Wisse, J. S. P. and de Arellano, J. V.-G., 2004: *Analysis of the role of the planetary boundary layer schemes during a severe convective storm*, Ann. Geophys., **22**, 1861–1874.

WMO, 2002: *54 Edition of the Executive Council*, WMO – Annex V, `http://www.wmo.int/pages/prog/arep/wwrp/documents/WWRPe.pdf`, **945**, 137pp (95–99).

WMO, 2006: *Guidelines on Using Information from EPS in Combination with Single Higher Resolution NWP Forecasts*, WMO - CBS Expert Team on EPS, `http://www.wmo.int/pages/prog/www/DPFS/Documentation/Guidelines_ET-EPS2%006.pdf`, p. 2.

WMO, 2007: *FM 94XIII Ext. BUFR Binary universal form for the representation of meteorological data*, `http://www.wmo.int/pages/prog/www/WMOCodes/Operational/BUFR/FM94REG-11-%2007.pdf`, pp. 1–12.

Xu, M., Bao, J.-W., Warner, T. T., and Stensrud, D. J., 2001: *Effect of Time Step Size in MM5 Simulations of a Mesoscale Convective System*, Mon. Weather Rev., **129**, 502–516, doi:10.1175/1520-0493(2001)129⟨0502:EOTSSI⟩2.0.CO;2.

Zängl, G., 2002: *An Improved Method for Computing Horizontal Diffusion in a Sigma-Coordinate Model and Its Application to Simulations over Mountainous Topography*, Mon. Weather Rev.–notes and correspondence, **130**, 1423–1432, doi:10.1175/1520-0493(2002)130⟨1423:AIMFCH⟩2.0.CO;2.

Zeng, X., Pielke, R. A., and Eykholt, R., 1992: *Estimating the Fractal Dimension and the Predictability of the Atmosphere*, J. Atmos. Sci., **49**, 649–659.

Zhang, D. and Anthes, R. A., 1982: *A High-Resolution Model of the Planetary Boundary Layer–Sensitivity Tests and Comparisons with SESAME-79 Data*, J. Appl. Meteorol., **21**, 1594–1609.

Zhang, D. and Fritsch, J. M., 1986: *Numerical simulation of the meso-β scale structure and evolution of the 1977 Johnstown flood. Part I: Model description and verification*, J. Atmos. Sci., **43**, 1913–1943.

Zou, X. and Xiao, Q., 1999: *Studies on the Initialization and Simulation of a Mature Hurricane Using a Variational Bogus Data Assimilation Scheme*, J. Atmos. Sci., **57**, 836–860.